



**CZECHOSLOVAK ASSOCIATION FOR CRYSTAL GROWTH**

 **Fyzikální ústav**  
Akademie věd ČR, v. v. i.



**Development of Materials Science  
in Research and Education**

*Proceedings of 20<sup>th</sup> Joint Seminar*

K. Nitsch  
Z. Kožíšek  
Editors

Bořetice, Kraví Hora  
Czech Republic

*September 1 – 3, 2010*

Published by the Czechoslovak Association for Crystal Growth (CSACG)  
CZ-162 00 Praha 6, Cukrovarnická 10, Czech Republic

Editors: K. Nitsch and Z. Kožíšek  
©2010 CSACG, Czech Republic. All rights reserved.

**ISBN 978-80-254-7237-8**

**The seminar is organized by**

**the Czechoslovak Association for Crystal Growth and  
the Slovak Expert Group of Solid State Chemistry and Physics**

under the auspices of

**the Institute of Physics, Academy of Sciences of the Czech Republic and  
the Slovak Society for Industrial Chemistry**

## **Conference Chairman**

### **Dr. K. Nitsch**

Chairman of the Czechoslovak Association for Crystal Growth  
Institute of Physics Academy of Sciences of the Czech Republic  
Cukrovarnická 10, 162 00 Praha 6, Czech Republic

Phone +420 220 318 557

Fax +420 233 343 184

E-mail: nitsch@fzu.cz

## **Conference Co-Chairman**

### **Prof. M. Koman**

Chairman of the Slovak Expert Group of Solid State Chemistry and Physics  
Faculty of Chemical and Food Technology SUT  
Radlinského 9, 812 37 Bratislava, Slovak Republic

Phone +421 259 325 622

Fax +421 252 493 198

E-mail: marian.koman@stuba.sk

## **Conference Secretary**

### **Miroslava Rodová**

Institute of Physics Academy of Sciences of the Czech Republic, Cukrovarnická 10,  
162 00 Praha 6, Czech Republic

Phone +420 220 318 429

Fax +420 233 343 184

E-mail: rodova@fzu.cz



# FOREWORD

This year's seminar "Development of Materials Science in Research and Education" is already the twentieth in the series started at Gabčíkovo in the Slovak Republic in 1991. It is organized by the Czechoslovak Association for Crystal Growth and the Slovak Expert Group of Solid State Chemistry and Physics under support of the Institute of Physics AS CR, Faculty of Chemical and Food Technology SUT Bratislava, and Slovak Society for Industrial Chemistry at a Moravian resort Bořetice situated about 30 km south-eastern from Brno. The objectives of this meeting were to offer the opportunity for the Czech and Slovak teachers and scientists and guests from other countries working in the field of crystal growth and materials science to present their recent results and to exchange ideas and information.

The scientific sessions cover the following topics of materials science:

1. Trends in development of materials research.
2. Education of materials science at the universities.
3. Information about the research programmes of individual institutions.
4. Information about equipment for preparation and characterisation of materials.
5. Results of materials research.

The sessions include talks and orally presented short contributions. The time allocated for talks is 30 minutes and for short contributions 20 minutes including the time for discussion. Although the official languages of the seminar are Czech and Slovak, the presentation of the abstracts is only in English.

This booklet contains the abstracts of all contributions, which reached us before July 31. The required camera-ready format of the abstracts makes it impossible for the editors to take any responsibility for the technical and language quality of the contributions. This responsibility rests entirely with the authors.

*Editors*



# CONTENTS

IMPORTANCE OF USING POLYMER LAYERS FOR SELECTIVE AREA GROWTH OF DIAMOND MICRO- AND NANOSTRUCTURES ..... 7

*Oleg Babchenko, Tibor Izak, Karel Hruška, Martin Ledinsky, Bohuslav Rezek, and Alexander Kromka*

MATERIAL MODELS FOR NUMERICAL SIMULATION OF MATERIAL FLOW IN THIXOTROPIC STATE ..... 9

*Mária Behúlová*

REGIONAL MATERIALS SCIENCE AND TECHNOLOGY CENTRE IN OSTRAVA ..... 11

*Jaromír Drápala and Miroslav Kursá*

DETERMINATION OF THE MEAN VALUE OF CRYSTAL GRAIN SIZE BY X-RAY DIFFRACTION SPOT COUNTING ..... 13

*Jaromír Galle, Zdenek Pala, Kamil Kolařík, and Nikolaj Ganev*

DIFFRACTION ANALYSIS OF RESIDUAL STRESSES IN THIN SURFACE LAYERS OF POLYCRYSTALLINE MATERIALS ..... 15

*Nikolaj Ganev, Zdenek Pala, and Kamil Kolařík*

CHALLENGES IN THE PREPARATION AND APPLICATION OF POROUS III-V SEMICONDUCTORS ..... 17

*Jan Grym and Dušan Nohavica*

INFLUENCE OF  $Sc^{3+}$  DOPING ON  $Pr^{3+}$  EMISSION IN EPITAXIAL SCINTILLATION GARNET LAYERS ..... 19

*Martin Hanuš, Miroslav Kučera, Martin Nikl, Karel Nitsch, Petr Průša, Jiří A. Mareš, and Zuzana Onderišinová*

USING OF SELF-ASSEMBLED GOLD NANO-SIZED DROPLETS FOR FABRICATION OF VERTICALLY ALIGNED DIAMOND NANORODS ..... 21

*Tibor Izak, Oleg Babchenko, Alexander Kromka, Karel Hruška, and Miroslav Michalka*

CRYSTAL STRUCTURES OF  $Cu(II)$  COMPLEXES WITH PYRIDYLMETHANOLS ..... 23

*Marian Koman, Jaroslava Maroszová, Ján Moncol', and Dušan Mikloš*

COBALT-BASED FERROMAGNETIC SHAPE MEMORY ALLOYS - PREPARATION, CHARACTERIZATION AND FUNCTIONAL PROPERTIES . . . . .	25
<i>Jaromír Kopeček, Markéta Jarošová, Karel Jurek, Jan Drahekoupil, Dušan Majtás, Silvie Ignáčová-Sedláková, and Oleg Heczko</i>	
SELECTIVE ETCHING PROCESSES FOR BESOI MANUFACTURING . . . . .	27
<i>Petr Kostelník</i>	
STRUCTURAL STUDIES OF ZNO-WO <sub>3</sub> -P <sub>2</sub> O <sub>5</sub> SYSTEM GLASSES . . . . .	29
<i>Ladislav Koudelka, Jiří Šubčík, Petr Mošner, and Ivan Gregora</i>	
KINETICS OF POLYMER NUCLEATION ON ACTIVE CENTERS . . . . .	31
<i>Zdeněk Kožíšek, Pavel Demo, Alexei Sveshnikov, and Petra Tichá</i>	
GROWTH OF DIAMOND FILMS AND CARBON NANOTUBES OVER LARGE AREAS BY LINEAR ANTENNA MICROWAVE PLASMA CVD DEPOSITION . . . . .	33
<i>Alexander Kromka, Oleg Babchenko, Tibor Izak, Marina Davydova, Stepan Potocky, and Bohuslav Rezek</i>	
FIGURE OF MERIT OF (Sb <sub>0,75</sub> Bi <sub>0,25</sub> ) <sub>2-x</sub> In <sub>x</sub> Te <sub>2,8</sub> Se <sub>0,2</sub> SINGLE CRYSTALS . . . . .	35
<i>Vladimír Kucek</i>	
DIELECTRICAL BEHAVIOUR OF CARBON BLACK - POLYMER COMPOSITES PREPARED FROM SOLUTION . . . . .	37
<i>Jan Lipták, Josef Sedláček, Ivana Pilarčíková, and Václav Bouda</i>	
MEASUREMENT OF THE SPECTRAL REFLECTANCE RATIO OF POLARIZED WAVES USED TO THIN-FILM THICKNESS DETERMINATION . . . . .	39
<i>Jiří Luňáček, Petr Hlubina, and Dalibor Ciprian</i>	
ALTERNATIVE METHOD TO THIN-FILM THICKNESS DETERMINATION USING THE SPECTRAL REFLECTANCE MEASUREMENT . . . . .	41
<i>Milena Luňáčková, Jiří Luňáček, Zdeněk Potůček, and Petr Hlubina</i>	
RESIDUAL STRESS OF THIN FILMS OF POLYCRYSTALLINE AND AMORPHOUS SILICON	43
<i>David Lysáček</i>	
INNOVATION OF TEACHING AIDS IN THE SUBJECT "MATERIALS FOR ELECTRO-TECHNOLOGY." . . . .	45
<i>Michal Madaj, Jaromír Drápala, and Miroslav Kursá</i>	

GAMMA AND ALPHA SPECTROSCOPY OF INORGANIC SCINTILLATORS, ESPECIALLY THOSE OF PR <sup>3+</sup> DOPED .....	47
<i>Jiří A. Mareš, Alena Beitlerová, Martin Nikl, Petr Průša, Miroslav Kučera, and Karel Nitsch</i>	
MEASUREMENT METHODS OF MECHANICAL PROPERTIES OF SOLDERS AND SOLDERED JOINTS.....	49
<i>Maroš Martinkovič, Roman Koleňák, and Katarína Pocisková Dimová</i>	
LOW TEMPERATURE HYDROGEN PLASMA TREATMENT OF DIAMOND FILMS BY LINEAR ANTENNA MICROWAVE PECVD SYSTEM .....	51
<i>Neda Neykova, Halyna Kozak, and Alexander Kromka</i>	
EFFICIENCY OF PHYSICAL CHEMISTRY TEACHING IN MATERIAL SUBJECTS .....	53
<i>Ivana Pilarčíková and Ivan Křivý</i>	
PHOTOLUMINESCENCE OF COPPER IONS IN SILICATE GLASS.....	55
<i>Zdeněk Potůček, Stanislava Stará, Zdeněk Bryknar, and Jarmila Špírková</i>	
THERMAL PROPERTIES AND CRYSTALLIZATION KINETICS OF LiY(PO <sub>3</sub> ) <sub>4</sub> GLASS .....	57
<i>Miroslava Rodová, Antonín Cihlář, Robert Král, Alexej Sveshnikov, and Karel Nitsch</i>	
LASER SCRIBING ON SOI WAFER .....	59
<i>Jan Šik and Petr Kostelník</i>	
COMBINED <sup>31</sup> P AND <sup>17</sup> O MAS NMR AND RAMAN STUDIES OF MOLYBDENO-PHOSPHATE GLASSES.....	61
<i>Jiří Šubčík, Ladislav Koudelka, Lionel Montagne, and Gregory Tricot</i>	
NUCLEATION OF PORTLANDITE .....	63
<i>Alexej Sveshnikov, Pavel Demo, Zdeněk Kožíšek, Petra Tichá, and David Ladman</i>	
IMPACT OF CRYSTAL-ORIGINATED DEFECTS ON MANUFACTURING OF ELECTRONIC DEVICES .....	65
<i>Lukáš Válek, Petr Kostelník, and Adam Klimsza</i>	
PD NANOLAYER FOR HYDROGEN SENSOR.....	67
<i>Roman Yatskiy, Karel Zdansky, Jan Grym, and Katka Piksová</i>	



# **ABSTRACTS**



## IMPORTANCE OF USING POLYMER LAYERS FOR SELECTIVE AREA GROWTH OF DIAMOND MICRO- AND NANOSTRUCTURES

O. Babchenko, T. Izak, K. Hruska, M. Ledinsky, B. Rezek, A. Kromka

Institute of Physics AS CR, Cukrovarnicka 10, CZ-16253 Praha 6, Czech Republic

*babchenko@fzu.cz*

Presently, several technological methods known as chemical vapor deposition (CVD) are routinely used to grow diamond thin film on variety of substrates with wide range of properties, i.e. surface morphology, crystallographic quality, chemical purity, crystal size, etc [1, 2]. Any diamond-based micro-electro-opto-mechanical prototype often requires structuring of diamond layer in a specific geometry and/or shape [3]. Dry etching plasma post-growth structuring with implementation of lithographical steps was successfully used in previous works [4-6]. However, the dry etching plasma process is quite complex and it requires a using of “*enough-resistive*” masking material (e.g. SiN<sub>x</sub> or Al<sub>2</sub>O<sub>3</sub>) to achieve process selectivity, i.e. etching of non masked diamond area and non-etching of masking material.

Previously we have shown that the selective area deposition (SAD), i.e. the strategy bottom-up, allowed a direct growth of micrometer sized diamond structures suitable for fabrication of field effect transistors [7, 8] (see Fig. 1 – concept 1).

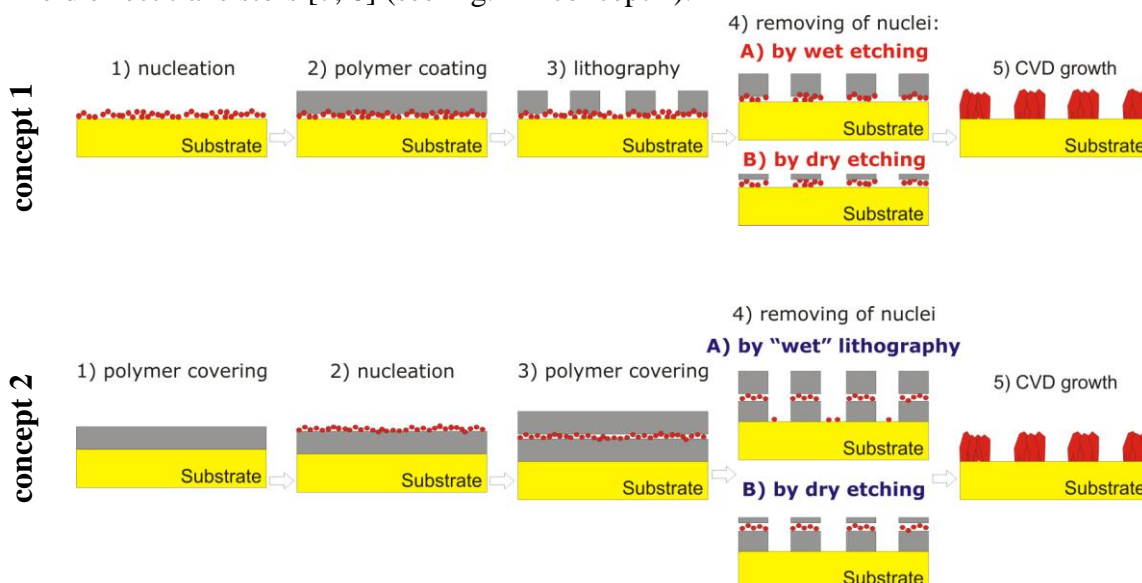


Fig. 1: Schematic drawing of two standard concepts for achieving SAD growth of diamond structures: **concept 1** uses *single* polymer layer used as mask and **concepts 2** uses two polymer layers, one is used as carrier and second as the mask.

The concept 1 used a “single” polymer layer. The seeding (or nucleation) layer was removed from areas outside the photoresist patterns by applying the wet etching procedure. In our case, buffered oxide etchant was used. During this procedure, the *top* surface of treated SiO<sub>2</sub> layer was partially removed.

As alternative to this solution we present the concept 2 where the SAD growth of diamond structures is achieved at minimal (or no) loading of the substrate surface (Fig. 1 – concept 2). This concept implements two photosensitive polymer layers: one used as the carrier and the second as the mask. The primary seeding layer is stacked between them. It should be noted that the growth of patterned diamond structures, either in the concept 1 or concept 2, was provided by microwave plasma enhanced chemical vapor deposition method [9].

Generally, the efficiency of the SAD growth is characterized by so called density of parasitic seeds which are found on the unwished areas after the CVD growth. In this meaning, the grown samples were studied by scanning electron microscopy, Raman spectroscopy and atomic force microscopy.

Figure 2 compares parasitic seed densities for different treatment processes used for achieving the SAD diamond growth. The concept 2 clearly achieves the lowest densities as low as  $10^5 \text{ cm}^{-2}$ .

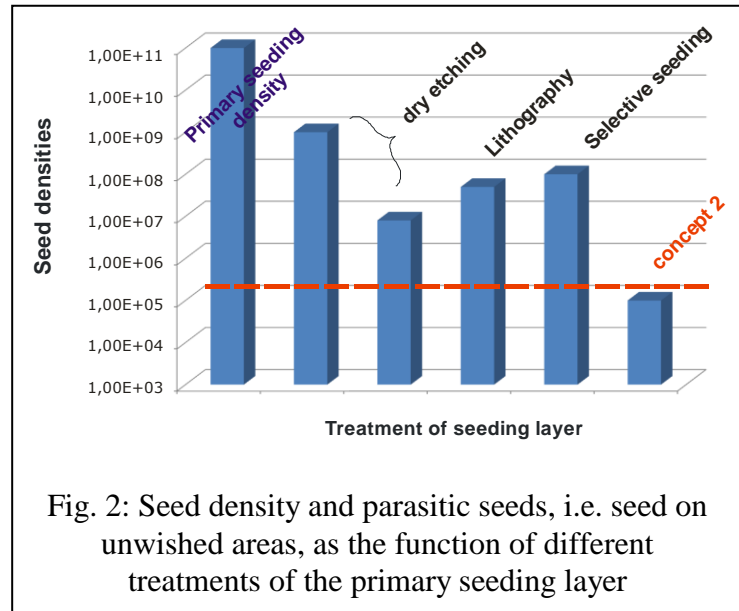


Fig. 2: Seed density and parasitic seeds, i.e. seed on unwished areas, as the function of different treatments of the primary seeding layer

The SAD growth which combines the concept 1 and 2 with EBL will be highlighted as strategy for growth of sub-micrometer sized diamond structures (100-500 nm).

*We acknowledge a financial support by AV0Z10100521, KAN400100701 (ASCR), IAAX00100902 (GAAV), M100100905 (GAAV), IM06002 (MSMT) and by the Fellowship J.E. Purkyne (ASCR). We would like to gratefully appreciate J. Potmesil and O. Rezek for technical assistance and preparation of samples, and K. Hruska for SEM measurements.*

- [1] E. Sevillano, B. Williams, *Diamond Films and Technology* 8/2 (1998) 73.
- [2] J.E. Butler, A.V. Sumant, *Chemical Vapor Deposition* 14/7-8 (2008) 145.
- [3] Y.Q. Fu, H.J. Du, J.M. Miao, *Jour. Mat. Proc. Technol.* 132/1-3 (2003) 73.
- [4] Y.H. Chen, C.T. Hu, I.N. Lin, *Applied Surface Science* 113 (1997) 231.
- [5] K. Hirabayashi, Y. Taniguchi, O. Takamatsu, T. Ikeda, K. Ikoma, N. Iwasakikurihara, *Applied Physics Letters* 53/19 (1988) 1815.
- [6] H.W. Liu, C.X. Wang, C.X. Gao, Y.H. Han, J.F. Luo, G.T. Zou, C. Wen, *Jour. Physics-Condensed Matter* 14/44 (2002) 10973.
- [7] A. Kromka, O. Babchenko, B. Rezek, M. Ledinsky, K. Hruska, J. Potmesil, M. Vanecek, *Thin Solid Films* 518/1 (2009) 343.
- [8] H. Kozak, A. Kromka, O. Babchenko, B. Rezek, *Sensor Letters* 8/3 (2010) 482.
- [9] A. Kromka, B. Rezek, Z. Remes, M. Michalka, M. Ledinsky, J. Zemek, J. Potmesil, M. Vanecek, *Chemical Vapor Deposition* 14/7-8 (2008) 181.

## MATERIAL MODELS FOR NUMERICAL SIMULATION OF MATERIAL FLOW IN THIXOTROPIC STATE

M. Behúlová

Slovak University of Technology in Bratislava, Faculty of Materials Science and Technology  
in Trnava, Paulínska 16, 917 24 Trnava, Slovak Republic

*maria.behulova@stuba.sk*

**1. Introduction.** In the framework of collaborative project of the Research Centre of Forming Technology at the West Bohemia University in Pilsen and the Faculty of Materials Science and Technology in Trnava, the models for numerical simulation and optimization of unconventional materials processing in semi-solid state are developed [1-3]. From the material point of view, the interest is focused on the high-alloyed steels with relatively high solidus and liquidus temperatures with the aim to produce small parts with very fine microstructures and improved material properties. In this paper, the chosen material models directly implemented to the program code ANSYS-Flotran CFD [4] or possible to define through the user subroutine and suitable for the numerical simulation of one-phase material flow in thixotropic state are briefly summarized and discussed. As the developing advanced technology of thixoforming is very fast, the time dependency of material properties can be neglected in this case.

**2. Material models.** The most simplest model describing the material flow is the classical pure Newtonian model (Fig.1a) with a linear relationship between shear rate  $\dot{\gamma}$  and shear stress  $\tau$

$$\tau = \eta \dot{\gamma} \quad (1)$$

with the viscosity  $\eta$  constant or depending on temperature and/or pressure.

Non-linear viscous fluids do not exhibit elastic properties but the relationship between strain rate and stress is nonlinear. Mostly, the Ostwald-de-Waele (Power law) model is applied for modelling the behavior of such fluids [4, 5]. The relationship takes a relatively simple form

$$\tau = K \dot{\gamma}^n \quad (2)$$

with only two parameters, the flow index  $K$  and the shear exponent  $n$ . For material flow in thixotropic state, the both parameters depend on the solid fraction [5, 6]. If the exponent  $n < 1$ , the equation (2) expresses the shear thinning, for  $n > 1$ , it describes the shear thickening (Fig.1b,c). Generally, thixotropic fluids are shear thinning, i. e. they viscosity decreases with increasing in shear rate [5, 6]. On the other hand it is supposed that at very low and very high shear rates, thixotropic materials become Newtonian. This fact can be expressed by the Cross model [7].

$$\eta = \eta_{\infty} + \frac{\eta_0 - \eta_{\infty}}{1 + K \dot{\gamma}^n} \quad (3)$$

where for the  $\dot{\gamma} \rightarrow 0$ ,  $\eta \rightarrow \eta_0$  and for  $\dot{\gamma} \rightarrow \infty$ ,  $\eta \rightarrow \eta_{\infty}$ .

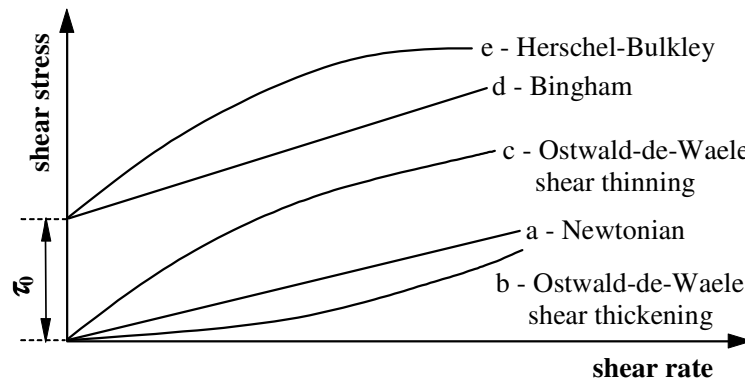


Fig. 1: Flow curves for chosen material models

There is some discussion in the scientific community if the thixotropic alloys display yield. The Bingham material model (Fig. 1d) supposes that the fluid exhibits a yield stress  $\tau_0$  and above this point the relationship between the shear rate and shear stress is linear [4, 7]

$$\tau = \tau_0 + k \dot{\gamma}. \quad (4)$$

The constant  $k$  is related to the viscosity. Some modification of Bingham model represents Herschel-Bulkley model considering a non-linear dependence of the shear stress on the shear rate (Fig. 1e,f)

$$\tau = \tau_0 + k \dot{\gamma}^n \quad (5)$$

**3. Conclusions.** The choice and application of a proper material model for the simulation of material flow in thixotropic state represent the fundamental assumption for the achievement of correct and sufficiently accurate results. Of course, more complex and sophisticated models require definition of higher number of not easily measured parameters.

*This research is supported by the VEGA MŠ SR and SAV within the project 1/0837/08, project 1M06032 Research Centre of Forming Technology and the joint Slovak and Czech Project SK-CZ-0180-09.*

- [1] D. Aišman, H. Jirková and B. Mašek, *Forming Technology of Small Parts in Semi-solid State*. In: Proceedings of the 20th International DAAAM Symposium, 2009, Vol. 20, No. 1, pp. 1895-1896, ISSN 1726-9679, ISBN 978-3-901509-70-4
- [2] B. Mašek, H. Jirková, D. Aišman and P. Hronek, *Thixoforming von Stahl - ein bisher unerforschtes Verfahren mit großem Potenzial*. In: XXIX. Verformungskundliches Kolloquium, Planneralm, Österreich, ISBN 978-3-902078-14-8, März 2010
- [3] H. Jirková, D. Aišman and B. Mašek *Unconventional structure of X210Cr12 steel obtained by thixoforming*. J. of Alloys and Compounds, Available online 3 March 2010.
- [4] ANSYS Theoretical Manual, Release 10.0, SAS IP, Inc., 2005.
- [5] G. Hirt and R. Kopp, *Thixoforming*. WILEY-VCH Verlag GmbH & Co. KGaA, Weinheim, 2009. ISBN 978-3-527-32204.
- [6] H. V. Atkinson, *Modelling of semi-solid processing*. Aachen : Shaker, 2008. ISBN 978-3-8322-7212
- [7] H. V. Atkinson, *Modelling the semisolid processing of metallic alloys*. Progress in Materials Science, Vol. 50, 2005, pp. 341–412

**REGIONAL MATERIALS SCIENCE AND TECHNOLOGY CENTRE  
IN OSTRAVA**

M. Kursa, J. Drápala

Vysoká škola báňská – Technical University of Ostrava, Faculty of Metallurgy and Materials Science, Av. 17. listopadu 15, 708 33 Ostrava – Poruba, Czech Republic

[Miroslav.Kursa@vsb.cz](mailto:Miroslav.Kursa@vsb.cz), [Jaromir.Drapala@vsb.cz](mailto:Jaromir.Drapala@vsb.cz)

New project “Regional Materials Science and Technology Centre (RMTVC)” concerns most importantly the Faculty of Metallurgy and Materials Engineering (FMME). Orientation of research and development of the FMME is in conformity with a long-term concept of the University focused into the following disciplines: metallurgy of metals (ferrous and non-ferrous), chemical metallurgy, materials engineering, forming and heat treatment.

The specific objective of the RMTVC is to build laboratories and teams that will develop, prepare, investigate and optimise advanced materials and technologies of their preparation for the application sphere. The centre will focus on the preparation of highly pure materials, special alloys, bio-medical materials, development of materials for high temperature applications, and power engineering, preparation of materials by advanced powder metallurgy technologies (magnetic materials, friction materials, composite materials, etc.), preparation of nano-crystalline materials based on non-ferrous metals, their alloys and steels prepared by severe plastic deformation, research of processes running in the liquid phase of reactors that affect the utility properties of materials, physical and mathematical modelling of processes materials forming, including forging, and application of the obtained findings in research and development of technology of forming the components for nuclear power engineering equipment. The complexity of technological solutions of material-technological issues will be further deepened by investigation of degradation processes of investigated materials caused by corrosion, high temperatures, stress states and embrittlement due to effects hydrogen, and their impact on the degradation mechanism and safety at operational application. From the material point of view this concerns new advanced materials, but also traditional structural materials, such as steel.

The proposed RMTVC centre will link its activities to the R&D activities of the applicant and its partner – the company Material & Metallurgical Research Ltd. and on the long-term mutual cooperation, the complexity of which in the field of metallurgy and processing of metallic materials will represent a unique working site in the context of the Czech Republic and will contribute significantly to the development of its material base.

The structure of the RMTVC centre was also subordinated to the envisaged outputs into the industrial sphere with a strong application potential. Organisational structure of the centre is divided into five departments:

1. Department of preparation of materials (laboratory of pure metals and laboratory of technology for preparation of special materials).
2. Department of powder technologies (laboratory of magnetic and ceramic materials, laboratory of friction composites).

3. Department of forming processes (laboratory processes of severe plastic deformation, laboratory materials with ultra fine-grained structure prepared by forming, laboratory of modelling and optimisation of the forming technologies).
4. Department of evaluation of materials properties (laboratory of structural analysis, laboratory of mechanical properties, laboratory of chemical analyses, laboratory of surface analysis and corrosion, laboratory of physical properties).
5. Department of experimental verification of technologies and applications (laboratory for experimental verification of technologies for the production of new materials and laboratory of modelling of processes in liquid and solid phases).

On the basis of the existing results of the research and development and in collaboration with potential customers in the application sphere the following research programs were formulated at preparation of the RMTVC project:

1. Development and optimisation of new technologies of highly pure materials, special metallic alloys and inter-metallic compounds with the defined structure and physical properties for applications in electronics, medicine, mechanical engineering and chemical industry.
2. Development and optimisation of processes of powder technologies for production of selected types materials and products
3. Control of specific properties of intensively rolled and thermo-mechanically processed materials by using their structural potential.
4. Research of metallic materials with ultra fine-grained structure (nano-structure), and development of the processes for their preparation
5. New sources of strength and toughness of materials for demanding technological applications.
6. Experimental verification of new technological procedures for metallic materials with high quality parameters.

The Department of preparation of materials consists of the "Laboratory of pure metals" and the "Laboratory of special materials". The focus of research and development activities of the "Laboratory of pure metals" is concentrated on the following key issues: Investigation of processes of refining metallic materials, preparation of single crystals and defined materials, determination of the origin and distribution of admixtures in the crystal and investigation of the physical-chemical properties of highly pure substances and of regularities of changes of their properties in dependence on their chemical composition, concentration of admixtures, crystalline defects and structural parameters. The project aims to build a research infrastructure of the laboratories of the Department of preparation of materials, as well as scientific-research teams that will develop, prepare and optimise the properties of advanced materials and technologies of their preparation for the application sphere.

*This work was supported by the Ministry of Education, Youth and Sports, Czech Republic, the project of OP VaVPI "Regional Materials Science and Technology Centre (RMTVC)" No. CZ.1.05/2.1.00/01.0040.*

## **DETERMINATION OF THE MEAN VALUE OF CRYSTAL GRAIN SIZE BY X-RAY DIFFRACTION SPOT COUNTING**

J. Galle<sup>(a)</sup>, N. Ganev<sup>(a)</sup>, Z. Pala<sup>(a)</sup>, K. Kolařík<sup>(a)</sup>,

(a) Czech Technical University in Prague, Faculty of Nuclear Sciences and Physical Engineering, Břehová 7, 115 19 Prague 1, Czech Republic

*j.galle@seznam.cz*

The mean value of crystal grain size and distribution of crystal grains size is one of the basic characteristics of polycrystalline materials. These quantities significantly influence mechanical, electrical and thermal properties. Very quick and accurate determination of both quantities allows the method of diffraction spots counting. This experimental technique is applicable to the materials with grain size between 1 – 100  $\mu\text{m}$ . The advantage of this method is very quick result assessment, because the method does not demand time consuming surface adjustment contrary to the standard optical and electron microscopy methods. Moreover, the specimen is not damaged during the surface adjustment. By means of the X-ray diffraction spots counting it is also possible to observe occurrence of the subgrains and the grains with small angle boundary which are not distinguishable by optical methods [2].

The main object of the experiments was determination of the real polycrystalline structure of precious metals sputtering targets by counting the X-ray diffraction spots and comparison with classical optical methods based on the scratch pattern.

Bragg diffraction occurs when X-ray radiation with wavelength  $\lambda$  comparable to atomic spacing impinges upon a crystalline sample. The waves are scattered by lattice planes having the interplanar distance  $d$ . The path difference between the two waves undergoing constructive interference is given by  $2d\sin\theta$ , where  $\theta$  is the scattering angle. Constructively interfering waves remain in phase since the path length of each wave is equal to an integer  $n$  multiple of the wavelength. This leads to Bragg's law  $2d\sin\theta=n\lambda$ , which describes the condition for constructive interference from successive crystallographic planes ( $hkl$ ) of the crystalline lattice [1].

If a monochromatic beam of X-ray radiation wide about 1 mm falls to a polycrystalline specimen with small grains, then many grains inside the irradiated volume diffract. Each grain diffracts the radiation in defined angle  $\theta$  independently of the other grains. Then the grain works as mirror, which reflects X-ray radiation. But the grains are variously oriented in respect to the direction of incident X-ray beam. It creates continuous diffraction ring. If the crystal grains are bigger than approximately 1  $\mu\text{m}$ , then continuous diffraction ring splits into separate spots. The number of diffraction spots is in a direct relation to the number of crystal grains inside the irradiated volume of the sample [1].

The diffraction pattern is recorded by 2D detector, namely imaging plate. The use of the imaging plate enables exposition time shortening and manipulation simplification compared with classical photographic film. Next advantage of the imaging plate is linear time dependence of blackening, which significantly simplifies procedure of data evaluation. The imaging plate consists of polymer board, which is coated with thin luminophore layer. When the X-ray photon fall to the luminophore, then one electron is released from  $\text{Eu}^{2+}$  ion

engaged in the material. These electrons are captured in vacancies where creates optical F-centres. The information about X-ray photon is consequently obtained by means of F-centre excitation through He-Ne laser irradiation. Finally the information is deleted from imaging plate through UV irradiation, when electrons are released form F-centres and consequently captured on  $\text{Eu}^{3+}$  ions.

The diffraction pattern is transferred from imaging plate to computers through a scanner. Image processing of diffraction patterns is performed using programme *Lucia*. This software enables automatic diffraction spots counting and simulation of various expositions. The diffraction pattern is processed like monochrome picture and a numeric value is assigned to ever pixel. This number determines value of pixel blackening. If pixels of given spot have higher value of blackening as threshold, than this spot is counted. Via change of threshold it is possible to simulate various exposure times from one picture. Time dependence of number of diffraction spots is needed for determination of crystal grains size distribution function.

Stephen-Barnes method [3] is used for mean value grain size determination. This method needs two expositions. Difference between darkening of spots on one picture is caused by difference in depth of irradiated volume in the sample. If the sample is exposed for time  $t_1$ , then we count  $M_1$  spots, which are caused by grains in depth  $d < d_1$ . When the sample is exposed for time  $t_2 > t_1$ , then we count  $M_2$  spots, which are caused by grains in depth  $d < d_2$ . Difference  $M_2 - M_1$  represents the number of all spots caused by grains from layer  $t = d_2 - d_1$ . Layer  $t$  is the thickness of irradiated volume. The mean value of grain size is given by the equation:

$$v = \frac{j\alpha Stg(\pi - 2\theta)\ln(T_1/T_2)}{2\mu(M_2 - M_1)(1 - \sec 2\theta)}$$

where  $j$  is number of equivalent  $hkl$  planes,  $\alpha$  is divergent angle,  $\theta$  is diffraction angle, and  $\mu$  is linear absorption coefficient.

*The research was supported by the MSM 6840770021 research project of the Ministry of Education, Youth and Sports of the Czech Republic and by the CTU project SGS 10-803000.*

- [1] I. Kraus, *Úvod do strukturní rentgenografie*, Academia, Prague (1985).
- [2] S. A. Saltykov, *Stereometrická krystalografie*, SNTL, Prague (1962).
- [3] R. A. Stephen, R. I. Barness,.: *J. Inst. Metals*, 60 (1937) 285.

## **DIFFRACTION ANALYSIS OF RESIDUAL STRESSES IN THIN SURFACE LAYERS OF POLYCRYSTALLINE MATERIALS**

N. Ganev<sup>(a)</sup>, Z. Pala<sup>(a)</sup>, K. Kolařík<sup>(a)</sup>

(a) Czech Technical University in Prague, Faculty of Nuclear Sciences and Physical Engineering, Břehová 7, 115 19 Prague 1, Czech Republic

*nikolaj.ganev@fjfi.cvut.cz*

Recently we have been witnessing a growth of interest in the surface qualities of solids. However, this fact is not surprising, when we become aware of the fact that any interaction with material is being realized over its free surface. Surface layers can influence in a decisive way the employment on the whole volume of material.

Residual stresses on the surface of polycrystalline materials and beneath it belong among the most important parameters of surface quality. Under elastic-plastic deformation, individual crystallites are differently deformed and this gives rise to microscopic internal stresses, which are accompanied by macroscopic stresses [1, 2]. It has been shown [3] that, in general, compressive residual stresses in the material can favourably reinforce the dynamic strength by about 50%; on the other hand, tensile RSs could reduce the dynamic strength by about 30%.

Stress measurement, especially that of residual stresses, represents one of the most wide-spread and technically important applications of X-ray diffraction. In Czech Countries this area of experimental physics has almost reached a 70 year old tradition. X-ray diffraction laboratory of the Czech technical university in Prague has the reputation for being the leading workplace for X-ray diffraction tensometry in the Czech Republic. During the last decade, the laboratory participated on numerous projects and grants. Following examples of solved problems illustrate the experience of the laboratory team with applications of X-ray stress measurements in materials science and mechanical engineering.

### **State of residual stress in surface layers of shot-peened steels**

Shot peening process consists of the controlled bombardment of the metal surface by spherical shot including steel shot, steel and stainless steel pieces of wire, ceramic or glass beads [4]. The treatment causes plastic flow of the surface layers, thereby inducing surface compressive stresses, change of microstructure and may cause phase transformation in the surface layers.

When the beneficial effect of imposed compressive residual stresses by shot peening is evaluated, usually only depth distribution of macroscopic (first kind) ones is taken into account. The unique ability of X-ray diffraction methods to determine both the macroscopic residual stress and mean value of micro-strain and crystalline size in the irradiated volume is not commonly applied for complete characterization of the degree of plastic deformation.

The set of analysed samples prepared from five steels was shot-peened by using two different intensities of blasting. The  $\sin^2\psi$  method was used for determination of

macroscopic residual stresses [2]. The single line Voigt function method was applied for determination of microstrains and crystallite size.

Results of experiments imply that relationships between macroscopic and microscopic stresses are independent on intensity of blasting for the particular material. Depth profiles of both types of stresses are similar for all five investigated steels. Parameters of the shot peening process have only a little effect on the magnitude of the compressive macrostress induced which is primarily a function of the mechanical properties of the material. Subsurface depth of these stresses depends on intensity of the process.

### **Surface properties of tool steel after electro-discharge machining**

Electro-discharge machining (EDM) belongs to chip-less unconventional working methods most widely used in the case of materials hardly workable by classical machining technologies. It is based on eroding and removing material from electrically conductive materials by use of consecutive electric sparks.

The experimental samples were made from Böhler W300 ferritic – perlitic steel which is widely used in die - sinking industries. One half of the samples was left in basic state, the other was tempered onto hardness 53 - 54 HRC. Two modes of machining, i.e. finishing and roughing were used. Residual stresses were determined by X-ray diffraction, Barkhausen noise and layer removal method. Phase composition of cut area was evaluated as well.

Phase analyses of samples machined by roughing mode exhibit similar phase composition in surface layer and are distinguished by higher content of gamma iron in comparison to finishing mode. The white layer appears consistent after etching and dendritic structure can be seen.

According to X-ray residual stress analysis, EDM generates tensile residual stresses (RS), which increase in value from the surface till the depth where they reach a maximum. This maximum value is around the ultimate tensile strength of the material. Lower values of RS on the surface compared to the maximum in the depth distribution are related to crack formation since the RS exceed the fracture strength of the material. The further decrease of RS from the point of maximum is due to the condition of mechanical balance between plastically deformed surface and elastically deformed bulk.

*The research was partly supported by the Project No 101/09/0702 of the Czech Science Foundation and by the Project MSM 6840770021 of the Ministry of Education, Youth and Sports of the Czech Republic.*

- [1] V. Hauk et. al.: Structural and Residual Stress Analysis by Nondestructive Methods, Elsevier, 1997.
- [2] I. Kraus, N. Ganev: Residual Stress and Stress Gradients, in: Industrial Applications of X-ray Diffraction, Marcel Dekker, New York, 2000, pp. 793–811.
- [3] A. G. Youtsos: Residual Stress and its Effect on Fracture and Fatigue, Springer, 2006.
- [4] J. Drahokoupil, N. Ganev, M. Čerňanský, P. Boháč, M. Stranyánek, R. Čtvrtlík: Stress and Hardness in Surface Layers of Shot-peened Steels. Z. Kristallogr. Supl. 27 (2008) pp. 89 – 96.

## CHALLENGES IN THE PREPARATION AND APPLICATION OF POROUS III-V SEMICONDUCTORS

J. Grym<sup>(a)</sup>, D. Nohavica<sup>(a,b)</sup>

(a) Institute of Photonics and Electronics ASCR, Chaberska 57, 182 51 Praha 8, Czech Rep.

(b) Institute of Physics ASCR, Cukrovarnická 10, 162 00 Praha 6, Czech Rep.

*grym@ufe.cz*

The emission of visible light from microporous Si has attracted an increasing interest in the investigation of porous semiconductors [1, 2]. Increasing number of papers is devoted to A<sup>III</sup>B<sup>V</sup> semiconductors mainly due to the significant changes of their optical properties, such as the photoluminescence intensity enhancement and the existence of the emission at above band gap energies, which can be explained by quantum size effects in nanocrystalline structures [3, 4]. Moreover, A<sup>III</sup>B<sup>V</sup> porous materials show new and engaging properties compared to porous silicon, such as pore morphology and pore propagation in bulk material [5-7]. Pore formation in A<sup>III</sup>B<sup>V</sup> materials has been reported in a number of recent papers; for a review, see [8-10]. On the contrary, the heat treatment of micropores and their technological applications have not been thoroughly investigated yet.

Epitaxial growth has always been a marriage of convenience between deposited layer and substrate. In the simplest case, both layer and substrate are of the same material, providing a perfect homoepitaxial match. Frequently, it is impractical to use the same material for both the layer and the substrate since certain large single crystals are not available, are immensely expensive, or their properties are inappropriate for the intended application. Many strategies have been suggested to achieve single-crystal thin films via epitaxy. Crystalline films are mechanically bonded to other materials to form composite substrates; crystals have been cut and rewelded, patterned and regrown, buffer layered and repolished [11]. Significant development in defect density reduction in semiconductor materials has been accomplished using epitaxial lateral overgrowth techniques [12]. Recently, semiconductor epitaxial growth has progressed to pseudomorphic, lattice mismatched systems where a small amount of strain is accommodated in very thin layers [13].

A new approach extending the critical layer thickness in highly mismatched heterostructures is nanoheteroepitaxy [14]. Nanoheteroepitaxy exploits the three-dimensional stress relief mechanisms that are available in nanoscale objects and applies this property to reduce the strain energy in lattice mismatched heterojunctions. While in conventional planar structures the epilayer can only deform vertically, in a nanopatterned substrate a selectively growing epilayer can deform vertically and laterally, and the strain energy decreases exponentially with the distance from the growth interface [15]. If the maximum strain energy is below the energy of dislocation formation, an epilayer with no mismatch defects of infinite thickness can be grown.

In this paper we report on the preparation of micropores in A<sup>III</sup>B<sup>V</sup>, their modification by the heat treatment and epitaxial overgrowth using the nanoheteroepitaxial approach. Both current-line oriented (CLO) and crystallographically oriented (CO) pores anodized at the substrate surface are transformed into microcavities and microlamellas. The transformation

takes place during the heat treatment of InP pores under phosphorus vapor and during the liquid phase epitaxy (LPE) overgrowth of porous InP and GaAs by InP, InAs, and InGaAs. The transformation process is described by the mass transport leading to lower energy state. Porous substrates may find applications in heteroepitaxial growth since the resulting structures exhibit quite improved properties without the requirement of any graded transition layers or significantly extended nucleation barriers during growth. Furthermore, a detailed investigation of the pore interaction with strain fields and structural defects existing in these materials is of tremendous interest [16].

*This work was supported by the Czech Science Foundation Grant P108/10/0253.*

- [1] Canham, L.T., *Silicon quantum wire array fabrication by electrochemical and chemical dissolution of wafers*. Applied Physics Letters, 1990. **57**(10): p. 1046-1048.
- [2] Lehmann, V. and U. Gosele, *Porous silicon formation: A quantum wire effect*. Applied Physics Letters, 1991. **58**(8): p. 856-858.
- [3] Anedda, A., et al., *Time resolved blue and ultraviolet photoluminescence in porous GaP*. Applied Physics Letters, 1995. **67**(22): p. 3316-3318.
- [4] Schmuki, P., et al., *Formation of visible light emitting porous GaAs micropatterns*. Applied Physics Letters, 1998. **72**(9): p. 1039-1041.
- [5] Delimitis, A., et al., *Controlled growth of porous networks in phosphide semiconductors*. Journal of Porous Materials, 2008. **15**(1): p. 75-81.
- [6] Föll, H., et al., *Engineering porous III-Vs*. III-Vs Review, 2003. **16**(7): p. 42-43.
- [7] Föll, H., et al., *How to make single small holes with large aspect ratios*. Physica Status Solidi - Rapid Research Letters, 2009. **3**(2-3): p. 55-57.
- [8] Föll, H., et al., *Pores in III-V Semiconductors*. Advanced Materials, 2003. **15**(3): p. 183-198.
- [9] Ulin, V. and S. Konnikov, *Electrochemical pore formation mechanism in III-V crystals (Part I)*. Semiconductors, 2007. **41**(7): p. 832-844.
- [10] Ulin, V. and S. Konnikov, *Electrochemical pore formation mechanism in III-V crystals (Part II)*. Semiconductors, 2007. **41**(7): p. 845-854.
- [11] *Substrate Engineering—Paving the Way to Epitaxy*. in *MRS Fall Meeting, Symposium O*. 1999: Materials Research Society.
- [12] Nishinaga, T., *Microchannel epitaxy: an overview*. Journal of Crystal Growth, 2002. **237-239**(Part 2): p. 1410-1417.
- [13] Atkinson, A., S.C. Jain, and A.H. Harker, *Strain, dislocations, and critical dimensions of laterally small lattice-mismatched semiconductor layers*. Journal of Applied Physics, 1995. **77**(5): p. 1907-1913.
- [14] Zubia, D. and S.D. Hersee, *Nanoheteroepitaxy: The Application of nanostructuring and substrate compliance to the heteroepitaxy of mismatched semiconductor materials*. Journal of Applied Physics, 1999. **85**(9): p. 6492-6496.
- [15] Luryi, S. and E. Suhir, *New approach to the high quality epitaxial growth of lattice-mismatched materials*. Applied Physics Letters, 1986. **49**(3): p. 140-142.
- [16] Sitnikova, A.A., et al., *Specific features of epitaxial-film formation on porous III-V substrates*. Semiconductors, 2005. **39**: p. 523-527.

**INFLUENCE OF Sc<sup>3+</sup> DOPING ON Pr<sup>3+</sup> EMISSION IN EPITAXIAL SCINTILLATION GARNET LAYERS**

M. Hanuš<sup>(a)</sup>, M. Kučera<sup>(a)</sup>, M. Nikl<sup>(b)</sup>, K. Nitsch<sup>(b)</sup>, P. Průša<sup>(b)</sup>, J. A. Mareš<sup>(b)</sup>,  
Z. Onderišinová<sup>(a)</sup>

(a) Charles University, Faculty of Mathematics and Physics, Ke Karlovu 5, 121 16, Prague, Czech Republic

(b) Institute of Physics v.v.i., AS CR, Cukrovarnická 10, 160 00, Prague, Czech Republic  
*hanus@karlov.mff.cuni.cz*

Yttrium (Y<sub>3</sub>Al<sub>5</sub>O<sub>12</sub>) and lutetium (Lu<sub>3</sub>Al<sub>5</sub>O<sub>12</sub>) aluminium garnets doped by rare earths such as Ce, Eu, Pr, are considered as very good scintillation materials. The garnets have chemical, mechanical, and radiation stability superior to most of scintillation materials and light yield is high, thus they are often used as scintillation screens [1]. For higher resolution in 2D imaging, it is necessary to use screens as thin as possible. To obtain such screens from a single crystal is complicated. By means of liquid phase epitaxy (LPE) we are able to produce such thin layers easily. Compared to Czochralski grown single crystals, the epitaxial layers can be prepared from a flux at much lower growth temperatures. As a result, there is lower structural disorder and lower concentration of defects in layers.

This work was motivated by endeavour to prepare Pr and Sc co-doped LuAG epitaxial layers and to determine their optimal concentrations for maximal conversion efficiency. The epitaxial garnet layers were grown by the isothermal dipping LPE from BaO-BaF<sub>2</sub>-B<sub>2</sub>O<sub>3</sub> flux. We used both YAG and LuAG substrates. The layers were characterized by optical absorption, photoluminescence, radioluminescence (RL), and by scintillation response using the alpha particles.

We prepared over 40 samples with various concentrations of Pr and Sc. Characteristic peaks of allowed 4f-5d transitions of Pr<sup>3+</sup> ions are at 240 and 282 nm in absorption spectra and corresponding 5d-4f emission is observed in the UV range between 290 and 420 nm. The intensity of Sc<sup>3+</sup>-related peak near 280 nm in the RL spectra diminishes while the Pr<sup>3+</sup>-related peak at 308 nm increases with increasing Sc concentration in layers. Likewise the integral RL intensity increases with growing Sc concentration in layers, Fig. 1. This shows on energy transfer from Sc<sup>3+</sup> to Pr<sup>3+</sup> ions. Measured photoelectron yield after irradiation by alpha particles produced by <sup>239</sup>Pu (5.16 MeV) is higher than in single crystals only for small concentrations of Sc and Pr. Furthermore, we observed lower fraction of slower components in the photoelectron yield and a bit better spectral resolution in epitaxial layers compared to single crystal counterparts. The photoelectron yield has its maximum for Sc concentration at 2.4 % but it decreases with increasing concentration of Sc, Fig. 2.

Despite very good emission properties, layers grown from the BaO flux have sometimes worse surface morphology. A fundamental problem of the BaO flux is complicated growth due to very high viscosity and surface tension of the BaO melt. The remaining melt tend to damage both layer and substrate after cooling down.

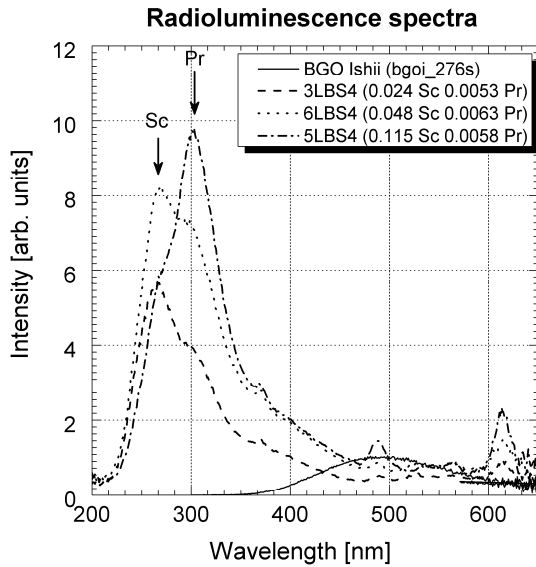


Fig. 1: Radioluminescence spectra of samples with nearly same Pr concentration and increasing Sc concentration (2.4, 4.8, and 11.5 %, respectively). The RL of BGO single crystal is shown for comparison.

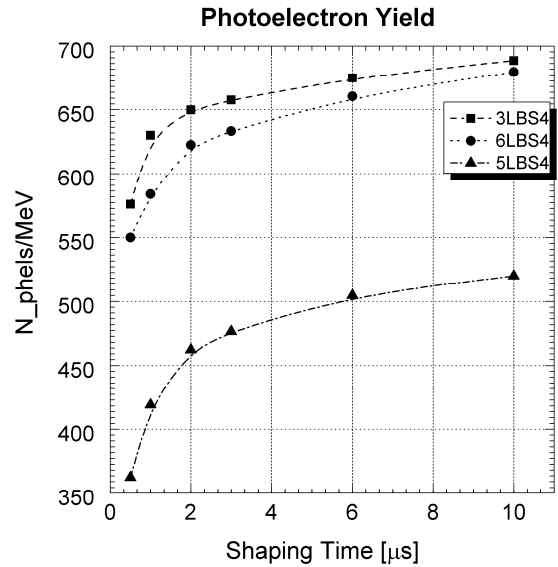


Fig. 2: Time dependence of photoelectron yield,  $N_{\text{phels}}$ , under  $\alpha$ -particle excitation in the range 0.5 – 10  $\mu\text{s}$  shaping times for the same samples as in Fig. 1

[1] J. Tous, K. Blazek, L. Pina, B. Sopko, Rad. Meas. 42 (2007) 925.

*Acknowledgments:*

*This work was supported from the Grant Agency AS CR, grant KAN 300100802, and from the Ministry of Education CR, research plan MSM0021620834. The work was also supported by the grant SVV-2010-261306.*

## **USING OF SELF-ASSEMBLED GOLD NANO-SIZED DROPLETS FOR FABRICATION OF VERTICALLY ALIGNED DIAMOND NANORODS**

T. Izak<sup>(a)</sup>, O. Babchenko<sup>(a)</sup>, A. Kromka<sup>(a)</sup>, K. Hruska<sup>(a)</sup>, M. Michalka<sup>(b)</sup>

(a) Institute of Physics AS CR, Cukrovarnicka 10, CZ-16253 Praha 6, Czech Republic

(b) International Laser Centre, Ilkovicova 3, SK-84104 Bratislava, Slovak Republic

*izak@fzu.cz*

Diamond is a multifunctional semiconductor material with wide interdisciplinary applications in biochemistry, biophysics, pharmacy and regenerative medicine. Recently, one of the highest interests in diamond field is related to the various biomedical [2,3] and chemical sensor applications [1], [4] For commercial application it is necessary to have reliable sensors and devices with high sensitivity, selectivity and reproducibility. One possibility to improve sensor detection properties is enlarging of the surface area by its nanostructuring or shaping. Using of nanopillars or nanocones resulted in improved sensitivity of diamond-based biomedical and chemical sensors. [1,5]

In this study we focus on plasma assisted thermal formation of nano-sized gold droplets from thin gold layer and using of such droplets for fabrication of vertically aligned diamond nanorods by dry etching plasma process (process known as top-down strategy).

First, nanocrystalline diamond thin films (NCD) were deposited on Si substrates by microwave plasma chemical vapour deposition (system Aixtron P6). Then, Au thin films with different thickness from 2.8 nm to 15.2 nm were thermally evaporated on the NCD films. Samples covered with gold layer were treated in microwave hydrogen plasma to form nano-sized gold droplets. The treatment conditions were following: temperature 500°C, power 1300 W, pressure 30 mbar, H<sub>2</sub> flow rate 300 sccm and process time 10 min. Etching of diamond films was performed by standard capacitively coupled plasma reactive ion etching (CCP-RIE) technique (Phantom III, Trion Technology). The etching parameters were following: pressure 90 mtorr, power 300 W, gas composition 40% O<sub>2</sub> in CF<sub>4</sub>, etching time 10 min. After the etching of diamond the gold mask was removed by wet etching using solution HNO<sub>3</sub>: HCl (1:3) for 5-10 min. The surface morphology of samples was characterized by Scanning Electron Microscopy (SEM).

We found that the hydrogen plasma treatment resulted in formation of gold droplets (or islands) whereas their size (or diameter) strongly depended on the primary gold thickness (Fig. 1a).

The 2.8nm thick Au layer formed round droplets with diameter from 10 to 20 nm. Increasing of Au thickness enlarged the size of formed droplets and their shape also changed. Treatment of 15.2 nm thick Au layer led in a formation of large droplets in diameter from 160 to 200 nm. Some droplets reveal ellipsoidal like geometry.

The origin of droplet formation is complex process where de-wetting of metal atoms, their surface migration, and clustering in droplets (islands) takes a place. In our case, surface reaction of carbon with gold are minimized due to chemical non-reactivity. However, the presence of hydrogen can significantly influence the surface migration i) through local overheating during production of hydrogen molecules (H<sub>2</sub>) from atomic

hydrogen, ii), due to surface potential of hydrogen terminated diamond which is known as strongly hydrophobic.

Formed gold nano-sized droplets were used as the masking material during reactive ion plasma etching. Using droplets of different size allowed a wide variability of surface structuring. Figure 1b shows SEM images of diamond structures after applying the plasma etching. It is important to note that rest of Au mask was removed by wet chemical etching before SEM measurements. We fabricated narrow and sharp diamond nanorods with varied filling factor (i.e. area of nanorods to the not-filled area). The filling factor varied due to variation of the droplet size and their density over the diamond surface.

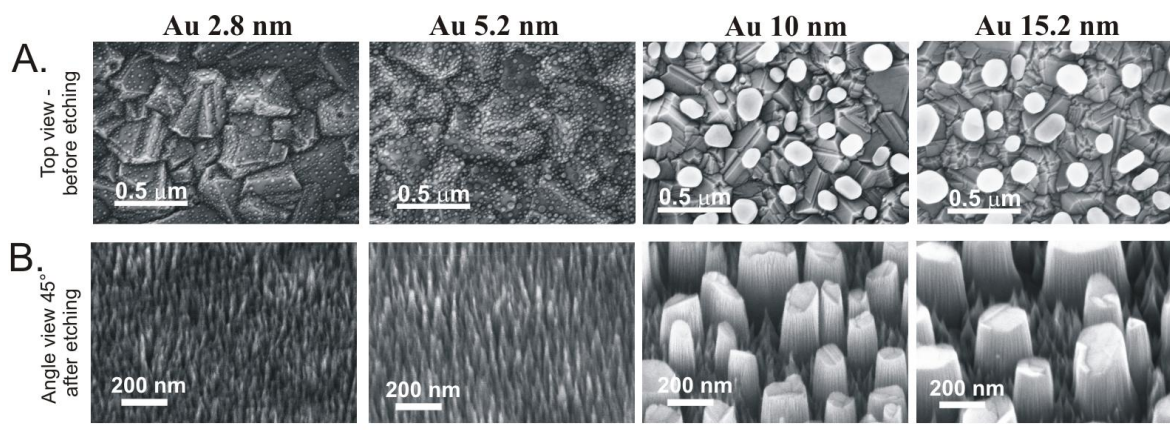


Fig. 1: SEM images of NCD surfaces with Au droplets for different thickness of gold layer after plasma annealing and before etching (A), and corresponding SEM images of structured diamond layer after the plasma etching (B).

This study show that implementation of self-assembled gold droplets as masking material for reactive ion etching treatment is useful, fast and cheap technological method for fabrication of vertically aligned diamond nanostructures (nanorods) suitable for fabrication of bio- and chemical-sensor devices, optical components or for fabrication of artificial substrates suitable well tuned for tissue engineering. Complementary study on nickel droplet formation will be discussed too.

*This work was supported by the Institutional Research Plan No. AV0Z10200521, by the projects No. IAAX00100902, KAN400100701, KAN400480701, M100100905 and by the Fellowships J. E. Purkyne.*

- [1] M. Davydova, A. Kromka, P. Exnar, M. Stuchlik, K. Hruska, M. Vanecek, M. Kalbac, *Phys. Stat. Sol. A* 206 (2009) 2070.
- [2] B. Rezek, L. Michalíková, E. Ukraintsev, A. Kromka, M. Kalbacova, *Sensors* 9 (2009) 3549.
- [3] H. Kozak, Z. Remeš, A. Kromka, M. Vaněček, *Hasselt Diamond Workshop 2009, SBDD XIV* (2009), p.97, March 2-4, Belgium
- [4] A. Kromka, M. Davydova, B. Rezek, M. Vanecek, M. Stuchlik, P. Exnar, M. Kalbac, *Diam. Rel. Mater.* 19 (2010) 196.
- [5] Y.S. Zou, Y. Yang, W. J. Zhang, Y. M. Chong, B. He, I. Bello, S.T. Lee, *Appl. Phys. Lett.* 92 (2008) 053105.

**CRYSTAL STRUCTURES OF Cu(II) COMPLEXES WITH PYRIDYLMETHANOLS**

M. Koman, J. Maroszová, J. Moncol', D. Mikloš

Department of Inorganic Chemistry, Slovak Technical University, Radlinského 9,  
812 37 Bratislava, Slovakia  
*marian.koman@stuba.sk*

One of the key areas of theory and applications of coordination chemistry is purposeful preparation, studying structure, chemical reactivity and biological activity of compounds, alone or as ligands in coordination compounds the use of which is promising in human and veterinary medicine and environment. In particular, structure research for the carboxylate copper and iron complexes with biologically active ligands has been performed [1]. Biological tests were carried out on selected bacteria, fungi and mushrooms (Staphylococcus aureus, Escherichia coli, Candida albicans, Candida parapsilosis, Rhizopus oryzae, Alternaria alternata, Botrytis cinerea, Microsporus gypseum). We found a series of relationships and correlations [2,3]. Results of biological tests have shown relationships between some physico-chemical properties and biological activity. This knowledge allows systematic approach to synthesis of new compounds with presumed physico-chemical and biological characteristics. Over the past ten years around 600 new carboxylate Cu(II) complexes with biologically active ligands have been prepared from this group of

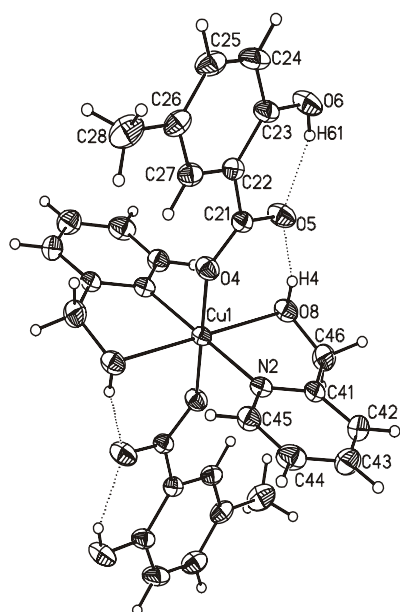


Fig. 1 The molecular structure of  $[\text{Cu}(5\text{-Mesal})_2(2\text{-mepy})_2]$

substances. For tens of compounds, of which single crystals have been prepared, their crystal and molecular structures were solved. Despite the number of experimental materials obtained in the different groups of complexes, there are different structural deviations, which do not correspond to the above trend. These variations are demonstrated with the structures of the Cu(II) complexes with 2-pyridylmethanol, 3-pyridylmethanol, 4-pyridylmethanol (2-, 3- and 4 - mepy).

With 2-pyridylmethanol preferential involvement of the chelating ligand in the coordination sphere of Cu(II) has been confirmed (Fig. 1). In the group with 3-pyridylmethanol complexes were confirmed priority bridge engaging 3-mepy in the coordination sphere. There were observed two types of coordination polymers, one-dimensional (1-D) chain and two-dimensional (2-D) network (Fig. 2). However, besides the presumed polymer composition  $[\text{Cu}(\text{RCOO})_2(3\text{-mepy})_2]_n$  the aqua monomer complex  $[\text{Cu}(3\text{-CH}_3\text{sal})_2(3\text{-mepy})_2(\text{H}_2\text{O})] \cdot \text{H}_2\text{O}$  was

prepared and characterized. Previous study of the relatively small group studied of the Cu(II) complexes with 4-pyridylmethanol has shown preferential involvement of the terminal 4-mepy in the coordination sphere of Cu(II).

### Development of Materials Science in Research and Education

Despite this fact complex  $[\text{Cu}_2(3,5\text{-}(\text{NO}_2)_2\text{bz})_4(\mu\text{-4-mepy})_2(4\text{-mepy})_2]\cdot 2\text{H}_2\text{O}$  has been prepared, where 4-mepy occurs as a bridge as well as terminal ligand and complex  $[\text{Cu}(3\text{-}(\text{NO}_2)\text{bz})_2(\mu\text{-4-mepy})_2]_n$  is polymeric (Fig. 3). These deviations from the trend may be due to strong inter- and intra-molecular hydrogen bonds of type O-H...O which create one-dimensional supramolecular chains or two-dimensional supramolecular networks that have a dominant effect on the stabilization of the molecular structures.

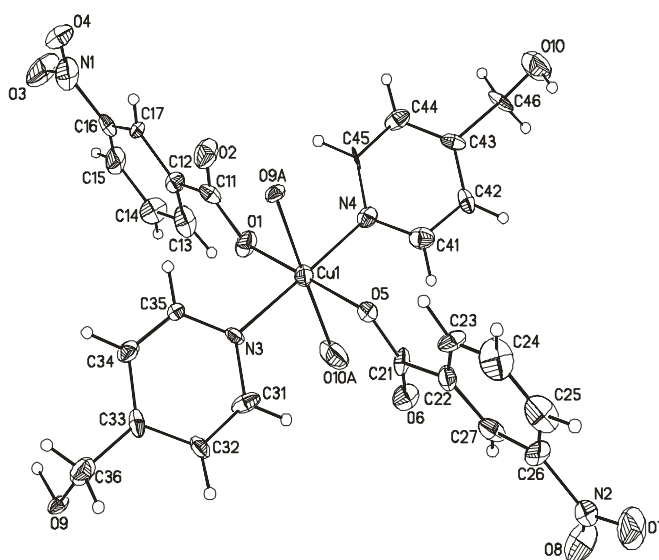
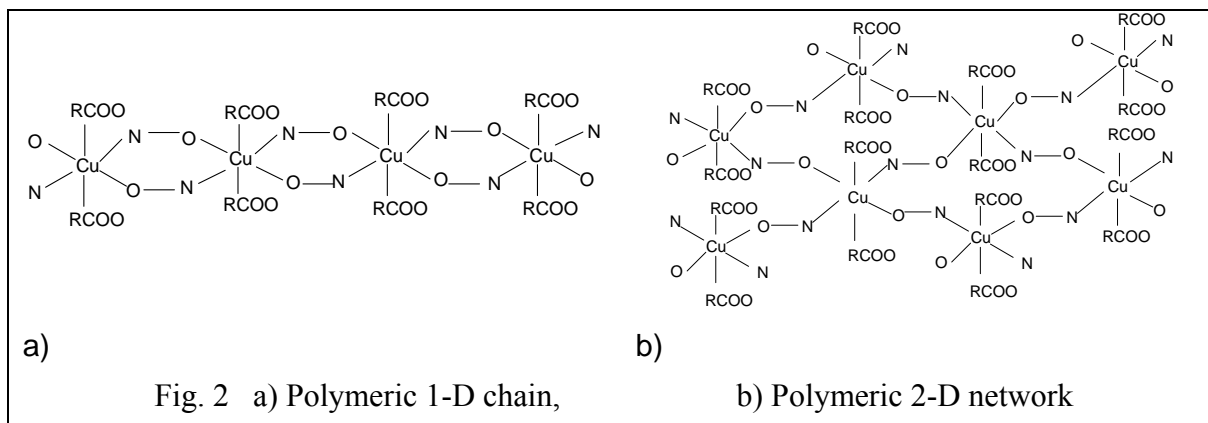


Fig. 3 The molecular structure of  $[\text{Cu}(3\text{-}(\text{NO}_2)\text{bz})_2(\mu\text{-4-mepy})_2]_n$

This work was supported by Slovak Ministry of Education (VEGA project 1/0562/10).

- [1] D. Valigura, M. Melník, M. Koman, L. Martiška, M. Korabik, J. Mrozinski, and T. Glowiak: *Inorg. Chem. Comm.* **7**(2004)548.
- [2] M. Koman, J. Moncol', D. Hudecová, B. Dudová, M. Melník, M. Korabik, and J. Mrozinski: *Polish J. Chem.* **75**(2001)975.
- [3] M. Koman, J. Moncol', V. Kuchtanin, M. Melník: *XXII. International Conference on Coordination and Bioinorganic Chemistry, Smolenice, 8 – 12 June, 2009*, Press of Slovak University of Technology (2009)141.

**COBALT-BASED FERROMAGNETIC SHAPE MEMORY ALLOYS -  
PREPARATION, CHARACTERIZATION AND FUNCTIONAL PROPERTIES**

J.Kopeček<sup>(a)</sup>, M. Jarošová<sup>(b)</sup>, K. Jurek<sup>(b)</sup>, J. Drahoukoupil<sup>(a)</sup>, D. Majtás<sup>(a)</sup>, S. Ignácová-Sedláková<sup>(a)</sup>, O. Heczko<sup>(a)</sup>

(a) Institute of Physics AS CR, Na Slovance 2, 182 21 Prague 8, Czech Republic

(b) Institute of Physics AS CR, Cukrovarnická 10, 162 00 Prague 6, Czech Republic

*kopecek@fzu.cz*

The cobalt-based shape memory alloys (SMA) are expected to be the new kind of so-called ferromagnetic SMAs [1]; this means alloys, in which the driving force for the martensitic phase transformation (direct or reverse) or martensitic variants reorientation can be the external magnetic field. This effect was described in stoichiometric compound Ni<sub>2</sub>MnGa [2]. The mechanical properties of Co-Ni-Al alloys are definitely better than the properties of Ni-Mn-Ga alloys; they are harder and they have better creep and fatigue properties. But, the structure of Co-Ni-Al alloy is more complicated as compared to NiMnGa alloys. There are two phases at least, but only one of them undergoes the martensitic transformation. The role of the non-transforming phase during the transformation is not recognised yet, but its presence is suitable for the successful shape memory effect (SME). Single-phase alloys have tendency to crack before achieving a reasonable plastic deformation. The presented abstract describes the progress on the structural study.

The structure of the investigated material Co<sub>38</sub>Ni<sub>33</sub>Al<sub>29</sub> is composed of two phases – an ordered matrix (Co,Ni)Al with space group Pm3m, structure type B2, and a disordered face centred cubic cobalt solid solution with space group Fm3m, structure type A2 [3], Fig. 1. The B2 phase matrix undergoes martensitic transformation into the tetragonal L0<sub>1</sub> structure (space group P4/mmm). The transformation mechanism is very similar to the Ni-Al alloy including precursors, tweed structure and softening of the phonon modes [4]. According to the phase diagram L1<sub>2</sub> structure (Co,Ni)<sub>3</sub>Al (space group Fm3m) exists in samples with sufficient amount of nickel. In our samples, this phase is observed under special kinetic conditions.

In order to study and to apply ferromagnetic shape memory effect (FSME), it is very convenient to have single-crystalline samples. The single-crystals for our study were prepared using vertical floating-zone method and Bridgman method. The structure and composition of the as-grown samples were published in Refs [5, 6].

A kind of metastable (quenched) equilibrium is necessary for the SME performance in these alloys. It was described just as quick cooling after homogenization annealing in literature, but significant changes are observed mainly in the matrix [7].

The set of various annealing temperatures was employed. All samples were quenched to the ice-cold water. The temperature of 1350 °C leads to the dissolving of the interdendritic precipitates of the A2 (fcc cobalt) phase, but the true temperature of dissolving is lower, probably close to 1300 °C, as was observed. The melting of the two-

phase structure damages the SME. The samples showing the superelasticity (stress induced martensitic transformation) have a two-phase structure.

Past works [8] reported quite high temperatures of the martensitic transformation, but we observed  $M_s \sim -73$  °C, which does not depend on the annealing temperature in the interval from 1250 °C up to 1350 °C. The hysteresis of the martensitic transformation enlarges with lowering of the annealing temperature. Although the martensitic transformation takes place at temperatures below  $-73$  °C, pinned martensitic structures were observed in various samples. The lamellae were pinned either by A2 interdendritic precipitates or by special shapes of the sample – thin edges. The details of the pinning configuration are under examination.

The samples performing interesting superelastic properties were prepared, but the microstructure governs the mechanical behaviour mainly through the interdendritic particles distribution and their dissolving during the annealing.

*Authors would like to acknowledge the financial support from the Grant Agency of the AS CR project IAA200100902 and Czech Science Foundation projects 101/09/0702 and P107/10/0824.*

- [1] O. Heczko, N. Scheerbaum, O. Gutfleisch, Magnetic Shape Memory Phenomena, in Nanoscale Magnetic Materials and Applications, edited by J.P. Liu et al. (Springer Science+Business Media, LLC), 2009, pp. 14-1.
- [2] Heczko O, Sozinov A, Ullakko K, IEEE Trans. Magn., 36, (2000), 3266-3268.
- [3] M. Hubert-Protopescu, H. Hubert, Aluminium-cobalt-nickel ternary alloys: a comprehensive compendium of evaluated constitutional data and phase diagram. Vol. 4: Al-Cd-Ce to Al-Cu-Ru, edited by G. Petzow & G. Effenberg (Weinheim: VCH) 1991, pp. 234.
- [4] Y. Murakami, D. Shindo, K. Oikawa, R. Kainuma, K. Ishida, Acta Mater., 50, (2002), 2173.
- [5] J. Kopeček, K. Jurek, M. Jarošová, et al., IOP Conf. Sci.: Mater. Sci. Eng., 7, (2010), 012013.
- [6] J. Kopeček, S. Sedláková-Ignácová, K. Jurek, M. Jarošová, J. Drahokoupil, P. Šittner, V. Novák: Structure development in Co<sub>38</sub>Ni<sub>33</sub>Al<sub>29</sub> ferromagnetic shape memory alloy, 8th th European Symposium on Martensitic Transformations, ESOMAT 2009, edited by Petr Šittner, Václav Paidar, Luděk Heller, Hanuš Seiner, 2009, article No. 02013.
- [7] Yu. I. Chumlyakov, I. V. Kireeva, E. Yu. Panchenko, E. E. Timofeeva, Z. V. Pobedennaya, S. V. Chusov, I. Karaman, H. Maier, E. Cesari and V. A. Kirillov, Russ. Phys. J., 51, (2008), 1016.
- [8] K. Oikawa, L. Wulff, T. Iijima, F. Gejima, T. Ohmori, A. Fujita, K. Fukamichi, R. Kainuma, K. Ishida, Appl. Phys. Lett., 79, (2001), 3290.

## SELECTIVE ETCHING PROCESSES FOR BESOI MANUFACTURING

P. Kostelník

ON Semiconductor, 1. máje 2230, 756 61 Rožnov pod Radhoštěm, Czech Republic  
*petr.kostelnik@onsemi.com*

Bond and etch-back (BESOI) technique is way of manufacturing silicon on insulator (SOI) wafers with very thin device layer and excellent thickness uniformity control. The BESOI wafer is produced by direct bonding of two wafers: handle and device wafers. A buried oxide layer (BOX) is prepared on one of the wafers before the bonding process. The BOX layer assures total electrical isolation of the to-be created device layer. Handle wafer is usually an arbitrary wafer since its role is only supporting of the thin device layer. The device layer is manufactured from the device wafer. In case of the BESOI technique, the device wafer consists of a sacrificial substrate wafer on which an etch-stop layer (either created by implantation or epitaxial deposition) and the device layer (epitaxial deposition) are formed. The sacrificial substrate wafer and the etch-stop layer are removed (by grinding and selective etching) after the bonding. Therefore only the well defined epitaxial device layer remains on the BOX and handle wafer providing the desired resistivity and thickness control.

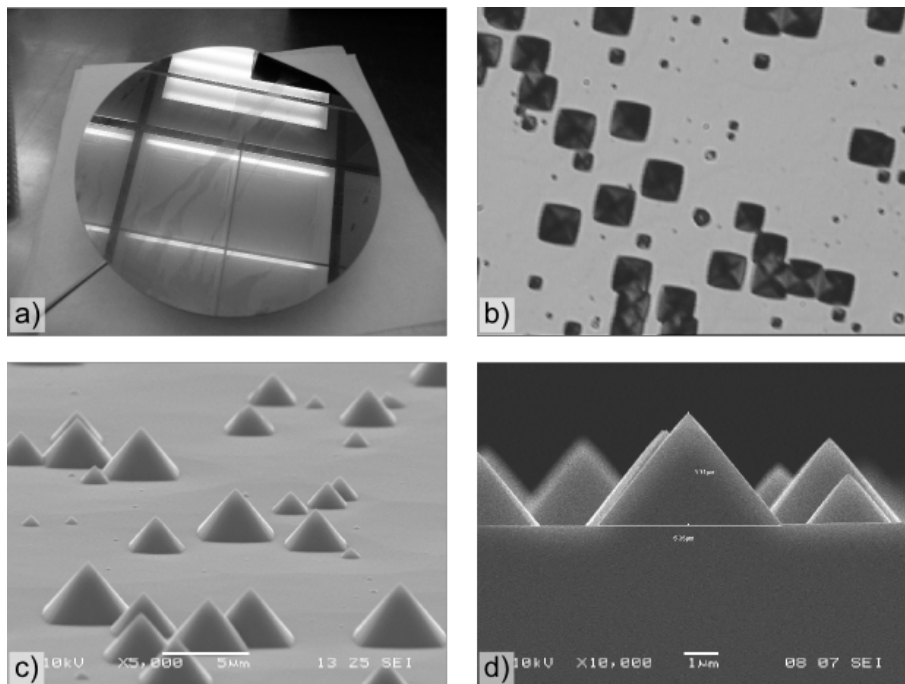


Figure 1: Surface defects on the wafers after TMAH etching: a) A full wafer photo showing haze on the surface, note that the geometrical pattern on the wafer is caused by the reflection of the clean room ceiling. b) An optical microscope image of the defects on the surface. Images c) and d) show SEM images of the defects.

Character of the etch-stop layer depends on the etchant used; etch-stop layers doped with C, N and B can be used. The most often used etch-stop layer is heavily boron doped

layer (doping level of  $10^{20}$  at/cm<sup>3</sup> and higher [1]). Such a high level of boron doping causes a severe strain in the interface of heavily and lightly doped material causing occurrence of dislocation defects due to the lattice mismatch. The strain may be reduced by using the B/Ge co-doped layer. The B/Ge concentration ratio of 1 : 2 to 1 : 8 may be used [2]. Such an etch-stop layer is the most desirable from the BESOI manufacturing process view and was used in our experiments.

BESOI selective etching consists of two different etching processes. The first one is intended for selective removal of the sacrificial substrate wafer, the second one to removal of the B/Ge co-doped etch-stop layer. The presented work is dedicated to study of these etching processes. We have used tetramethyl ammonium hydroxide (TMAH) with addition of ammonium persulfate (APS) and megasonic agitation as the selective etchant for the first etching process and HNA (mixture of hydrofluoric, nitric and acetic acids) as the selective etchant for the second etching process. Etch rate, composition, process conditions and selectivity of these etchants are discussed as well with problems one may come into contact such as etch defects (see Figure 1). All the results are presented and discussed on a 6" wafer scale (see Figure 2).

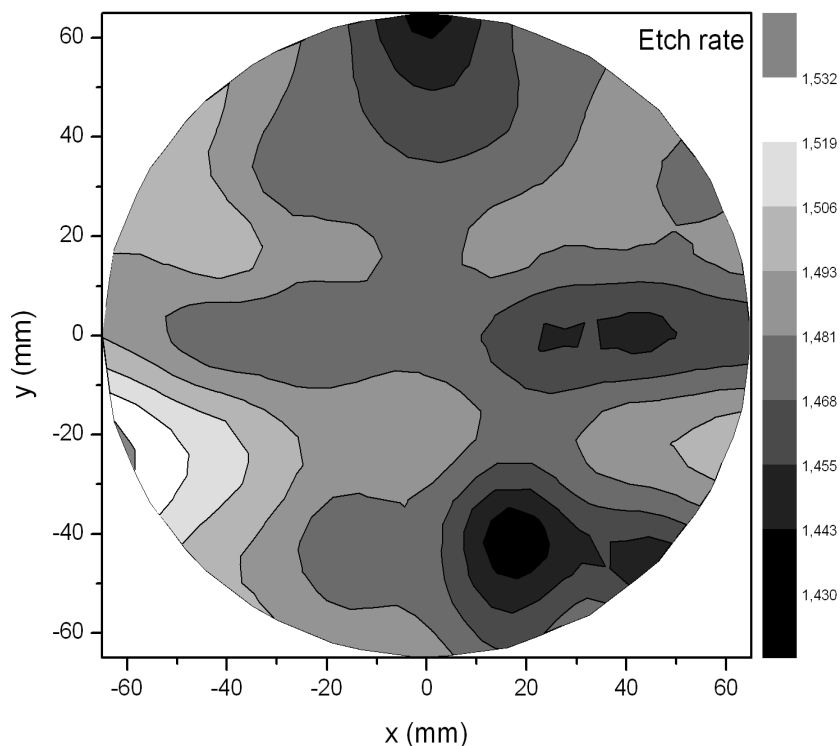


Figure 2: Wafer scale example of the TMAH etch-rate of a lightly doped single silicon.

- [1] H. Baumgart, T.J. Letavic, R. Egloff, Evaluation of wafer bonding and etch back for SOI technology, *Philips J. Res.*, 49 (1995) 91.
- [2] S. Tatic-Lucic, W. Zhang, N. Navneet, Etch-stop characteristics of heavily B/Ge-doped silicon epilayer in KOH and TMAH, *Sensors and Actuators A*, 123-124 (2005) 640.

## STRUCTURAL STUDIES OF ZnO-WO<sub>3</sub>-P<sub>2</sub>O<sub>5</sub> SYSTEM GLASSES

L. Koudelka<sup>(a)</sup>, J. Šubčík<sup>(a)</sup>, P. Mošner<sup>(a)</sup>, I. Gregora<sup>(b)</sup>

(a) Department of General and Inorganic Chemistry, Faculty of Chemical Technology,  
University of Pardubice, 532 10 Pardubice, Czech Republic

(b) Institute of Physics AS CR, Na Slovance 2, 182 21 Prague, Czech Republic  
*ladislav.koudelka@upce.cz*

Transition-metal containing glasses have attracted attention of several recent papers due to their electronic properties and high ionic conductivities in alkali phosphate-based glasses [1, 2]. Molybdenum oxide MoO<sub>3</sub> and tungsten oxide WO<sub>3</sub> belong to transition metals which are able to form glasses with glass-forming oxides, like P<sub>2</sub>O<sub>5</sub>, over a wide range of composition. This contribution is devoted to the study of structure of ZnO-WO<sub>3</sub>-P<sub>2</sub>O<sub>5</sub> glasses by Raman and <sup>31</sup>P MAS NMR spectroscopies.

Glasses of this system were synthesized from reagent grade ZnO, H<sub>3</sub>PO<sub>4</sub> and WO<sub>3</sub> in platinum crucible heated slowly at first up to 600 °C to remove water with final melting at 1100-1260°C, according to the composition. After 20 min heating at the maximum temperature, the melt was poured into a graphite mould and cooled slowly to room temperature. Glass-forming region obtained under these conditions in the studied ternary system is shown in Fig. 1. For the investigation of their structure glasses were studied in three compositional series X: (100-x)[0.5ZnO-0.5P<sub>2</sub>O<sub>5</sub>]-xWO<sub>3</sub>, Y: (50-y)ZnO-yWO<sub>3</sub>-50P<sub>2</sub>O<sub>5</sub> and Z: zZnO-20WO<sub>3</sub>-(80-z)P<sub>2</sub>O<sub>5</sub>

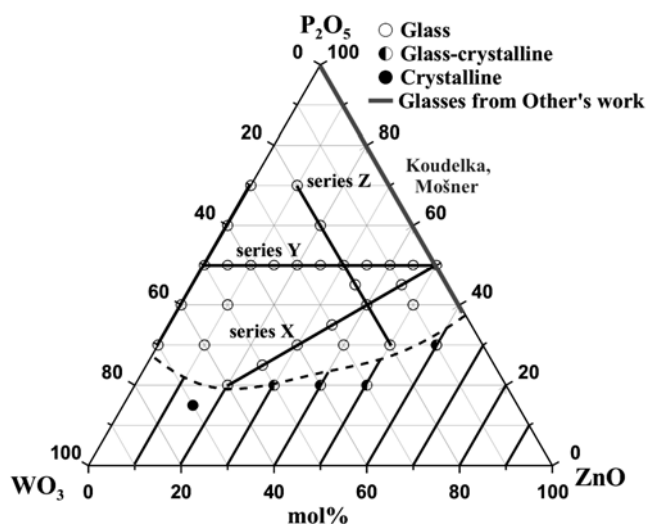


Fig. 1: Glass-forming region and composition of studied glasses in the ZnO-WO<sub>3</sub>-P<sub>2</sub>O<sub>5</sub> system.

In the compositional series X: (100-x)[0.5ZnO-0.5P<sub>2</sub>O<sub>5</sub>]-xWO<sub>3</sub> homogeneous glasses were prepared in the broad concentration region of 0-60 mol% WO<sub>3</sub>. Their glass transition temperature (T<sub>g</sub>) increases with increasing WO<sub>3</sub> content within the range of 460-622°C.

Their  $^{31}\text{P}$  MAS NMR spectra show on a steady depolymerization of phosphate chains by the incorporation of tungstate structural units as evidenced by a downfield shift of the NMR signal from -31.1 ppm to -11.8 ppm. Raman spectra reveal the existence of  $\text{WO}_6$  and  $\text{WO}_4$  units in the glasses with a low  $\text{WO}_3$  content and increasing clustering of  $\text{WO}_6$  units via W-O-W bonds at the glasses with a high  $\text{WO}_3$  content, as concluded from the presence of a broad vibrational band at 804-843  $\text{cm}^{-1}$  in their Raman spectra [3].

In the compositional series (Y)  $(50-y)\text{ZnO}-y\text{WO}_3-50\text{P}_2\text{O}_5$  homogeneous glasses were prepared in the whole concentration region of 0-50 mol%  $\text{WO}_3$ . Their  $^{31}\text{P}$  MAS NMR spectra reveal one broad signal showing downfield shift from -31 ppm ( $\text{Q}^2$  units) for the glass with  $x = 0$  up to -22 ppm ( $\text{Q}^1+\text{Q}^2$  units) for the glass with  $x = 45$  mol%  $\text{WO}_3$ . Also their Raman spectra show on a limited depolymerization of phosphate chains in this series as confirmed by a slow shift of the dominant Raman band 1207  $\text{cm}^{-1}$  to lower wavelengths. With increasing  $\text{WO}_3$  content in the glasses the strength of the new dominant band at 992-1000  $\text{cm}^{-1}$  in Raman spectra increases. This band was ascribed to the vibrations of W-O and W=O bonds in  $\text{WO}_6$  octahedra, which are present also in the crystalline  $\text{WO}_3$ .

In the compositional series (Z)  $z\text{ZnO}-20\text{WO}_3-(80-z)\text{P}_2\text{O}_5$  glasses were prepared in the concentration region of 10-50 mol%  $\text{WO}_3$ . Their  $^{31}\text{P}$  MAS NMR spectra reveal the presence of  $\text{Q}^2$  and  $\text{Q}^3$  units in the glasses with 10 and 20 mol% ZnO and  $\text{Q}^1$  and  $\text{Q}^0$  units in the glass with 50 mol% ZnO. Raman spectra show at low ZnO content a dominant band at 995-997  $\text{cm}^{-1}$ , ascribed to vibrations of  $\text{WO}_6$  octahedra, accompanied by the vibrational band at 923  $\text{cm}^{-1}$  at high ZnO content ascribed to the formation of  $\text{WO}_4$  tetrahedra. The presence of a broad Raman band at 844  $\text{cm}^{-1}$  in the glass with 50 mol% ZnO shows on some clustering of tungstate structural units via W-O-W bonds.

Raman spectra were also studied in the glass series  $(100-x)\text{P}_2\text{O}_5-x\text{WO}_3$ . These spectra are characterized by a narrow dominant vibrational band with the maximum at 999-1000  $\text{cm}^{-1}$  (vibrations of  $\text{WO}_6$  octahedra) and a broad band at 784-805  $\text{cm}^{-1}$  (vibrations of W-O-W bonds), the strength of which increases with  $\text{WO}_3$  content.

Investigation of properties of the glasses of ZnO- $\text{WO}_3$ - $\text{P}_2\text{O}_5$  ternary system showed that additions of  $\text{WO}_3$  to the zinc phosphate glasses improve their chemical durability and increase also their glass transition temperature due to the presence of stronger W-O bonds and to the reticulation of glass structure.

*The authors thank to prof. L. Montagne for the measurement of  $^{31}\text{P}$  MAS NMR spectra. This work was supported by the Grant No. P106/10/0283 of the Grant Agency of CR and the research project KAN301370701 of the AS CR.*

- [1] C. Mercier, G. Palavit, L. Montagne, C. Follet-Houttemane, *A survey of transition-metal containing phosphate glasses*, C. R. Chemie 5 (2002) 693.
- [2] B. V. R. Chowdari, K. L. Tan, W.T. Chia, *Structural and physical characterization of  $\text{Li}_2\text{O}:\text{P}_2\text{O}_5\text{-MO}_3$  ( $M = \text{Cr}_2, \text{Mo}, \text{W}$ ) ion conducting glasses*, Mat. Res. Soc. Symp. Proc. Vol. 293 (1993) 325.
- [3] T. Sekiya, N. Mochida, S. Ogawa, *Structural study of  $\text{WO}_3\text{-TeO}_2$  glasses*. J. Non-Cryst. Solids 176 (1994) 105.

## KINETICS OF POLYMER NUCLEATION ON ACTIVE CENTERS

Z. Kožíšek<sup>(a)</sup>, P. Demo<sup>(a,b)</sup>, A. Sveshnikov<sup>(a,b)</sup>, P. Ticháček<sup>(b)</sup>.

(a) Institute of Physics, Academy of Sciences of the Czech Republic, Cukrovarnická 10,  
162 00 Prague 6, Czech Republic

(b) Czech Technical University in Prague, Faculty of Civil Engineering, Thákurova 7,  
165 29 Prague 6, Czech Republic

*kozisek@fzu.cz*

Nucleation is process leading to formation of a new phase from supercooled melt or super-saturated solution. During this process it is necessary to overcome some energetical barrier called nucleation barrier at critical size (critical number of molecules forming the nucleus). This barrier decreases with increasing supercooling and thus nucleation is more probable. Undercritical nuclei have tendency to shrink and supercritical nuclei grow to macroscopic size.

Nucleation agent is added to polymer melt to increase the ability of crystallization of polymer. Formation of nuclei on nucleation agent is more probable due to lower energy barrier of nucleation. Crystalline polymer has better physical properties and that is why one needs to increase rate of formation of nuclei.

We have already analyzed [1, 2] the total number of nuclei of polyethylene formed within supercooled melt near its critical size. In polymer systems the building units of new crystalline phase are not single molecules, but repeating units of polymer chain (e. g. CH<sub>2</sub> for polyethylene). We have shown that our model is in good coincidence with experimental data of the total number of nuclei near critical size.

Recently, relative number of nuclei near critical size was measured for polymer crystallization [3, 4, 5]. From the viewpoint of these new experimental data, we have reanalyze our model of polymer nucleation to determine total number of nuclei and temporal dependency of the number of nuclei near critical size using the same input data as in our previous work [1]. Total number of nuclei coincided with experimental data, but the number of nuclei failed. That is why we have modified thermodynamic model to determine the total number of nuclei and relative number of nuclei – see Figs. 1, 2. In both cases we succeeded to find kinetic and thermodynamic parameters to get coincidence in both these characteristics of nucleation process. We have used standard kinetic model of nucleation on active centers [1, 2]. Number of active centers is depleted during phase transition process due to formation of nuclei.

In most cases computed total number of nuclei is compared with experimental data, but temporal dependency of the number of nuclei near critical size is not known in experimental measurements. Unique experimental technique of Okada et al. [3, 4, 5] succeeded to measure relative number of nuclei near critical size during nucleation process. It is shown that it is necessary to take into account in our model [1] both these dependencies to determine thermodynamic and kinetic parameters (interfacial energy, activation barrier of diffusion across the phase interface, number of active centers) correctly.

Time delay determined by numerical solution of kinetic equations coincides with experimental data for nucleus size  $i = 6900$  (the number of repeating units forming the nucleus), but is lower for smaller size  $i = 940$  (see Fig. 1b). Time delay of nucleation is predominantly

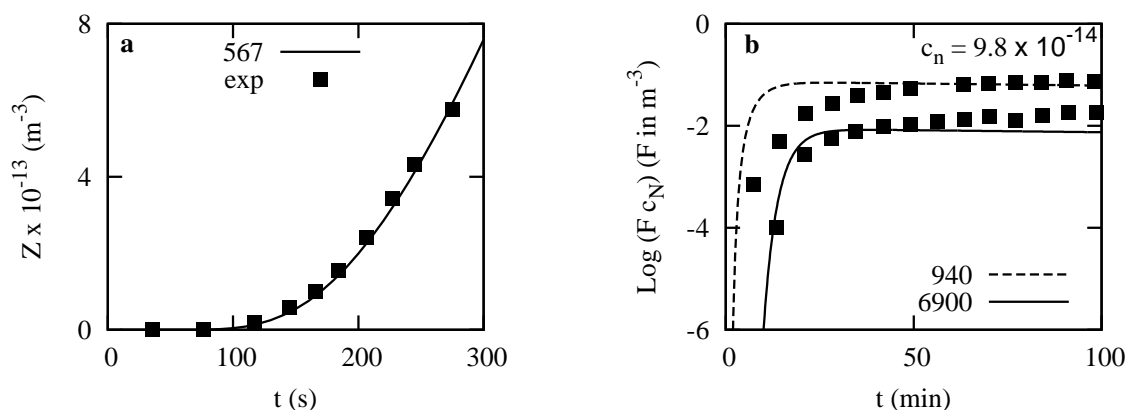


Fig. 1: Total number of nuclei (a) and number of nuclei (b) as a function of time at size 567 (a), 940 and 6900 (b). Full lines and dashed line correspond to numerical solution of kinetic equations, squares to experimental data.

determined by kinetic barrier of nucleation,  $E$ , which determines the probability of transition of monomers (repeating units of polymer chain) from liquid phase near phase interface to crystalline phase.  $E$  could depend on nucleus size and this dependence was not taken into account in our model. This is one possibility how to explain lower time delay determined from our model for smaller nuclei.

*This work was supported by the Grant No. IAA100100806 of the Grant Agency of the Academy of Sciences of the Czech Republic.*

- [1] Z. Kožíšek, M. Hikosaka, P. Demo, and A.M. Sveshnikov, *Nucleation kinetics of folded chain crystals of polyethylene on active centers*, J. Chem. Phys. 121 (2004) 1587.
- [2] Z. Kožíšek, M. Hikosaka, P. Demo, and A.M. Sveshnikov, *Nucleation kinetics of polymer formation on nucleation agent*, J. Cryst. Growth 275 (2005) e79.
- [3] K. Okada, K. Watanabe, T. Urushihara, A. Toda, M. Hikosaka, *Role of epitaxy of nucleating agent (NA) in nucleation mechanism of polymers*, Polymer 48 (2007) 401.
- [4] K. Okada, K. Watanabe, I. Wataoka, A. Toda, S. Sasaki, K. Inoue, M. Hikosaka, *Size distribution and shape of nano-nucleus of polyethylene simultaneously determined by SAXS*, Polymer 48 (2007) 382.
- [5] K. Okada, K. Watanabe, A. Toda, S. Sasaki, K. Inoue, M. Hikosaka, *Supercooling ( $\Delta T$ ) dependence of nano-nucleation of PE by SAXS and proposal of a new nucleation theory*, Polymer 47 (2007) 1116.

## GROWTH OF DIAMOND FILMS AND CARBON NANOTUBES OVER LARGE AREAS BY LINEAR ANTENNA MICROWAVE PLASMA CVD DEPOSITION

A. Kromka, O. Babchenko, T. Izak, M. Davydova, S. Potocky, B. Rezek

Institute of Physics AS CR, Cukrovarnicka 10, CZ-16253 Praha 6, Czech Republic

*kromka@fzu.cz*

Large area radio frequency (rf) plasma processes at 13.56 MHz have been commonly used in microelectronic industry. However, these processes are limited in coupling of rf energy to the process gases and thus, lower efficiency in atom ionization/excitation is achieved. Shifting of plasma processes to higher frequency, like microwave frequencies working at 2.45 GHz, can significantly increase plasma density and ionization ratio [1].

This relation is well known in chemical vapor deposition of diamond thin films. Growth of diamond films is well controllable in microwave plasma processes whereas using of rf frequency resulted in poor growth of lower quality films (i.e. films with high amount of non diamond carbon phases, low growth rate, etc.). Additionally, microwave plasma processes are not using metal electrodes which minimize the pollution of grown films from electrode material. Finally, microwave plasma CVD processes can simply implement substrate bias (rf or dc) independently of applied microwave power [2].

Commonly used method for coupling microwave plasma in CVD deposition of diamond films are “point” ball plasma system which use principles of dielectric windows (NIMIR system, Japan), a set of  $\lambda/4$  antennas (Astex systems, USA) or their combinations (ellipsoidal or “Egg” system, Fraunhofer Inst. Freiburg, Germany).

Microwave based surface wave-discharge (SWD) system represents an alternative solution to above proposed systems. Besides of all SWD configurations, the linear antenna microwave configuration is the most promising solution for large area deposition of diamond thin films. In this system, plasma is propagated along the central metal antenna (copper) and plasma is generated along the outside part of quartz tubes located in the vacuum chamber [2, 3]. First prove of using SWD plasma in linear antenna configuration for diamond

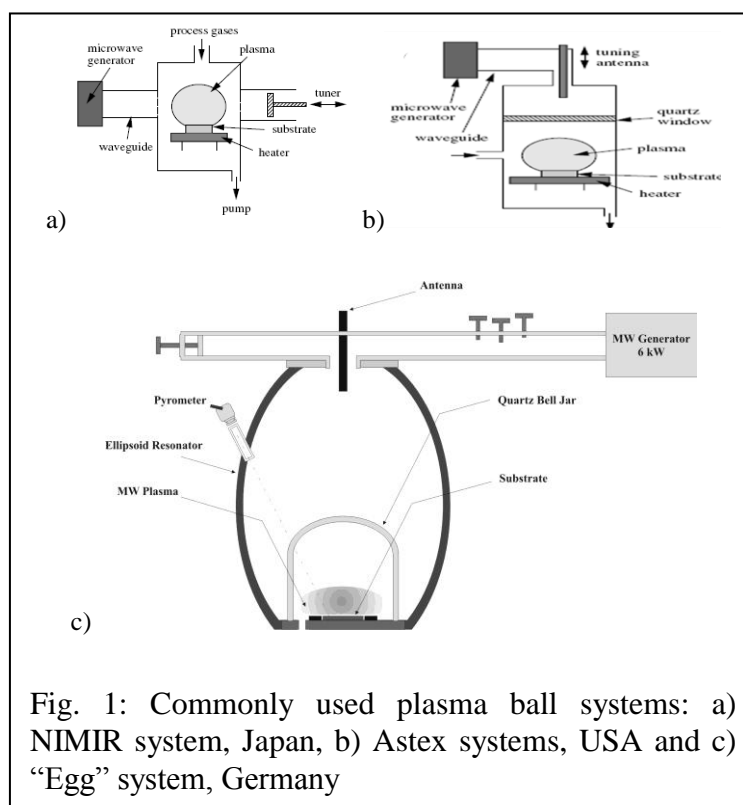


Fig. 1: Commonly used plasma ball systems: a) NIMIR system, Japan, b) Astex systems, USA and c) “Egg” system, Germany

growth was shown by Hasegawa group, who grow optically transparent and smooth NCD films over large areas (30x30 cm<sup>2</sup>) [4]. Typical size of diamond crystals was in the range from 5 to 20 nm. Unfortunately, up to our best knowledge, the relation between the film properties (i.e. morphology, sp<sup>2</sup> to sp<sup>3</sup> carbon content) and the deposition parameters have not been published yet.

In the present work, we show the correlation between the process parameters and morphology of diamond films grown from CO<sub>2</sub>/CH<sub>4</sub>/H<sub>2</sub> gas mixture by linear antenna microwave plasma CVD method (modified system AK 400, Roth & Rau, Germany). We found that standard pressure (2 mbar) resulted in growth of smooth films with relatively high amount of sp<sup>2</sup> bonded carbon species (Fig. 1b). As the pressure decreased down to 0.1 mbar, films become rough consisting of well faceted diamond crystals while the amount of sp<sup>2</sup> bonded carbon decreased significantly down (Fig. 2b). The suitability of the presented deposition system for growth of carbon nanotubes was tested too. We found that combining linear antenna microwave plasma with the rf substrate bias resulted in growth of carbon nanostructures under pre-defined angle to the substrate base (Fig. 2c).

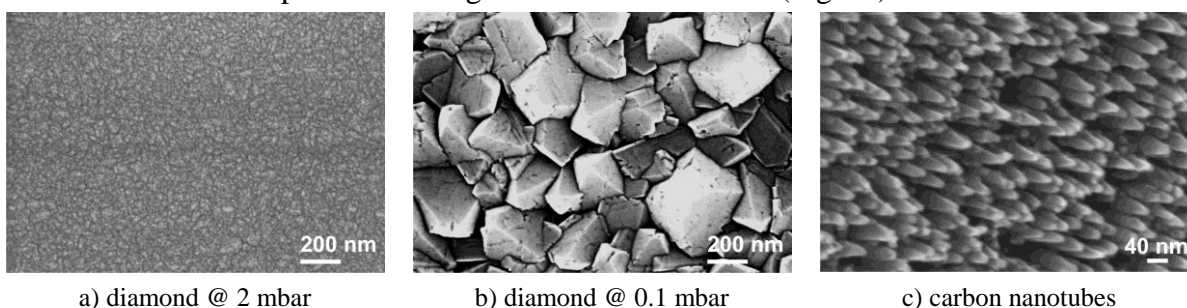


Fig 2: Surface morphology of diamond films (a, b – top view) and carbon nanotubes (c – view at 45°) grown by linear antenna microwave plasma CVD process

The main advantage of using linear antenna microwave plasma system in growth of carbon allotropes is its simple scale up, i.e. the antenna length can be prolonged up to meter and the antenna can be multiplied. Additional challenging multifunctional uses of SWD plasma in linear antenna configuration will be also pointed out.

*We acknowledge a financial support by AV0Z10100521, KAN400100701 (ASCR), IAAX00100902 (GA AV), M100100905 (GA AV), IM06002 (MSMT) and by the Fellowship J.E. Purkyne (ASCR). We would like to gratefully appreciate J. Potmesil and O. Rezek for technical assistance and preparation of samples, and K. Hruska for SEM measurements.*

- [1] K. Muraoka, C. Honda, K. Uchino, T. Kajiwara, K. Matsuo, M. Bowden, W.Z. Park, Y. Hirakawa, K. Tanaka, M. Maeda, T. Okada, *Rev. Sc. Instr.* 63/10 (1992) 4913.
- [2] H. Schlemm, A. Mai, S. Roth, D. Roth, K.M. Baumgartner, H. Muegge, *Sur. Coat. Tech.* 174 (2003) 208.
- [3] D. Roth, B. Rau, S. Roth, J. Mai, K.H. Dittrich, *Sur. Coat. Tech.* 74-75/1-3 (1995) 637.
- [4] K. Tsugawa, M. Ishihara, J. Kim, M. Hasegawa, Y. Koga, *New Diamond & Frontier Carbon Technology* 16/6 (2006) 337.
- [5] J. Kim, K. Tsugawa, M. Ishihara, Y. Koga, M. Hasegawa, *Plasma Sour. Sc. & Tech.* 19/1 (2010) 015003.

## **FIGURE OF MERIT OF $(\text{Sb}_{0.75}\text{Bi}_{0.25})_{2-x}\text{In}_x\text{Te}_{2.8}\text{Se}_{0.2}$ SINGLE CRYSTALS**

V. Kucek

Faculty of Chemical Technology, University of Pardubice, Studentská 573, 532 10  
Pardubice, Czech Republic

*vladimir.kucek@gmail.com*

Nowadays, we observe a boom in search of alternative power resources. One of the alternatives are thermoelectric effects. Research on thermoelectric (TE) materials is thus one of very active fields of research. Effectivity of a TE material is expressed in terms of so called TE figure of merit  $ZT$ ,  $ZT = \sigma S^2 T / \kappa$  ( $\sigma$ - electrical conductivity,  $S$ - Seebeck coefficient,  $\kappa$ - thermal conductivity,  $T$ - absolute temperature) [1]. It is well known that properly doped  $(\text{Sb}_{0.75}\text{Bi}_{0.25})_2\text{Te}_3$  is used as p-type legs of thermoelectric modules working in the vicinity of room temperature. It was shown that small concentrations of In can be beneficial for thermoelectric properties of  $(\text{Sb}_{0.75}\text{Bi}_{0.25})_2\text{Te}_3$  as it enhances the  $ZT$  value by as much as 30% in the low temperature region [2]. This contribution represents results on  $(\text{Sb}_{0.75}\text{Bi}_{0.25})_2\text{Te}_{2.8}\text{Se}_{0.2}$  (low temperature) system doped with indium.

The starting polycrystalline materials of nominal compositions  $(\text{Sb}_{0.75}\text{Bi}_{0.25})_{2-x}\text{In}_x\text{Te}_{2.8}\text{Se}_{0.2}$  were synthesized from the elements of 5N purity in conical quartz ampoules evacuated to  $10^{-3}$  Pa. The synthesis consisted of heating the reaction mixture at 1073 K for 48 hours. The single crystals were grown using a modified Bridgman technique. A conical quartz ampoule, containing the synthesized material, was placed in upper (warmer) part of the Bridgman furnace, where it was kept at 1000K for 24 hours. The ampoule was then lowered into a temperature gradient of 80K/cm at a rate of 1.3 mm per hour. The single crystals 60 mm long and 10 mm in diameter were easily cleavable along the 0001 plane. The orientation of the crystals was performed using Laue back-diffraction technique. The samples of dimensions for measurement were cut from the middle part of single crystals with a spark erosion machine. The lattice parameters of the single crystals were determined from powdered samples by X-ray diffraction analysis using D8-Advace diffractometer (Bruker AXE, Germany) with Bragg-Brentano  $\theta$ - $\theta$  geometry. Seebeck coefficient and thermal conductivity were determined using a longitudinal steady-state technique in a cryostat equipped with a radiation shield. Thermal gradients were measured by means of fine Au:Fe/Chromel thermocouples, and a miniature strain gauge served as a heater. For the Seebeck probes fine copper wires were used that have previously been calibrated, and their thermopower contribution was subtracted from the measured sample thermopower. Electrical conductivity was studied using a Linear Research ac bridge with 16 Hz excitation. All presented physical parameters are in-plane parameters, i.e. they were measured in perpendicular direction to trigonal axes  $c$ . Measurements of the electrical resistivity and the Seebeck coefficient have an absolute error of about 1% . Thermal conductivity is measured with an accuracy of 5%.

Indium that is incorporated in the host structure enters the cation sublattice and forms uncharged point defects  $\text{In}_{\text{Me}}^{\times}$ . Although nominally electrically inactive, indium causes a change in free hole concentration due likely to the interaction of indium with the native point

defects. Therefore In induces a change in the strength and character of charge carrier scattering. In all, a small concentration of In  $x \approx 0.02$  seems to be beneficial for thermoelectric properties since it enhances the figure of merit of  $(\text{Sb}_{0.75}\text{Bi}_{0.25})_{2-x}\text{In}_x\text{Te}_{2.8}\text{Se}_{0.2}$  by more than 15% over the values measured on the undoped  $(\text{Sb}_{0.75}\text{Bi}_{0.25})_2\text{Te}_{2.8}\text{Se}_{0.2}$  below room temperature (Fig. 1). This increase is primarily due to decreasing thermal conductivity and increasing Seebeck coefficient. Low concentration doping of tetradymite-type crystals with indium is worth of further exploration with respect to its potential to improve low temperature thermoelectric properties through the optimization of free carrier concentration and/or selenium content.

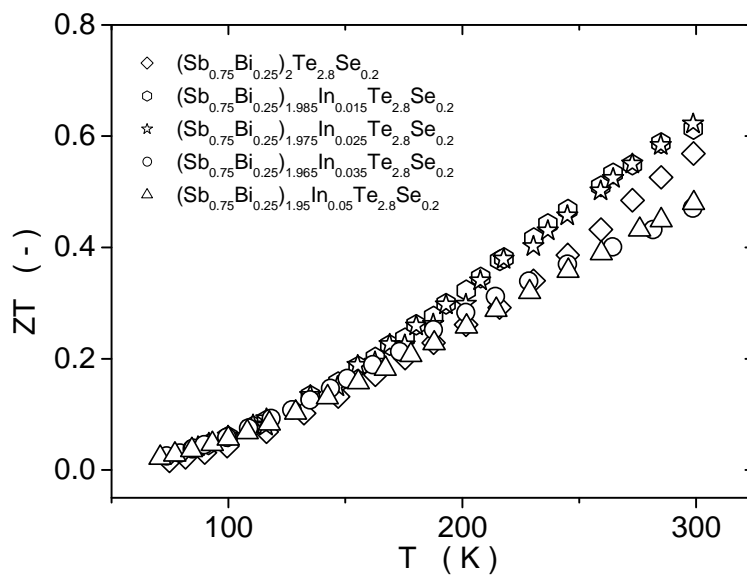


Fig. 1: The dimensionless figure of merit  $ZT$  as a function of temperature for  $(\text{Sb}_{0.75}\text{Bi}_{0.25})_{2-x}\text{In}_x\text{Te}_{2.8}\text{Se}_{0.2}$  single crystals.

*This research was supported by the Ministry of Education, Youth and Sports of the Czech Republic under the project MSM 0021627501.*

- [1] G. S. Nolas, J. Sharp, H. J. Goldsmid, *Thermoelectrics / Basic Principles and New Material Developments*, Springer-Verlag Berlin Heidelberg, p. 128 (2001).
- [2] C. Drasar, A. Hovorkova, P. Lostak, H. Kong, C.-P. Li and C. Uher, *J. Appl. Phys.* 104, 023701 (2008).

## **DIELECTRICAL BEHAVIOUR OF CARBON BLACK – POLYMER COMPOSITES PREPARED FROM SOLUTION**

J. Lipták, J. Sedláček, I. Pilarčíková, V. Bouda

Faculty of Electrical Engineering, Czech Technical University in Prague,  
166 27 Prague 6, Czech Republic  
*liptak@fel.cvut.cz*

### ***Introduction***

When the carbon black (CB) is used as filler in polymer matrix, CB agglomerates are formed due to activity of van der Waals forces. When the concentration of the CB reaches the percolation value the continuous electrically conductive network is formed in the composite. Therefore the composite behaviour can change from insulator to conductive one. Dependence of conductivity on CB concentration shows the sharp rise [1] (percolation threshold). The electrical conductivity decreases when temperature increases because the CB network is gradually broken out (PTC effect). It is widely used for self-controlling heating cables or screening desks etc. Also, the network in the bulk increases the viscosity [2] of the composite. The composites of conductive polymers with fullerenes are intensively studied for organic solar cells applications [3]. It was pointed out [4] that the agglomeration of CB is reasonably influenced by electric field [4-6] and ion concentration [4]. There are a small amount of different ions inside CB particles from the production process. In our previous work [4] it was shown that the presence or absence of ions in the composite plays reasonable role for agglomeration of CB due to their strong influence to van der Waals forces. This work deals with the structure and consequently electrical properties of carbon black – polystyrene (PS) composites with different amount of ions.

### ***Experimental***

*Sample preparation:* Two series of the samples were prepared. 1. Composites with dry CB. It was dried on the hot plate at temperature 120 °C up to constant weight. 2. Composites with CB (DCB-deionised CB) with lower concentration of ions which were extracted in water. The ions extraction was verified by the measurement of the water conductivity. CB and DCB were dried up to constant weight and mixed with polystyrene in toluene with loading from 2%w to 8%w and dispersed and pulverized by IKA rotational homogenizer at speed 20000 rpm for the 2 minutes. After that, the ultrasonic homogenizer Sonopuls UW 3200 (Bandelin) with the power 40 W for the time 3 x 1 minutes was used. The plate composites CB(DCB) – PS with the diameter 40 mm and the thickness from 0,05 mm to 0,2 mm were prepared from the solutions by simple coating into Petri dishes and thin layers on cover glasses by the method of spin coating.

*Electrical measurements:* The impedance analysis (capacitance  $C$  and resistance  $R$  in parallel scheme) in the frequency region 100 Hz to 1 MHz included DC measurement was carried out with the PM 6306 RLC meter FLUKE with the voltage from 0,5 to 2 V.

In normal direction measurements the plate condenser with micro shift was used. Resistivity  $\rho$  (Ohm m) and more simple quantities  $e1(-)$  and  $e2(-)$  proportional to the components of complex permittivity were evaluated according formulae as follows:

$$\rho = \frac{RS}{d}, \quad e1 = \frac{Cd}{\epsilon_0 S}, \quad e2 = \frac{d}{Rf} \quad \text{Eq. 1}$$

where  $f$  is the measuring frequency,  $\epsilon_0$  is permittivity of vacuum and  $d$  is thickness of the sample. In planar direction the van der Pauw method with Al dot contacts was used.

### Results and discussion

The results from AFM microscope (Fig. 1) are in agreement with optical observation [4]. The final structure of the composite with DCB is more homogeneous and finer than that with CB.

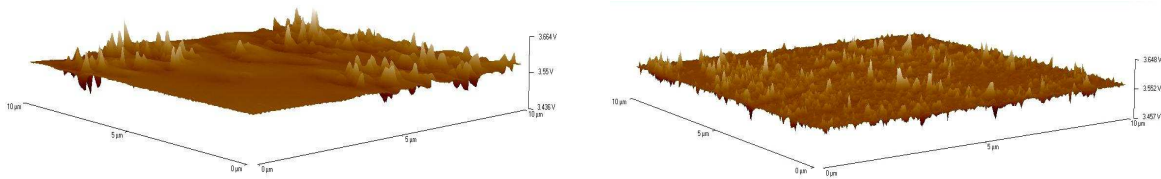


Fig. 1: Surface electrical potential of the sample with the thickness 0.1 mm and a) 4% CB and b) 4% DCB obtained from the AFM microscope.

The impedance measurements show the monotonically decrease of both  $e1$  and  $e2$  (Eq.1) with frequency. DC resistivity decreases with increasing CB (DCB) content, but the magnitude depends on measuring voltage (Fig. 2). It decreases when the voltage is higher. The resistivity of the samples with DCB is in the most cases lower in comparison with the samples with CB.

### Conclusions

In this work it was shown that both CB – PS composite structure and electrical properties of the CB – PS composites can be reasonably influenced by the concentration of ions in CB. The frequency dependences results are typical for partially conductive materials with space charge polarization. The decrease of the resistivity with increasing voltage implies that the mechanism of the conductivity is not ohmic, but the microscopic brake down or tunnelling phenomena can take place.

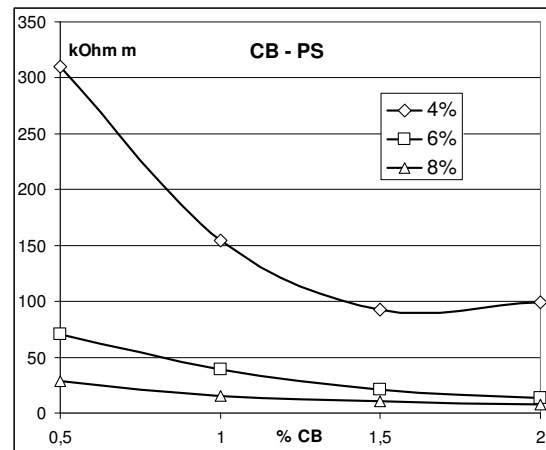


Fig. 2: Resistivity as a function of measuring voltage for the samples CB- PS

*This research has been supported by the research project MSM6840770021.*

- [1] Miyasaka, K. et al., J. Mat. Sci. 17 (1982) 1610.
- [2] Lakdawala, K., Salovey, R., Polymer Engineering and Science, 27 (1987) 1043.
- [3] Bjorklund, G. S., Baer, T. M., Photonics Spectra (2007) 70.
- [4] Lipták, J., Bouda, V., Nanocon, Rožnov pod Radhoštěm, 2009 vol. 1, p. 196.
- [5] Prasse, T. et al., Appl. Phys. Lett., 72, (1998) 290.
- [6] Lipták, J., The 18th joint seminar DMSRE 2.-5.9. 2008, Hnanice.

## MEASUREMENT OF THE SPECTRAL REFLECTANCE RATIO OF POLARIZED WAVES USED TO THIN-FILM THICKNESS DETERMINATION

J. Luňáček <sup>(a)</sup>, P. Hlubina <sup>(a)</sup>, D. Ciprian <sup>(a)</sup>

(a) Department of Physics, VŠB-Technical University of Ostrava, 17. listopadu 15,  
708 33 00 Ostrava-Poruba, Czech Republic

*jiri.lunacek@vsb.cz*

This paper deals with measuring the wavelength dependence of the reflectance ratio  $R_p(\lambda)/R_s(\lambda)$ , or  $\tan^2 \Psi(\lambda)$ , where  $\Psi(\lambda)$  is the ellipsometric angle, at a fixed angle of incidence. An experimental set-up is shown in Fig. 1.

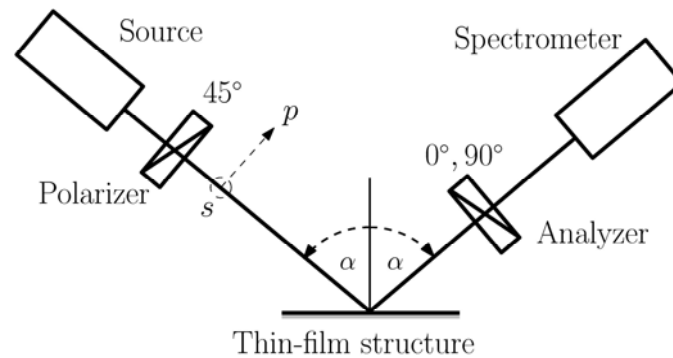


Fig. 1. Experimental setup for measuring the wavelength dependence of the reflectance ratio  $R_p(\lambda)/R_s(\lambda)$  of a thin-film for the angle of incidence  $\alpha$ .

The procedure consists of three steps: first, with the source blocked, the background spectrum  $I_{bkg}(\lambda)$  is measured, second, with the analyzer oriented perpendicularly to the plane of the incidence, the reflection spectrum  $I_s(\lambda)$  for  $s$  polarization is measured, and third, with the analyzer oriented parallel to the plane of the incidence, the reflection spectrum  $I_p(\lambda)$  for  $p$  polarization is measured. The reflectance ratio  $R_p(\lambda)/R_s(\lambda)$  of the structure is given by

$$R_p(\lambda)/R_s(\lambda) = [I_p(\lambda) - I_{bkg}(\lambda)] / [I_s(\lambda) - I_{bkg}(\lambda)]. \quad (1)$$

These spectral reflectance ratios  $R_p(\lambda)/R_s(\lambda)$  consist of maxima whose number and positions depend on the thickness of a thin film (see Fig. 2.). An approximate linear relation between the thin-film thickness and a wavelength of the maximum of the reflectance ratio for a specific angle of incidence is revealed, provided that the wavelength-dependent refractive index of the thin film is known and the substrates are weakly absorbing. The relation permits the calculation of the thin-film thickness from the measured spectral reflectance ratio by using one maximum only, as is demonstrated theoretically for SiO<sub>2</sub> thin film on a Si substrate [1].

Application of this method is showed experimentally for the same system thin-film structure with different thicknesses of the SiO<sub>2</sub> thin film (see Fig. 3.).

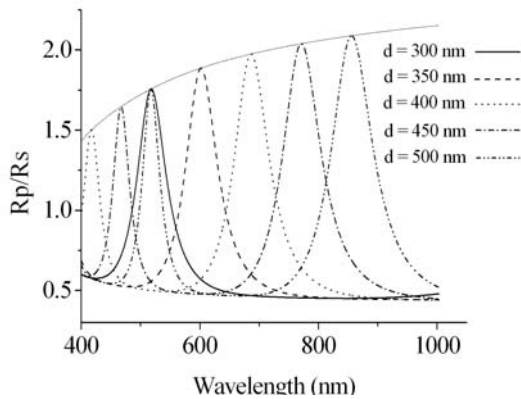


Fig. 2. Theoretical dependence of the reflectance ratio  $R_p(\lambda)/R_s(\lambda)$  for  $\alpha = 45^\circ$  and a SiO<sub>2</sub> thin-film of different thicknesses on the Si substrate.

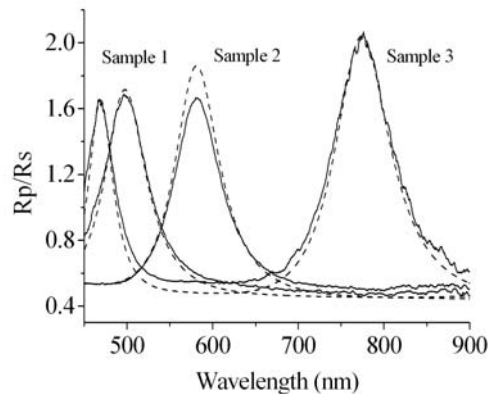


Fig. 3. Measured (solid) and theoretical (dashed) dependences of the ratio  $R_p(\lambda)/R_s(\lambda)$  for  $\alpha = 45^\circ$  and three different samples of the SiO<sub>2</sub> thin film.

The results are compared with those given by the algebraic fitting method, and very good agreement is confirmed (see Table 1). Details of these methods are presented in [1, 2].

Sample No.	$t$ (min)	$\alpha$ (°)	$\lambda_{\max,1}$ (nm)	$d$ (nm)	$d_{\text{fit}}$ (nm)
1	122	30	530,89	287,4	286,6
		45	497,62	288,5	287,7
		60	459,83	288,6	286,5
2	212	30	624,57	338,9	338,6
		45	580,97	337,8	337,5
		60	567,03	338,2	337,3
3	326	30	830,02	451,9	450,8
		45	775,03	452,5	451,9
		60	715,05	452,7	452,4

**Table 1.** Oxidation times  $t$ , angles of incidence  $\alpha$ , wavelengths  $\lambda_{\max,1}$ , thicknesses  $d_{\text{fit}}$  and  $d$  of the SiO<sub>2</sub> thin films.

*This work was supported by the Grant MSM6198910016 and by the regional Grant CZ. 1.05/2.1.00/01.0040.*

- [1] P. Hlubina, J. Luňáček, D. Ciprian, Maxima of the spectral reflectance ratio of polarized waves used to measure the thickness of a nonabsorbing thin film. *Optics and Lasers in Engineering* 48 (2010) 786.
- [2] P. Hlubina, D. Ciprian, J. Luňáček, Spectral interferometric technique to measure ellipsometric phase of a thin-film structure. *Optics Letters* 34 (2009) 2661.

**ALTERNATIVE METHOD TO THIN-FILM THICKNESS DETERMINATION  
USING THE SPECTRAL REFLECTANCE MEASUREMENT**

M. Luňáčková<sup>(a)</sup>, J. Luňáček<sup>(b)</sup>, Z. Potůček<sup>(c)</sup>, P. Hlubina<sup>(b)</sup>

(a) Department of Mathematics and Descriptive Geometry, VŠB - Technical University of Ostrava, 17. listopadu 15, 708 33 Ostrava - Poruba, Czech Republic

(b) Department of Physics, VŠB - Technical University of Ostrava, 17. listopadu 15, 708 33 Ostrava - Poruba, Czech Republic

(c) Department of Solid State Engineering, Faculty of Nuclear Sciences and Physical Engineering, Czech Technical University in Prague, Trojanova 13, 120 00 Praha 2, Czech Republic

*milena.lunackova@vsb.cz*

We propose an alternative reliable and accurate measurement of the reflectance spectrum of thin-film structures without the knowledge of the calibration function of a reference mirror. This procedure consists of two steps: First, the relative reflectance spectrum of a thin-film structure is measured using a non-calibrated mirror (or the calibration function of the reference mirror is not valid furthermore [1]), and second, the relative reflectance spectrum of a bare substrate of the thin-film structure is measured with the same reference mirror. Then the relationship between the relative spectral reflectance of the thin-film structure and the known absolute spectral reflectance of a standard bare wafer allows for obtaining the absolute reflectance spectrum of the structure.

The first step is the same as in a standard method with the calibrated mirror

$$R_{\text{abs}}(\lambda) = C_{\text{mirror}}(\lambda)R_{\text{meas}}(\lambda), \quad (1)$$

where  $C_{\text{mirror}}(\lambda)$  is the wavelength-dependent calibration (correction) function of the reference mirror. The second step consists of the replacement of the thin-film structure by a bare wafer of the structure of the known reflectance in the primary arm of the spectrometer. Because the conditions in the secondary arm with the mirror are not changed, we suppose that  $C_{\text{mirror}}(\lambda)$  is unchanged too and we can write equation for absolute spectral reflectance of the wafer  $R_{\text{wafer abs}}(\lambda)$

$$R_{\text{wafer abs}}(\lambda) = C_{\text{mirror}}(\lambda)R_{\text{wafer meas}}(\lambda), \quad (2)$$

where  $R_{\text{wafer meas}}(\lambda)$  is the wavelength-dependent measured relative reflectance of the wafer. Finally, we eliminate simply the unknown calibration function of the mirror by dividing Eqs. (1) and (2) and we can write a new relation between the relative and the absolute reflectance spectra of the thin-film structure

$$R_{\text{abs}}(\lambda) = C_{\text{wafer}}(\lambda)R_{\text{meas}}(\lambda) = \frac{R_{\text{wafer abs}}(\lambda)}{R_{\text{wafer meas}}(\lambda)}R_{\text{meas}}(\lambda), \quad (3)$$

On the basis of Eq. (3), a new correction function  $C_{\text{wafer}}(\lambda)$  can be constructed. Moreover, the absolute reflectance spectrum of the thin-film structure measured in this way (2-nd method) can be compared with the theoretical reflectance to determine the thin-film thickness.

This method was successfully tested on a uniform SiO<sub>2</sub> thin film grown by thermal oxidation on different B- and P-doped Si substrates. These substrates served as bare wafers

and the measured absolute reflectance spectra were compared with the results of a standard method (1-st method) using the known calibration function of the reference mirror. The reflectance spectra obtained by both methods were compared with the theoretical ones to determine the thin-film thicknesses. Small thickness changes due to different Si substrates were resolved and compatibility of the results of both measurement methods was confirmed (see Table 1).

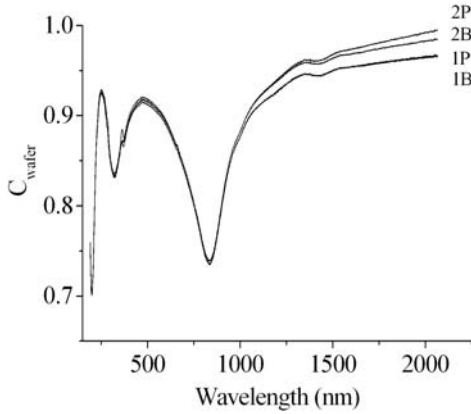


Fig. 1. Correction functions for all samples using refractive indices and extinction coefficients of undoped Si from [2].

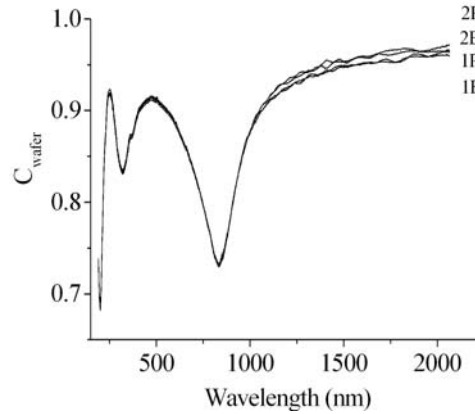


Fig. 2. Correction functions for all samples using refractive indices and extinction coefficients of Si from the ellipsometric data.

Wavelength range 192 – 2066 nm.

Table 1. Comparison of the thicknesses  $d$  and correlation coefficients  $C_{fit}$  determined by using various methods for a  $\text{SiO}_2$  thin film on the doped Si substrates.

Wavelength range: 250 – 2066 nm.

Sample	$N_D$ ( $\text{cm}^{-3}$ )	1-st method (a)		1-st method (b)		2-nd method (a)		2-nd method (b)	
		$d_{fit}$ (nm)	$C_{fit}$	$d_{fit}$ (nm)	$C_{fit}$	$d_{fit}$ (nm)	$C_{fit}$	$d_{fit}$ (nm)	$C_{fit}$
1B	$1.74 \times 10^{15}$	283.54	0.99983	283.43	0.99965	283.53	0.99989	283.42	0.99985
2B	$1.31 \times 10^{19}$	280.84	0.99985	280.73	0.99981	280.93	0.99997	280.81	0.99996
1P	$2.30 \times 10^{15}$	276.23	0.99991	276.13	0.99983	276.39	0.99991	276.14	0.99995
2P	$3.16 \times 10^{19}$	279.16	0.99969	278.94	0.99985	279.16	0.99990	279.01	0.99997

(a) optical parameters of undoped Si from [2]

(b) optical parameters of doped Si from ellipsometric data

*This work was supported by the Grants MSM6198910016 and MSM 6840770021, and by the regional Grant CZ. 1.05/2.1.00/01.0040.*

[1] D. Poelman, P.F. Smet, Methods for the determination of the optical constants of thin films from single transmission measurements: a critical review, *J. Phys. D: Appl. Phys.* 36 (2003) 1857.

[2] E. D. Palik, *Handbook of Optical Constants of Solids*, Academic Press, Orlando, 1995.

## RESIDUAL STRESS OF THIN FILMS OF POLYCRYSTALLINE AND AMORPHOUS SILICON

D. Lysáček

ON Semiconductor, 1. máje 2230, 756 61 Rožnov pod Radhoštěm, Czech Republic

*david.lysacek@onsemi.com*

The strong competitive conduct in IC industry forces the producers of the raw silicon wafers to the continuous price-cutting behavior. Therefore, projects leading to decreasing of the wafer unit cost are unavoidable in order to be able to compete. One of the most effective method leading to significant reduction of the unit cost of silicon wafer is decreasing of the wafer thickness. However, decreasing of the wafer thickness results in the excessive wafer warping if polycrystalline silicon layer is deposited on the wafer back side (Fig. 1).

This phenomenon is caused by high residual stress of the polycrystalline silicon layers. Knowledge of the dependences of the residual stress on the deposition conditions is than necessary for development of the process of deposition of the polycrystalline silicon layers allowing controlled wafer shaping.

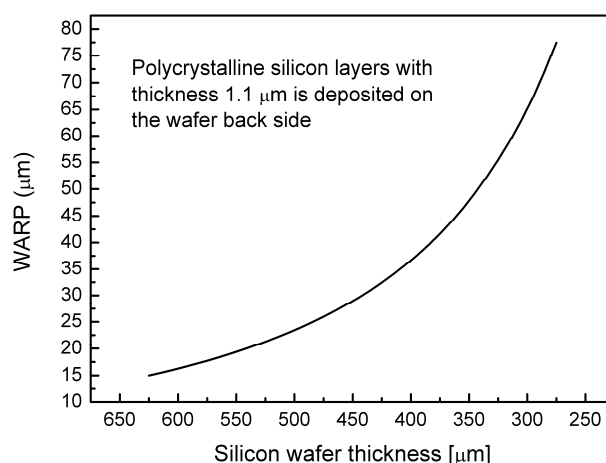


Fig. 1: Dependence of the silicon wafer warping on the thickness of the silicon wafer. Wafer warping is caused by polycrystalline silicon layer deposited on the wafer backside. WARP is parameter characterizing warping of the wafer [1].

LPCVD (Low Pressure Chemical Vapor Deposition) technique was used for deposition of the polycrystalline silicon layers on the wafer back side. The most important parameters of this technique are deposition temperature and deposition pressure.

Dependences of the residual stress of the polycrystalline silicon layers on the deposition temperature were measured for two constant deposition pressures 110 and 280 mTorr. The range of the deposition temperature was from 570 to 627°C. Deposition temperatures below 600°C were taken intentionally in order to get amorphous silicon layers. The thickness of the layers was 1.1 μm. Residual stress of the polycrystalline silicon layer  $\sigma_f$  was calculated from the curvature radius  $R$  of the wafer using Stoney's equation:

$$\sigma_f = \frac{E}{6(1-\nu)} \cdot \frac{t_s^2}{t_f} \cdot \left( \frac{1}{R} - \frac{1}{R_0} \right) \quad (1)$$

where  $E$  is Young's modulus,  $\nu$  is Poisson's ratio,  $t_s$  is thickness of the silicon wafer and  $t_f$  is thickness of the layer.

From the dependences of the residual stress on deposition temperature (Fig. 2) is evident that layers deposited at temperatures above 600°C for deposition pressure 280 mTorr as well as layers deposited above 580°C for deposition pressure 110 mTorr induce compressive residual stress. Compressive stress is denoted by the negative sign. Those layers (right from the grey areas in Fig. 2) are polycrystalline. Compressive stress of the polycrystalline silicon layers is the consequence of Vollmer – Weber mode of thin film growth. Residual stress of the polycrystalline silicon layers decreases with increasing deposition temperature.

Layers deposited below 580°C for deposition pressure 280 mTorr are amorphous and induce compressive residual stress. Layers deposited below 585°C for deposition pressure 110 mTorr are amorphous and induce tensile residual stress (denoted by the positive sign). Layer deposited at 585°C and 280 mTorr is amorphous and induces tensile residual stress as well. Tensile stress of the amorphous layers is a result of the partial crystallization of the amorphous layer during its deposition. Crystallization of amorphous silicon is followed by volume contraction of the layer which results in tensile stress.

Resolutions whether layer is polycrystalline or amorphous were done using SEM and is reported elsewhere [2].

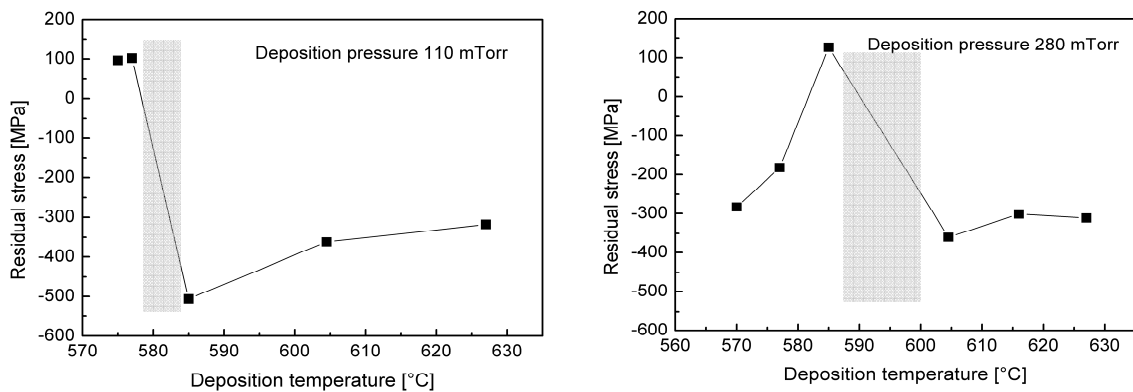


Fig. 2: Residual stress of the amorphous and polycrystalline silicon layers deposited on the backside of the silicon wafer. On the left side from the grey areas were layers amorphous. Grey areas denote transition region between amorphous and polycrystalline silicon. Polycrystalline layers are right from the grey area.

- [1] MF657, *Standard Test Method for Measuring Warp and Total Thickness Variation on Silicon Slices and Wafers by a Non-contact Scanning Method*, Semiconductor Equipment and Materials International (SEMI) 2007.
- [2] D. Lysáček, *Thin films of polycrystalline silicon*, Doctoral thesis, Brno University of Technology, 2010.

## **INNOVATION OF TEACHING AIDS IN THE SUBJECT „MATERIALS FOR ELECTRO-TECHNOLOGY“**

M. Madaj, J. Drápala, M. Kursá

Vysoká škola báňská – Technical University of Ostrava, Faculty of Metallurgy and Materials Science, Av. 17. listopadu 15, 708 33 Ostrava – Poruba, Czech Republic  
[michal.madaj@seznam.cz](mailto:michal.madaj@seznam.cz)

The task of the project „Personalization of tuition through e-learning“ (registration number CZ.1.07/2.2.00/07.0339) with support of MŠMT ČR and European social fund in the Czech Republic is to improve the quality of university textbooks in technical subjects at VŠB-Technical University of Ostrava. New teaching supports utilizing procedures, methods and tools, updating, distribution and evaluation of education and administration of knowledge applying network technologies and computers, thus e-learning, have been elaborated for some subjects. Study supports will serve for both the combined form of study and the full-time education and they will be available in the university computer network (Intranet), global network (Internet) or university e-courses. E-learning teaching aids utilize texts and presentations with references, animated sequences, video images, voice commentaries, own notes and communications with lecturers and students, tests and electronic models of processes, etc.

The main target group in the subject „Materials for electro-technology“ are students of the first and fourth years of the Faculty of Electrical Engineering and Computer Science and Faculty of Metallurgy and Materials Engineering at VŠB-TU Ostrava. It is an innovation of teaching aids and study support for the students who make the acquaintance of basic materials, procedures and processes utilized in electrical engineering, microelectronics and optoelectronics.

The subject “Materials for electro-technology“ presents general foundations for studying the electrical engineering specializations and provides students with the survey of materials used for construction of devices of electrical engineering and microelectronics. It deals especially with electrical, magnetic, physico-chemical, mechanical and other properties of substances and relates them to the material composition and internal structure. The subject frame is formed by twelve chapters, the first of them is „Introduction“. It presents the theory of conductivity, bonds between atoms, electron theory of metallic state, cohesive forces of solids, cohesive energy of metals, band theory for classical and transit metals. The second chapter has the title „Structure of materials“ and it includes basic characteristics of crystalline substances, which means the basic types of crystal lattices, Miller indices of planes and directions, Brillouin zones for conductors, insulators and semiconductors. Furthermore, it includes crystal lattice defects, single crystalline, polycrystalline and amorphous materials, solid solutions, intermetallic phases and modifications at phase transformations. The third chapter contains formation of alloys, phase diagrams, intermetallic compounds and their physical properties. The fourth chapter deals with conductive materials, physical principle of electrical conductivity of metals and basic properties of electrical conductivity of metals, special conductive materials, carbon materials, contact materials and materials with shape memory. The fifth chapter includes resistive materials, materials for thermo-electrical transformation, fuses, bimetals, solders.

The sixth chapter is entitled „Theory of superconductivity, low- and high-temperature superconductivity“. The seventh chapter deals with the theory of magnetism, magnetically soft and hard materials, their properties, ferrites, materials for magnetic record and metallic glasses. This chapter also includes production technologies and areas of their application. The eighth chapter characterizes methods of material refining and structure improvement, creating thin layers, diffusion and implantation of particles. Great attention is paid to such crystallization methods as the zone refining, directional crystallization, distillation, Czochralski method and other methods of crystalline and single crystal preparation. The ninth chapter enables students to understand more deeply the theory of semiconductors, elementary, compound and oxide materials. In addition, the planar-epitaxial technology of production of integrated circuits is presented. The tenth chapter includes materials for optoelectronics, thermoelectric materials, solar cells, liquid crystals, ferroelectrics. The eleventh chapter is entitled „Dielectrics and insulators, polymers“ and it includes the description of properties and structure of insulators, polarization and permittivity of dielectrics, electrical conductivity of insulators, dielectric strength of insulators, basic kinds of breakdowns, non-electrical properties of insulators and a survey of utilized materials. Moreover, gaseous, liquid and solid insulators, both organic and inorganic, and their applications are characterized. The last twelfth chapter includes construction materials, ceramic and composite materials, essential mechanical and technological tests of materials.

The text itself is suitably supplemented with animations, video-records and presentation CD-ROMs from the field of technology of semiconductors.

It follows from the characterisation above that the subject „Materials for electro-technology“ content and range cover a number of technical disciplines. The development in the area of materials for electro-technology, optoelectronics and microelectronics requires innovations and updating of teaching aids in all specializations applying modern teaching methods and computer technologies. It results in a better explanation, illustration and consequently a better understanding of the taught topics by the students.

*This work is supported by Ministry of Education Youth and Sport of the Czech Republic and European social fund in the frame of the solution of project „Personalization of tuition through e-learning“, number: CZ.1.07/2.2.00/07.0339.*

## REFERENCES

- [1] Šarmanová, Jana. *Personalizace výuky prostřednictvím e-learningu* [online]. 3. 7. 2006, 29. 6. 2010 [cit. 2010-06-29]. Personalizace výuky prostřednictvím e-learningu. Dostupné z WWW: <<http://www.person.vsb.cz>>.
- [2] Kuchař, Lumír; Drápala, Jaromír. *Metalurgie čistých kovů : Metody rafinace čistých látek*. první. Nadácia R. Kammela : [s.n.], 2000. 185 s. ISBN 80-7099-471-1.

**GAMMA AND ALPHA SPECTROSCOPY OF INORGANIC SCINTILLATORS,  
ESPECIALLY THOSE Pr<sup>3+</sup>-DOPED**

J.A. Mareš<sup>(a)</sup>, A. Beitlerová<sup>(a)</sup>, M. Nikl<sup>(a)</sup>, P. Průša<sup>(a),(b)</sup>, M. Kučera<sup>(c)</sup>, K. Nitsch<sup>(a)</sup>

(a) Institute of Physics AS CR, Cukrovarnická 10, 162 00 Prague 6, Czech Republic

(b) Czech Technical University in Prague, Faculty of Nuclear Sciences and Physical Engineering, Břehová 7, 115 19 Prague 1, Czech Republic

(c) Faculty of Mathematics and Physics, Charles University, Ke Karlovu 5, 121 16 Prague 2, Czech Republic

*amares@fzu.cz*

Basic concept of Hybrid Photo Detectors (HPD) or Hybrid Photo Multipliers (HPMT) combines vacuum sealed photocathode and Si-PIN diode as anode and is known more than 50 years [1]. Considerable improvement of these detectors is connected with a development of more efficient Si-PIN diodes [1]. Though HPMT multipliers exhibit much lower gain compared with the classical PMT dynode multipliers they are less noisy and can be easily calibrated in photoelectrons compared with the classical PMT [1,2].

HPMT detector was employed at characterization of scintillation properties of heavy, fast, radiation hard and low light yield (around 10-20 ph/MeV) PbWO<sub>4</sub> (PWO) crystal selected for electromagnetic or photon calorimeters at LHC CMS and ALICE CERN's projects, (see [www.cern.ch](http://www.cern.ch)) [2]. The latest interesting development of HPD detectors is connected with the use of silicon pixel array instead of one Si-PIN diode as anode. This Si-pixel HPD multiplier (1024 pixels) is used at CERN LHCb RICH detector of Cherenkov's radiation which consists of 500 these special HPDs. Besides these "large" applications also smaller experimental set-ups use HPMT multipliers, especially to measure scintillation properties of different wide band gap materials of much higher light yields than that of PWO [2,3].

During last years extended research of scintillation properties was performed on fast Ce<sup>3+</sup> or Pr<sup>3+</sup>-doped Lu or Y aluminum perovskite or garnet crystals (or even on epitaxial crystalline layers) but also on Lu or Y silicates and other crystals [1-3] mainly using set-ups with classical PMT multipliers and only a few ones using the HPMT multipliers. The highest light yield (~ 60000,0 ph/MeV) was reached on LaCl<sub>3</sub>:Ce and LaBr<sub>3</sub>:Ce ones. This paper has two main goals: (i) to describe the method of gamma and alpha spectroscopy of scintillators – the use of the HPMT multiplier in scintillation studies of wide band gap materials (properties as photoelectron and light yields, energy resolution, proportionality, time properties, etc.) in the energy range 10 keV - 2 MeV and (ii) to summarize scintillation properties of various mainly Pr<sup>3+</sup>-doped scintillators of Y-Lu aluminum garnet structures. Finally, we also mention a new possibility to investigate scintillation properties of thin epitaxial layers using the HPMT and  $\alpha$ -ray particle excitation [3] and possible imaging applications.

Selected examples of scintillation response of  $N_{\text{phels}}(E)$  photoelectron yields of Pr-doped LuAG crystals compared with those of YAP:Ce and undoped LuAG are presented in

Fig 1. Time dependence of  $N_{\text{phels}}(t)_{\text{rel}}$  photoelectron yield of selected LuAG:Pr thin layers are given in Fig. 2. These results and the other ones will be summarized.

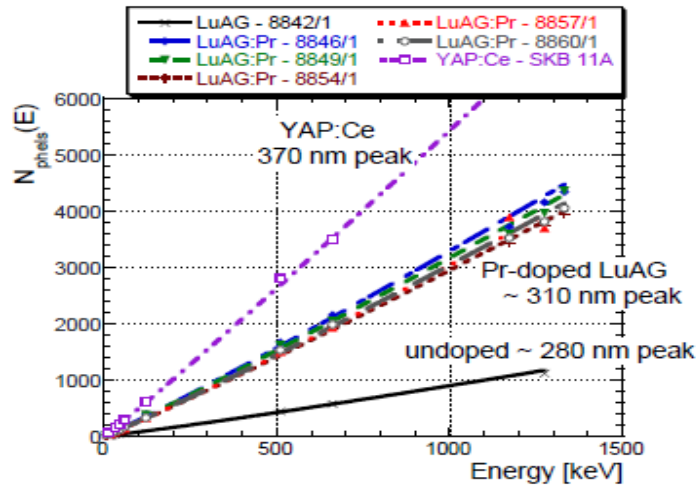


Fig. 1:  $N_{\text{phels}}(E)$  scintillation photoelectron yield as function of energy measured with LuAG, LuAG:Pr and YAP:Ce crystals

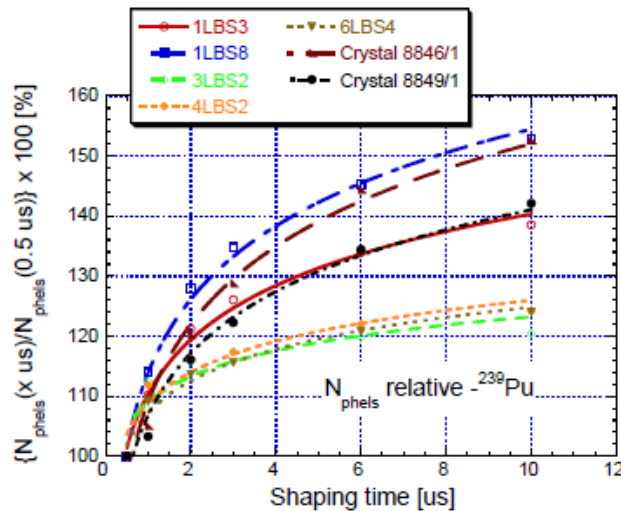


Fig. 2: Time development of  $N_{\text{phels}}(t)_{\text{rel}}$  yield for LuAG:Pr crystals and thin LPE grown epitaxial layers

*This work was supported by the Grant No. 202/08/0893 of the Czech Science Foundation.*

- [1] J. A. Mareš, C. D'Ambrosio, Opt. Mat. 30 (2007) 22.
- [2] J. A. Mareš, M. Nikl, K. Blažek, K. Nejezchleb, C. D'Ambrosio, Proc. of 8-th Intern. Conf. on Inorg. Scintillators and their Use in Scientific and Industrial Applications (SCINT'05), Kharkov, 2006, Ukrajina, p. 138.
- [3] P. Průša, M. Nikl, J.A. Mareš, M. Kučera, K. Nitsch, A. Beitlerová, Phys. Stat. Sol. A 206 (2009) 1494.

## MEASUREMENT METHODS OF MECHANICAL PROPERTIES OF SOLDERS AND SOLDERED JOINTS

M. Martinkovič, R. Koleňák, K. Pocisková Dimová

Slovak University of Technology Bratislava, Faculty of Materials Science and Technology in Trnava, Institute of Production Technologies, J. Bottu 25, 917 24 Trnava  
*maros.martinkovic@stuba.sk*

### Introduction

There has been significant research to improve properties of lead free-solders during last years [1]. At present, much effort is devoted to investigate the relations between microstructure and mechanical properties of these materials and compare new lead free-solders properties with led ones using to recent time. It is necessary to investigate mechanical properties of soldered joints too.

### Measurement of bulk solder specimens properties

Bulk solder specimens are prepared from small ingots melted in aluminium mold. The specimens of about 40x5x2 mm with the gauge length of 16 mm must be selectively polished before testing. Bulk solders specimens before and after tensile test are on fig. 1.

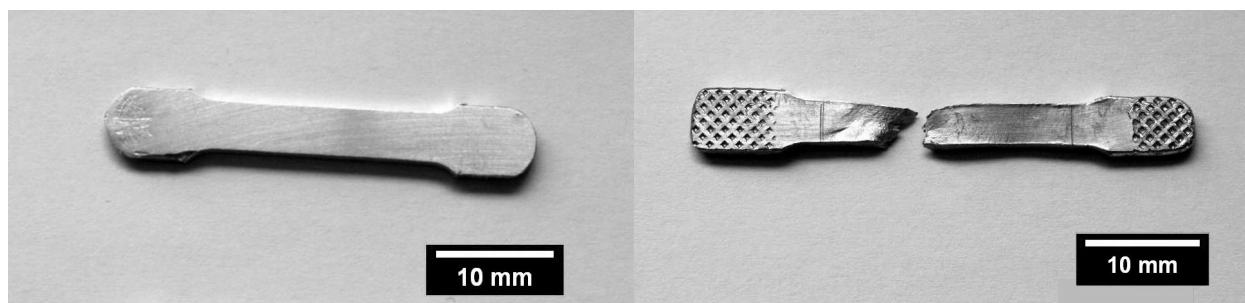


Fig. 1: Bulk solders specimens before and after tensile test

Force – extension diagrams are drawn by the testing machine and the maximum force to failure for each bulk solder specimen is determined. The obtained diagrams are digitalized and the values of relative toughness ( $\text{mJ/mm}^3$ ) are determined from the area under the recorded loading curve. The ductility is determined from gauge length before and after the test. The values of ultimate tensile strength are determined by dividing the maximum force applied in the tensile test with the original cross-sectional area of the tested solder specimen.

### Measurement of soldered joints properties

Two types of soldered joints are manufactured. First type - soldered lap-joints is prepared from sheets with size 20 x 10 x 0.8 mm. Each sheet was shortly polished on P1200 SiC abrasive paper. To prepare the soldered joints, the solder alloy and the flux were placed between two sheets and heated on the hot plate. To ensure immobility during the process a special facility from aluminium was designed. Finished joints (see fig. 2) were subsequently cooled on a stainless steel pad. Only shear strength of joints can be measured. The shear strength of solder lap-joints is determined by dividing the maximum shear load by the area of the solder lap-joint.

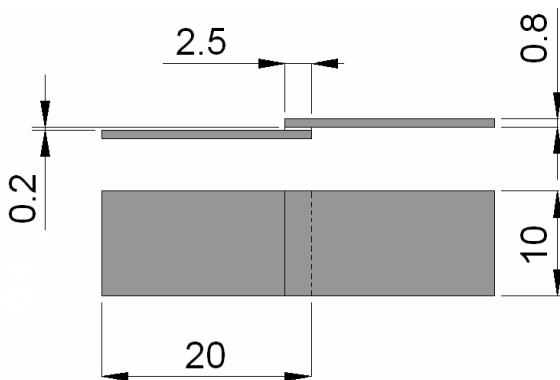


Fig. 2: Solder lap-joint

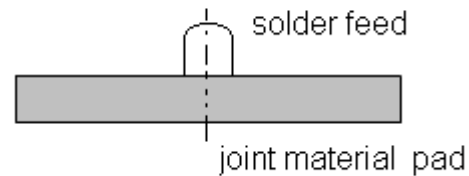


Fig. 3: Solder feed-joint

Second type - solder feed with diameter 5 mm and high 2.5 mm on (see fig. 3) with diameter 16mm and high 1.5mm is prepared on a hot plate at appropriate technological conditions using special facility from aluminium. Shear strength of solder-pad interface and toughness –fracture energy can be measured. Universal testing machine with shear strength adaptor is used. Fracture energy –toughness of bond is calculated from area under the curve in force- displacement diagram.

### **Conclusion**

These measurement methods of mechanical properties of solders and soldered joints were used for a lot of experiments. To use small tensile test specimen have some advantages. Only 4 grams of solder material is enough to obtain two main mechanical properties of solder alloy – ductility and tensile strength and toughness – fracture energy too. Soldered lap-joints probe led only to obtaining of shear strength, but solder feed probe can be used to obtain not only value of shear strength, but fracture energy –toughness of bond too. Only about 0.4g of solder material is needful for this probe and after testing the both materials (feed and pad) can be used for further utilization.

*This work was supported by VEGA Grants No. 1/0381/08, 1/0842/09 which are supported by Slovak Republic Ministry of Education*

### **Literature**

- [1] Martinkovič, Maroš - Drienovský, Marián: Comparison of mechanical properties and microstructure of lead-free solders and soldered joints. In: Acta Metallurgica Slovaca Conference. - ISSN 1338-1660. - No. 1, Special Issue : 14th International Symposium on Metallography, 28th - 30th April 2010, Stará Lesná, Slovak Republic (2010), s. 277-280

## **LOW TEMPERATURE HYDROGEN PLASMA TREATMENT OF DIAMOND FILMS BY LINEAR ANTENNA MICROWAVE PECVD SYSTEM**

N. Neykova, H. Kozak, A. Kromka

Institute of Physics AS CR, Cukrovarnická 10, CZ-16253 Praha 6, Czech Republic  
*neykova@fzu.cz*

Diamond is a perspective material for advanced devices in bio- and electronic applications because of unique optical, electrical and biocompatible properties. Undoped diamond is generally considered to be a very good insulator, but also exhibits p-type surface conductivity (SC) and negative electron affinity when it is terminated by hydrogen plasma. The best SC induced by H-plasma can be achieved on mono-crystalline diamond. However, nano-crystalline diamond (NCD) films are more desirable material considering low cost and large area deposition on different substrates. Our recent results demonstrated that NCD films exhibit high enough surface conductivity suitable for fabrication of electronic devices. For example, ion-sensitive and solid-state field effect transistors (FETs) were fabricated [1]. Up to now, the H-termination of NCD films was performed at relatively high substrate temperatures ( $T_{\text{sub}} \geq 600^\circ\text{C}$ ). For many bio- or electronic applications, H-termination at high temperatures is an ineligible technological process, because of a partial or complete damage of the passivating layer (used in bio-FETs), metal electrodes or other electronic parts. Therefore, hydrogen termination at low temperature is essential for such applications.

In this work we report on H-termination of NCD films at low temperature. Its effect on NCD surface conductivity, chemical properties of passivating layer, and metal contacts is presented. NCD films (thickness 600 nm, grain size 250 nm) were deposited on Si/SiO<sub>2</sub> substrates (10×10mm<sup>2</sup>) from a CH<sub>4</sub>/H<sub>2</sub> gas mixture in a microwave plasma enhanced chemical vapor deposition (PECVD) system [2]. To investigate the influence of H-termination on the diamond surface conductivity, Au interdigitated contacts (IDCs) were fabricated on NCD surface using optical lithography and lift-off technique. H-termination of NCD films was performed in a temperature range from 150 to 400°C in linear microwave antenna PECVD system. The surface conductivity of H-terminated NCD patterns was characterized by current-voltage (I-V) characteristics. As an electronically insulating layer was used SU-8 photoresist which is well known as insulating and biocompatible material. Plasmatcally and thermally induced changes of SU-8 before and after plasma treatment were investigated by Raman spectroscopy and interference-free reflectance-absorbance spectroscopy of p-polarized IR light at Brewster's angle of incidence.

We found that the sheet surface conductivity of NCD films increased with increasing the substrate temperature. The sample treated (hydrogenated) at 150°C exhibited the lowest sheet surface conductivity in the range of  $10^{-11} \div 10^{-10} (\Omega/\square)^{-1}$  at 1V. The highest surface conductivity ( $1.7 \times 10^{-6} (\Omega/\square)^{-1}$  at 1V) was observed of the sample hydrogenated at 400°C. The “breaking temperature, i.e. the temperature at the highest gradient of sheet conductivity, was 200°C.

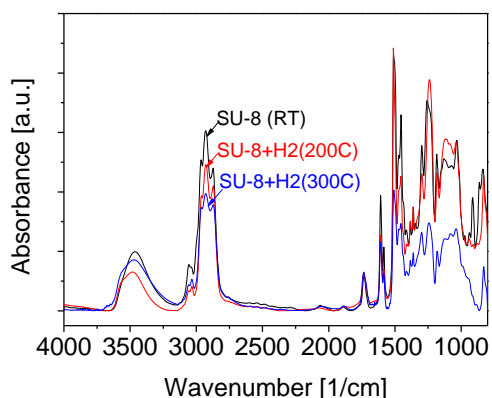


Fig. 1: IR absorbance spectra of SU-8 measured before and after hydrogen plasma treatment at 200 and 300°C.

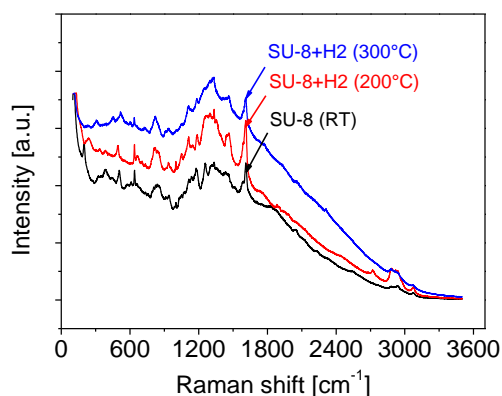


Fig. 2: Raman spectra of SU-8 measured before and after hydrogen plasma treatment at 200 and 300°C, respectively.

The IR and Raman spectra of SU-8, i.e. the study on its stability before and after hydrogen plasma processing, are shown in Fig.1 and Fig.2. All the spectra show comparable features and no significant change of polymer was observed up to 200°C. However, the hydrogen plasma treatment provided at 300°C resulted in its partial degradation and etching of SU-8 polymer from some areas was observed.

However, it is clear from electrical measurements that the H-termination at 200°C is enough to obtain the diamond films with good surface conductivity.

Our results confirmed that low temperature hydrogenation by novel linear antenna microwave PECVD represents a promising alternative for large area hydrogen termination without damage or destroying of metal or other electronic parts. Passivating SU-8 polymer and Au contacts withstand plasma treatment up to 200°C. Electrical measurements confirmed that good enough surface conductivity can be induced at such low temperature.

The present work opens a new technological window for possible applications of diamond thin films in semiconductor engineering.

*This work was supported by the grants IAAX00100902, KAN400100701, M100100905 and by the Centrum nanotechnology LC510.*

- [1] H. Kozak, A. Kromka, L. Michalikova, B. Rezek, Direct growth of nanocrystalline diamond field-effect transistor microstructures, *Sensor Letters*, 8 (2010) 482.
- [2] A. Kromka, B. Rezek, M. Kalbacova, V. Baresova, J. Zemek, C. Konak, M. Vanecek, *Adv. Eng. Mater.*, 11 (2009) B71.

## **EFFICIENCY OF PHYSICAL CHEMISTRY TEACHING IN MATERIAL SUBJECTS**

I. Pilarčíková<sup>(a)</sup>, I. Křivý<sup>(b)</sup>

(a) Czech Technical University in Prague, Faculty of Electrotechnical Engineering,  
Technická 2, 166 27 Prague 6, Czech Republic

(b) University of Ostrava, Faculty of Science, 30. dubna 22, 701 03 Ostrava 1,  
Czech Republic  
*pilarcik@fel.cvut.cz*

Universities are generally considered to be top institutes of an educational system as they provide graduates with high level of knowledge and values carried off to their prospective careers and lives. During last twenty years, the demands for academic education upgrading are frequently spoken in context of qualitative development, institutional and curricular changes in the area of the educational system. Pedagogic research in the field of academic education and training is rather sporadic and theoretical disciplines like Academic pedagogy and Academic didactics have no requested response to the academic ground.

Our research was focused on finding physical chemistry teaching efficiency in material engineering subjects at CTU, Faculty of Electrical Engineering. In the course of ten years, initially individual subject Physical chemistry, formerly for all FEE students, had been reduced to four lectures within the scope of one of introductory material subjects. These four lectures represent a necessary minimum needed for further study of material subjects. Their content consist of three topics: atomic structure, couplings, and material states of aggregation.

The research was realized in the subject Introduction to electrotechnical materials that is compulsory one in the bachelor course Electro-engineering and informatics registered into winter semester of the first class. The subject's program includes all selected chapters of Physical chemistry related to our research.

One parallel class including 314 students divided to 16 study groups represented a sample for statistic treatments. Foreigners whose perfect language knowledge cannot be supposed were displaced from this sample. After this reduction 300 respondents remained in this sample.

Teaching efficiency was evaluated using three non-standardized knowledge tests:

- before teaching (input knowledge of students);
- immediately after subject matter completion (output test);
- at semester end (preserve knowledge test).

At the same time, we dealt with the question how the following factors influence students' knowledge:

- type of secondary school attended by students before university entrance;
- sex;
- grade achieved by parents;
- residence city size.

At first, using a questionnaire, we collected some demographic data supposed to have an influence on the subject knowledge. This information was obtained by means of structured (closed) and half-closed questions.

**Input data**

sex	No	CS	SSS	STC	B	SOL	SWL	UE	a	b	c	d
men	284	171	103	10	12	48	153	71	15	59	125	85
women	16	12	4	0	1	3	7	5	0	2	10	4

**Legend of abbreviation:**

- No number of students
- CS comprehensive school
- SSS secondary specialized school
- STC secondary training college
- B basic
- SOL secondary without leaving examination
- SWL secondary with leaving examination
- UE university education
- a to d residence city size (a – up to 500, b -500 to 10,000, c -10,000 to 100,000 and d – over 100,000)

The results obtained using all three didactic tests were treated statistically. All calculations were carried out by means of the standard **statistic programme system NCSS 97**. [1]

At first, standard tests were performed for normal distribution of all quantitative variables (point assessment of tests *T1*, *T2*, and *T3*). The results of testing showed that it is not possible to reject null hypothesis on distribution normality. The Figures 1-3 show histograms (together with density curves) for the variables *T1*, *T2*, and *T3*. Null hypothesis on distribution normality could not be rejected even for samples of less size (e.g. samples containing data for women). However, this implies that we can use the following parametrical tests in subsequent statistic treatments:

- two-sample T-test,
- paired T-test,
- one-way analysis of variance (ANOVA).

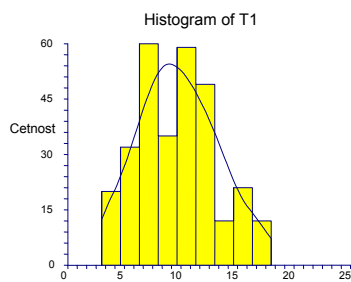


Fig. 1: Histogram for T1

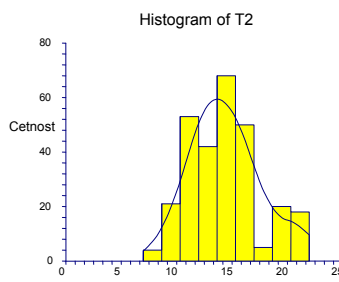


Fig. 2: Histogram for T2

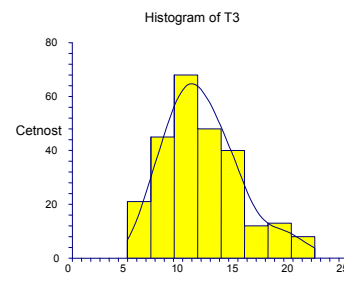


Fig. 3: Histogram for T3

Statistical analysis provided the following results:

- knowledge of students does not depend on their sex,
- knowledge of students coming from gymnasium are significantly better as compared with that of graduates of other types of secondary schools,
- effects of both grade of parents and residence city size on students' knowledge is found to be statistically significant,
- level of students' knowledge decreases significantly with time distance from subject matter presentation.

[1] NCSS 97. *Statistical System for Windows*. Keysville: Number Cruncher Statistical Systems, 1997.

## PHOTOLUMINESCENCE OF COPPER IONS IN SILICATE GLASS

Z. Potůček<sup>(a)</sup>, S. Stará<sup>(b)</sup>, Z. Bryknar<sup>(a)</sup>, J. Špírková<sup>(b)</sup>

(a) Czech Technical University in Prague, Faculty of Nuclear Sciences and Physical Engineering, Trojanova 13, CZ-120 00 Praha 2, Czech Republic

(b) Department of Inorganic Chemistry, Institute of Chemical Technology, Technická 5, CZ-166 28 Praha 6, Czech Republic

*zdenek.potucek@jfifi.cvut.cz*

Optical materials activated by  $\text{Cu}^+$  ions attract attention because of possible application of luminescence of  $\text{Cu}^+$  ions in tunable lasers for the visible spectral region [1, 2]. This luminescence associated with the interconfigurational transition  $3d^94s^1 \rightarrow 3d^{10}$  in  $\text{Cu}^+$  ion was observed in the near ultraviolet and almost in the whole visible spectral region in various glassy and crystalline materials activated by  $\text{Cu}^+$  ions. Glasses are more suitable for this application than crystalline materials because luminescence emission band is much broader in consequence of strong additional inhomogeneous broadening of corresponding electronic transition resulting from a variation of environment of  $\text{Cu}^+$  ions in the amorphous glass structure. Moreover glasses can be often technologically simply produced with high optical quality and excellent homogeneity up to very large dimensions and a spectral position of the  $\text{Cu}^+$  emission band can be influenced by modifying a glass composition. In particular, silicate glasses possess several advantages such as high transparency in the desired wavelength region, potentially low cost, and a very good compatibility with the most commonly used optical fibers.

We designed a composition and preparation procedure of novel Cu-doped sodium-zinc silicate optical glass that was doped by addition of  $\text{Cu}_2\text{O}$  to the batch. The glass batch weighed out from high purity powders of  $\text{SiO}_2$ ,  $\text{Na}_2\text{O}$ ,  $\text{ZnO}$ , and  $\text{Al}_2\text{O}_3$  was homogenized and melted in a platinum crucible in oxidation atmosphere at  $1450\text{ }^\circ\text{C}$  for 4 hours. The glass bars obtained by multistep cooling of the homogeneous melt in a stainless-steel mould were re-annealed and cut into rectangular plates with thickness of 1.5 mm. Then both large faces of the plates were polished to optical quality. Prepared samples of the Cu-doped sodium-zinc silicate glass were optically homogeneous and defect-free. In order to detect optically active centers related to Cu ions and to obtain their optical properties a study of room temperature absorption within the spectral region 200 – 3000 nm and temperature behavior of photoluminescence emission spectra within the spectral region 350 – 1600 nm was performed on samples of the prepared glasses with various Cu content up to 0.3 at. %.

The undoped glass was colorless and revealed absorption only in the UV spectral region below 320 nm. Cu-doping resulted in appearance of strong additional absorption in the UV spectral region below 350 nm and much weaker nearly unresolved broad absorption bands extending approximately between 500 and 1400 nm that originate from various types of centers related to  $\text{Cu}^{2+}$  ions appearing in the glass during the melting process due to partial oxidation of  $\text{Cu}^+$  ions [2]. Additional absorption in the UV spectral region is probably related to the interconfigurational  $3d^{10} \rightarrow 3d^94s^1$  transitions of  $\text{Cu}^+$  ions and to charge transfer transitions between  $\text{Cu}^{2+}$  and  $\text{O}^{2-}$  ions [2, 3].

Emission spectra of photoluminescence of prepared Cu-doped glasses excited in the region of additional UV absorption revealed three broad bands peaking near 530, 1020, and 1210 nm at room temperature. The emission bands peaking near 1020 and 1210 nm were attributed to electronic transitions in  $\text{Cu}^{2+}$  ions in octahedral and cubic coordination of oxygen, respectively. Luminescence of these  $\text{Cu}^{2+}$  centers could be also excited via a corresponding absorption band contributing to absorption observed for wavelengths longer than about 500 nm. The intensive emission band peaking near 530 nm is typical for photoluminescence of  $\text{Cu}^+$  ions occupying sites with the tetragonally distorted octahedral coordination of oxygen in the silicate glass [3]. Integral intensity of this emission band increased with increasing Cu content in the prepared sodium-zinc silicate glass reaching the maximum near 0.1 at. %. Such behavior is probably a consequence of the presence of  $\text{Cu}^{2+}$  centers in the glass that absorb part of excitation light owing to overlap of very strong charge transfer absorption bands of  $\text{Cu}^{2+}$  ions in the UV region with the excitation bands of photoluminescence of  $\text{Cu}^+$  ions. Moreover, photoluminescence of  $\text{Cu}^+$  ions can be also quenched by certain types of  $\text{Cu}^{2+}$  centers. Since an appreciable amount of  $\text{Cu}^{2+}$  ions is evidently undesirable in the Cu-doped glass for a potential application in tunable lasers emitting in the visible spectral region, optimization of both atmosphere and temperature conditions used for preparation of the studied glass is necessary in order to achieve the sufficient stabilization of  $\text{Cu}^+$  ions in the glass. However, Cu-doped glass exclusively activated by  $\text{Cu}^+$  ions is rather difficult to obtain because both the oxidation of  $\text{Cu}^+$  to  $\text{Cu}^{2+}$  and reduction of  $\text{Cu}^+$  to  $\text{Cu}^0$  and growth of  $\text{Cu}^0$  colloids must be prevented.

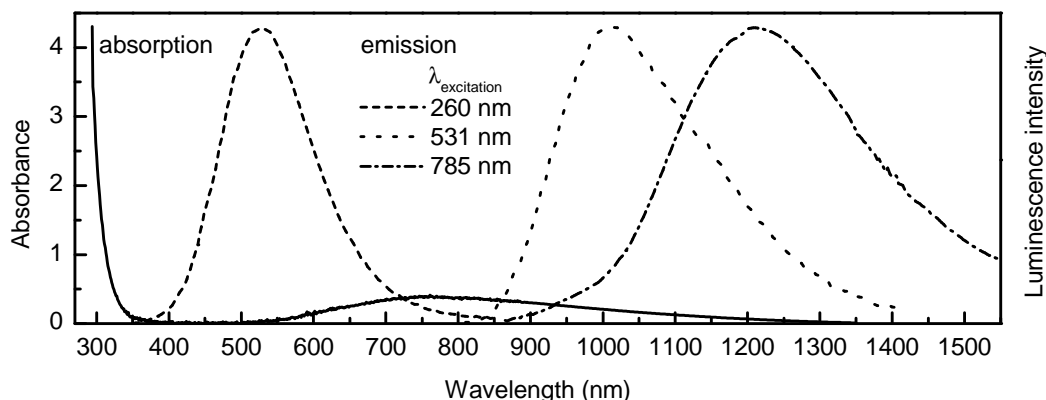


Fig. 1: Spectral dependence of Cu-induced absorption and normalized photoluminescence emission spectra of Cu-doped (0.3 at. %) sodium-zinc silicate glass at room temperature.

*This work was supported by the grant No. 106/09/1937 of the Grant Agency of the Czech Republic and by the projects MSM 6840770021 and MSM 6046137302.*

- [1] G. S. Kruglik, G. A. Scripko, A. P. Shkadarevich, N. N. Ermolenko, O. G. Gorodetskaya, M. V. Belokon, A. A. Shagon, and L. E. Zolotareva, *Copper-doped alumoborosilicate glass: spectroscopic characteristics and stimulated emission*, J. Lumin. 34 (1986) 343.
- [2] Y. Fujimoto and M. Nakatsuka, *Spectroscopic properties and quantum yield of Cu-doped  $\text{SiO}_2$  glass*, J. Lumin. 75 (1997) 213.
- [3] R. Debnath and S. K. Das, *Site-dependent luminescence of  $\text{Cu}^+$  ions in silica glass*, Chem. Phys. Lett. 155 (1989) 52.

## THERMAL PROPERTIES AND CRYSTALLIZATION KINETICS OF Er:LiY(PO<sub>3</sub>)<sub>4</sub> GLASS

M. Rodová, A. Cihlář, R. Král, A. Sveshnikov and K. Nitsch

Institute of Physics AS CR, Cukrovarnická 10, 162 00 Praha 6, Czech Republic  
rodova@fzu.cz

This contribution deals with study on thermal properties of phosphate glass with a nominal composition of Er:LiY(PO<sub>3</sub>)<sub>4</sub> when searching new scintillation glasses. Its aim is to determine fundamental kinetics parameters of crystallization of the supercooled melt of the above mentioned glass composition by means of the Johnson-Mehl-Avrami (JMA) model and to discuss applicability of this model using the  $y(\alpha)$  and  $z(\alpha)$  functions.

The standard nucleation-growth JMA model is expressed by the time dependence of the transformed volume fraction  $\alpha$  given by  $\alpha = 1 - \exp[-k(t)^n]$ , where  $n$  is the Avrami exponent,  $k$  the reaction rate constant and  $t$  is the time. By inserting the constant temperature increase  $T = \beta t + T_0$  into the above equation, where  $\beta$  is the heating rate and  $T_0$  is the initial temperature, and after taking the double logarithms a relation in the form  $\ln[-\ln(1 - \alpha)] = n \ln k + n \ln(T - T_0) - n \ln \beta$  was received. This makes it possible to evaluate the experimental data obtained by non-isothermal DSC and DTA.

The transformation conditions specified by the model need not fully agree with real transformation process [1] and so a state can arise, when the model is not able to describe running process with a sufficient truth. Hence procedures were proposed that are able to determine so-called applicability limits of the JMA model [2,3]. One of the most frequently used method to determine these limits is a test using  $y(\alpha) = \Phi \exp E_C / RT$  and  $z(\alpha) = \Phi T^2$  functions, where  $\Phi$  is the measured heat flow and  $E_C$  is the energy of crystallization, suggested for the description of experimental DTA and DSC traces. Both  $y(\alpha)$  and  $z(\alpha)$  functions are normalized between (0;1) and are independent of heating rate  $\beta$ . If the maximum of the  $z(\alpha)$  function is located at 0.632 the JMA model will describe correctly the crystallization of supercooled melt.

The glass with a composition of LiY(PO<sub>3</sub>)<sub>4</sub> with 1 mol % of Er<sup>3+</sup> as dopant was prepared by a direct synthesis of Li<sub>2</sub>CO<sub>3</sub> and YPO<sub>4</sub> with some excess of P<sub>2</sub>O<sub>5</sub> and doping ErPO<sub>4</sub> at 1200°C [4]. Crystallization kinetics was studied by non-isothermal DSC at heating rates of 2, 5, 8, 10, 18, 25, 40 and 48 K/min from room temperature to 1100°C on powdered samples of 30±5 mg and the particle size between 90 - 106 μm. Thermal properties of this glass measured at 10 K/min were as follows: temperature of glass transformation  $T_G = 413^\circ\text{C}$ , crystallization  $T_C = 726^\circ\text{C}$  and melting  $T_M = 926^\circ\text{C}$ .

Avrami exponent  $n$  was determined from the plots of  $\ln[-\ln(1 - \alpha)]$  on both  $\ln(T - T_0)$  (for individual heating rates) and on  $\ln \beta$  (for 8 different temperatures between 975 and 1084°C). While the former were nearly linear and parallel ones, the latter dependences were not linear or parallel ones.

Actual results obtained when describing the crystallization of supercooled melt with a composition of Er:LiY(PO<sub>3</sub>)<sub>4</sub> according to the JMA model provoke questions, due to the

above mentioned facts, whether this model is able at all to describe correctly crystallization of the supercooled melt studied. That is why the test of the JMA applicability to our melt was performed by means of  $y(\alpha)$  and  $z(\alpha)$  functions.

The normalized  $y(\alpha)$  and  $z(\alpha)$  functions are shown in Figs. 1 and 2 but only for the least and the greatest used heating rates of 2 and 48 K/min, respectively. The shapes of functions at the given rates are similar to each other. The maximum of the  $y(\alpha)$  decreases as  $\alpha$  increases, from  $\alpha$  value equal to 0.501 (at 2 K/min) to 0.378 (at 48 K/min). The maximum decrease of the  $z(\alpha)$  is from  $\alpha = 0.508$  (at 2 K/min) to 0.405 (at 48 K/min).

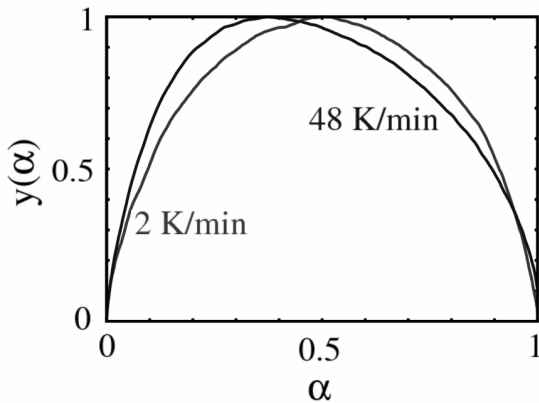


Fig. 1. Normalized  $y(\alpha)$  function obtained from non-isothermal DSC at heating rates of 2 and 48 K/min.

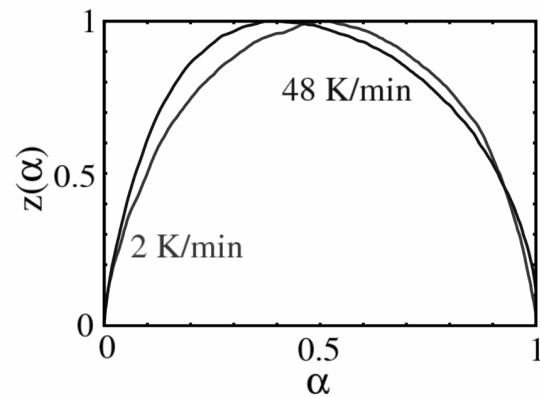


Fig. 2. Normalized  $z(\alpha)$  function obtained from non-isothermal DSC at heating rates of 2 and 48 K/min.

The maximum of the  $z(\alpha)$  function does not reach its characteristic value of  $\alpha_p^\infty = 0.632$  at any heating rate.

When searching new scintillating glasses, thermal properties of Er:LiY(PO<sub>3</sub>)<sub>4</sub> glass were studied. The fundamental parameters of the JMA model were determined but the differences in the Avrami exponent  $n$  obtained from experimental data by means of different procedure as well as the failure of linearity and parallelism of dependences of  $\ln[-\ln(1-\alpha)]$ , on  $1/T$  and on  $\ln \beta$  evoked great mistrust of usefulness of the JMA model to describe crystallization kinetics of molten Er:LiY(PO<sub>3</sub>)<sub>4</sub>. Using  $y(\alpha)$  a  $z(\alpha)$  functions it was confirmed that the JMA model is not able to describe correctly the crystallization kinetics of the supercooled melt with a composition of Er:LiY(PO<sub>3</sub>)<sub>4</sub>.

*This work was supported from the Grant Agency of the AS CR (No. KAN 300100802).*

- [1] H. Yinnon, D.R. Uhlmann, J. Non-Cryst. Solids 54 (1983) 253.
- [2] J. Málek, J. Therm. Anal. Calorim. 56 (1999) 763.
- [3] J. Málek, Thermochim. Acta 267(1995) 61; 355(2000) 239.
- [4] K. Nitsch, M. Rodová, J. Therm. Anal. Calorim. 91 (2008) 137.

## LASER SCRIBING ON SOI WAFER

J. Šik, P. Kostelník

ON Semiconductor, 1. máje 2230, 756 61 Rožnov pod Radhoštěm, Czech Republic  
*jan.sik@onsemi.com*

The light with the wavelength of  $1.06\ \mu\text{m}$  ( $1.17\ \text{eV}$ ) from Nd:YAG laser is used for silicon wafer laser scribing. The energy of the light is close to the indirect silicon bandgap and due to low absorption in this region the penetration depth of light into the wafer is relatively high. On the other hand, light absorption is increasing with increasing temperature; light is absorbed and creates well defined deep holes with edge slag rings in silicon. These ‘points’ create text for wafer marking (see Fig. 1).

We observed decreased scribe depth and diameter of holes at SOI wafer edge, where light interference fringes are seen (Fig. 1). These are indicating a gradient in device layer thickness, which causes laser light reflectivity fluctuations. At a high reflectivity condition the laser scribe is shallower and narrower as at a low reflectivity conditions. Scribe depth and diameter are roughly constant for reflectivity of up to 0.6; but decrease dramatically above 0.6 [1].

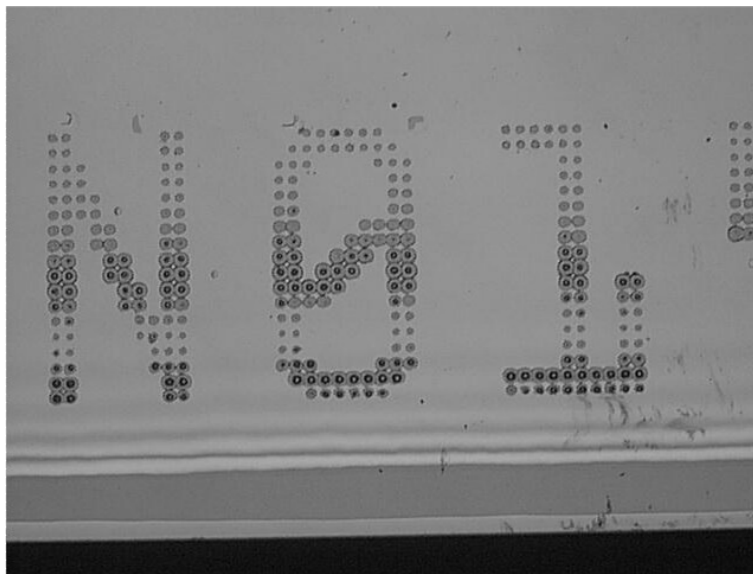


Fig. 1: Example of a laser scribe on SOI wafer. Decreased scribe depth and diameter of holes were observed.

Modeled reflectivity spectrum for SOI with  $1\ \mu\text{m}$  buried oxide (BOX) and  $3\ \mu\text{m}$  top device layer is in Fig. 2. The feature related to the first direct electronic transition in silicon  $E_1$  at  $3.4\ \text{eV}$  and starting interferences in device layer when penetration depth of the light approaches first silicon – oxide interface are clearly visible. BOX causes fluctuating interferences (beats) in reflectivity spectrum. The distance between maxima and minima is decreasing with increasing device layer and BOX thickness (see Fig. 2).

We proposed and modeled slight modifications (10% BOX thickness increase and surface oxide layer) of the SOI systems to reduce reflectivity value and its variation and thereby reduce shallow points in the wafer label (Fig. 3).

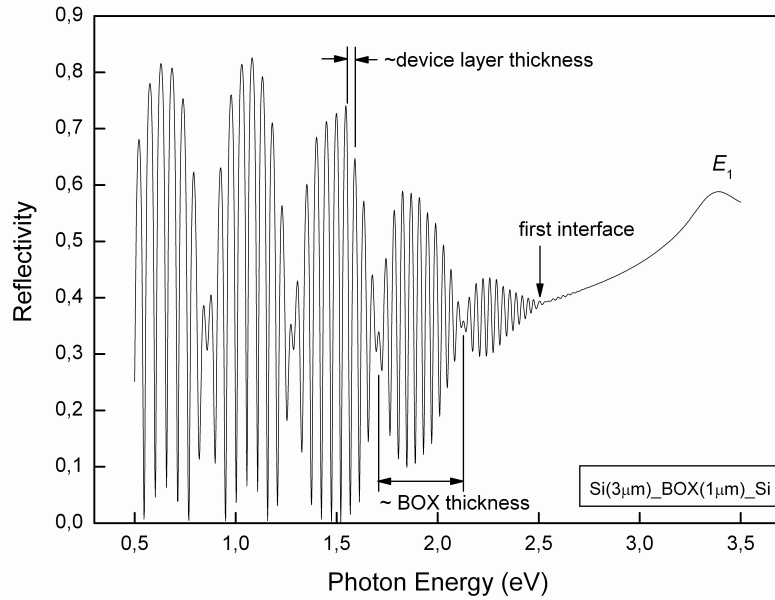


Fig. 2: Modeled reflectivity spectrum of the SOI with 1  $\mu\text{m}$  BOX and 3  $\mu\text{m}$  device layer.

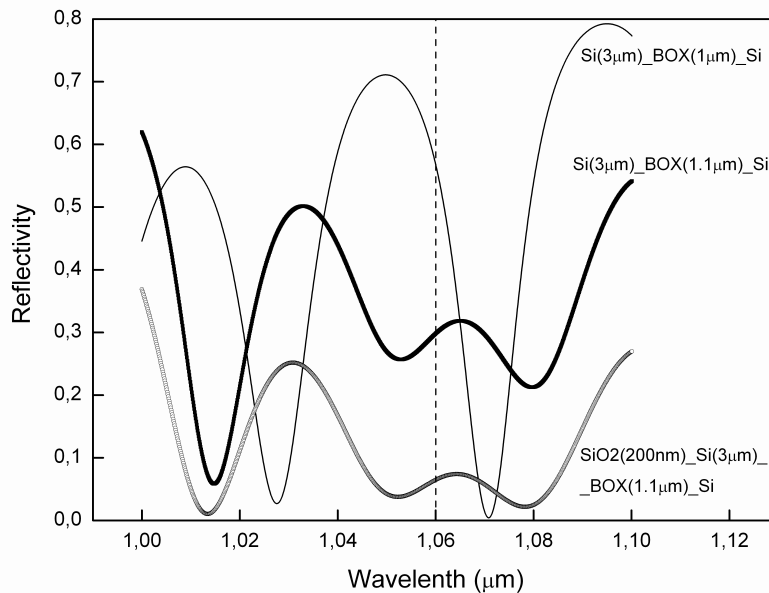


Fig. 3: Reflectivity spectra for SOI systems proposed to reduce reflectivity value and its variation and thereby reduce shallow points in the wafer label.

[1] Source: internal information from Le Laboratoire d'Électronique et de Technologies de l'Information (LETI), Grenoble.

**COMBINED  $^{31}\text{P}$  AND  $^{17}\text{O}$  MAS NMR AND RAMAN STUDIES  
OF MOLYBDENO-PHOSPHATE GLASSES**

J. Šubčík<sup>(a)</sup>, L. Koudelka<sup>(a)</sup>, L. Montagne<sup>(b)</sup>, G. Tricot<sup>(b)</sup>

(a) University of Pardubice, FChT, Studentská 95, 53210 Pardubice, Czech Republic

(b) University of Science & Technologies of Lille, UCCS, 59655 Villeneuve d Ascq, France

*jiri.subcik@student.upce.cz*

Phosphate glasses with additions of molybdenum oxide are prospective materials for electrical applications due to their high ionic conductivity [1]. Moreover, the knowledge of molybdenum oxide behavior in the phosphate based glasses and its role in the glass structure is important for management of radioactive waste. This contribution is devoted to the study of structure of phosphate-based glasses doped with molybdenum oxide with a focus on the role of  $\text{MoO}_3$  itself.

Glasses of the system  $(100-x)(0.5\text{ZnO}-0.5\text{P}_2\text{O}_5)-x\text{MoO}_3$  in the range of 0-70 mol%  $\text{MoO}_3$  were prepared by heating the calcined reaction mixture up to 900-1200°C and pouring the glass melt into the graphite mould. By slow cooling the melt in air the glass blocks with size about  $6\times 30\times 30\text{ mm}^3$  were formed. Raman spectra were measured on the bulk samples and for the NMR measurements the glass blocks were powdered in the mortar.

$^{31}\text{P}$  MAS NMR spectrum of the base glass  $50\text{ZnO}-50\text{P}_2\text{O}_5$  reveals one strong signal at  $\sim -31$  ppm, typical for metaphosphate glasses, corresponding to the resonance of  $\text{Q}^2$  phosphate units with two bridging oxygen atoms. With additions of  $\text{MoO}_3$  new Mo-O-P bonds are created hence the number of non-bridging oxygen atoms gradually increases and phosphate chains are shortened. This is reflected in the  $^{31}\text{P}$  NMR spectra by increasing the intensity of two new signals shifted upfield that correspond to the resonance of  $\text{Q}^1$  and  $\text{Q}^0$  units. In the glass with 70 mol%  $\text{MoO}_3$  the phosphate structure is highly depolymerized and the phosphate entities are present mostly in the form of isolated  $\text{P}(\text{OMo})_4$  units.

Raman spectra reveal incorporation of  $\text{MoO}_3$  to the glass structure in the form of  $\text{MoO}_6$  octahedra. Except that  $\text{MoO}_6$  octahedra are linked to the phosphate units by Mo-O-P bonds, they link together by common vertices creating Mo-O-Mo bonds. Presence of the latter bond is reflected in the Raman spectra by evolving the new band at  $891\text{ cm}^{-1}$  which is present in the spectra of all glasses. It follows that Mo-O-Mo bonds are present in the glass structure in an entire compositional range. Moreover, with increasing  $\text{MoO}_3$  content the number of Mo-O-Mo linkages increases. In the structure of glasses with a high  $\text{MoO}_3$  content the  $\text{MoO}_6$  octahedra link together by the common edges and form clusters of several molybdate units. This is reflected by broadening of Raman band at  $891\text{ cm}^{-1}$  to lower wavenumbers and shifting its maximum down to  $849\text{ cm}^{-1}$ .

The presence of Mo-O-Mo bonds was determined from Raman spectra. To our knowledge Mo-O-Mo bond has never been proven in glasses by any other method. Therefore, to prove this type bond in the glass structure, we have measured  $^{17}\text{O}$  MAS NMR for the sample  $x=20$  mol%  $\text{MoO}_3$ , which contains this type bond according to its Raman spectrum.

Prior to the measurement, the sample was enriched with  $^{17}\text{O}$  isotope to overcome its poor natural abundance (0.04%). The enrichment was performed on the powdered glass

sample by the enriched water at 550°C for 5 h. The acquisition was carried out on a high static field spectrometer (18.8 T) at a frequency of 108.5 MHz with a 3.2 mm probe operating at a spinning frequency of 20 kHz. A pulse length of 1.2  $\mu$ s and a radiofrequency of 55 kHz was used to acquire 2400 transients separated by a recycling time of 1 s. The  $^{17}\text{O}$  chemical shift reference is tap water.

According to Raman and  $^{31}\text{P}$  MAS NMR spectra there are several oxygen sites contained in the structure of the investigated glass. Therefore the  $^{17}\text{O}$  MAS NMR spectrum is supposed to show several resonance signals. These are the bridging oxygen site P-O-P, non-bridging oxygen sites Zn-O-P and Mo-O-P and also the Mo-O-Mo site.

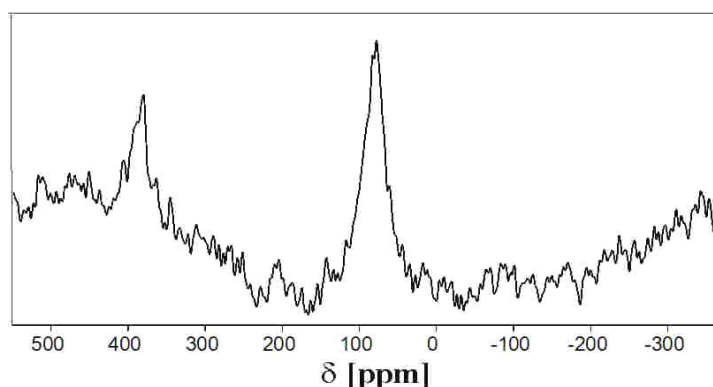


Fig. 1:  $^{17}\text{O}$  MAS NMR spectrum of the enriched glass sample with composition 40ZnO-20MoO<sub>3</sub>-40P<sub>2</sub>O<sub>5</sub>.

$^{17}\text{O}$  MAS NMR spectrum of the glass sample is shown in fig. 1. The spectrum shows two distinct signals with chemical shift values  $\sim 80$  ppm and  $\sim 380$  ppm. The signal at 80 ppm was ascribed to the resonance of non-bridging oxygen atoms of both Zn-O-P and Mo-O-P sites as well as in other phosphate glasses [2]. The latter signal at 380 ppm was ascribed to the resonance of Mo-O-Mo site as well as in  $^{17}\text{O}$  NMR spectra of some aqueous solutions of molybdenum complexes where the signal was found at 350-400 ppm [3].

As mentioned above the structure of the investigated glass should reveal also the signal corresponding to resonance of P-O-P site at  $\sim 120$  ppm [2]. This resonance likely makes part of the strong signal in the range of 20-150 ppm and longer acquisition would be needed to obtain the well resolved signal for this type site.

*The authors are grateful for the financial support from the research project No. 0021627501 of the Ministry of Education of Czech Republic and to the project SG300001.*

- [1] B.V.R. Chowdari, K.L. Tan, W.T. Chia, R. Gopalakrishnan, *X-ray photoelectron spectroscopic studies of molybdenum phosphate glassy system*, J. Non-Cryst. Solids 119 (1990) 95.
- [2] M. Zeyer, L. Montagne, V. Kostoj, G. Palavit, D. Prochnow, C. Jäger,  *$^{17}\text{O}$  nuclear magnetic resonance study of Na<sub>2</sub>O-P<sub>2</sub>O<sub>5</sub> glasses*, J. Non-Cryst. Solids 311 (2002) 223.
- [3] R.I. Maksimovskaya, G.M. Maksimov,  *$^{95}\text{Mo}$  and  $^{17}\text{O}$  NMR Studies of Aqueous Molybdate Solutions*, Inorg. Chem. 46 (2007) 3688.

## NUCLEATION OF PORTLANDITE

A. Sveshnikov<sup>(a,b)</sup>, P. Demo<sup>(a,b)</sup>, Z. Kožíšek<sup>(a)</sup>, P. Tichá<sup>(b)</sup>, D. Ladman<sup>(b)</sup>

(a) Institute of Physics AS CR, Cukrovarnická 10, 162 00 Prague 6, Czech Republic

(b) Czech Technical University in Prague, Faculty of Civil Engineering, Thakurova 7,  
165 29 Prague 6, Czech Republic

*sveshnik@fzu.cz*

The mixture of a cement with water starts a cascade of complex hydration reactions, leading in the final to the setting of a cement paste and the origination of a concrete [1]. The role of a starting material is played by tricalcium  $C_3S$  or dicalcium  $C_2S$  silicate (in the following text the chemical designations are used: C = CaO, S =  $SiO_2$ , H = OH). Their hydration produces a calcium hydroxide  $Ca(OH)_2$ . When the supersaturation of CH molecules, defined as a ratio of actual CH concentration to its equilibrium concentration, reaches high enough values, the nucleation of CH clusters starts. The calcium hydroxide nucleates in the form of hexagonal plates (see Fig. 1), also known as portlandite phase.

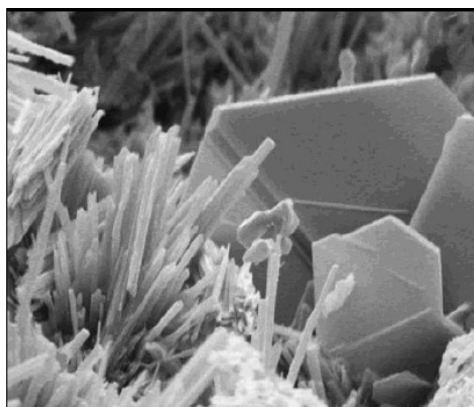


Fig. 1. Hexagonal portlandite CH plates surrounded by ettringite needles (photo by U.S. Department of Transportation)

In this paper we theoretically study the nucleation of portlandite clusters, which understanding is very important for the description of calcium silicate hydrate CSH formation at later stages of cement paste setting.

The driving force of CH nucleation is the supersaturation

$$S = \frac{C_{ACT}}{C_{EQ}},$$

where  $C_{ACT}$  represents the actual concentration of  $Ca(OH)_2$  molecules within solution and  $C_{EQ}$  is their equilibrium concentration, which can be determined from the solubility curve of calcium hydroxide in water [2]. We suppose, that the cluster has a shape of a hexagonal plate with radius  $r$  and height  $h$  (see Fig. 2).

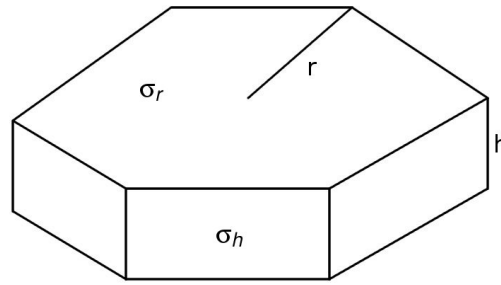


Fig. 2. The assumed shape of a portlandite cluster and the surface energies.

The total Gibbs energy required to form a cluster of size  $n$  consists of volumic and surface contributions and can be written as

$$\Delta G = \Delta G_v + \Delta G_s = -kT \frac{3\sqrt{3}r^2h}{2v} \ln S + 3\sqrt{3}r^2\sigma_r + 6rh\sigma_h,$$

where  $k = 1.38 \times 10^{-23}$  J/K is Boltzmann constant,  $T$  stands for temperature (in K),  $\sigma_r$  (resp.  $\sigma_h$ ) is surface energy of basis (resp. lateral) area, and  $v$  is the volume of the unit cell of portlandite ( $1.65 \times 10^{-28} m^3$ ). From extremum of  $\Delta G$  one can calculate the critical sizes of the portlandite cluster:

$$r_c = \frac{4\sigma_h v}{\sqrt{3}kT \ln S}, \quad h_c = \frac{4\sigma_r v}{kT \ln S}.$$

Clusters smaller than a critical one dissolve, while larger ones become stable and may further grow to macroscopic sizes. For the barrier of nucleation, which has to be overcome by CH-clusters in order to become growable we obtain

$$\Delta G_c = \frac{16\sqrt{3}\sigma_h^2\sigma_r v^2}{(kT \ln S)^2}.$$

Typical values of water to cement ratio,  $w/c$ , are spanned between 0.3 and 10. Taking a CH supersaturation from [2], we can estimate the critical sizes and the nucleation barrier to be  $r_c \in (5.9 \text{ nm}, 7.5 \text{ nm})$ ,  $h_c \in (1.0 \text{ nm}, 1.3 \text{ nm})$ ,  $\Delta G_c \in (7.9 \text{ eV}, 12.7 \text{ eV})$ .

It can be readily seen, that under common conditions neither the critical size nor nucleation barrier does not significantly change. However, the situation is quite different in the case of nucleation rate, which exponentially depends on  $\Delta G_c$ :

$$I \sim \exp\left(-\frac{\Delta G_c}{kT}\right), \quad \frac{I_{\max}}{I_{\min}} = \exp\left[-\frac{(\Delta G_c^{\max} - \Delta G_c^{\min})}{kT}\right] \approx 120.$$

Consequently, the rate of production of growable portlandite increases more than 100 times with decreasing  $w/c$  ratio.

*This study was supported by Ministry of Education and Youth of the Czech Republic, Project No. CEZ MSM 6840770003 and by the Grant No. IAA100100806 of the Grant Agency of the Academy of Sciences of the Czech Republic.*

[1]H. F. Taylor, *Cement Chemistry* (2<sup>nd</sup> edition), Thomas Telford, (2004).

[2]E. M. Gartner, et al., in: *Structure and Performance of Cements*, edited by J. Bensted and P. Barnes, chapter 3, Spon Press, (2001).

## **IMPACT OF CRYSTAL-ORIGINATED DEFECTS ON MANUFACTURING OF ELECTRONIC DEVICES**

L. Válek, P.Kostelnik, A.Klimsza

ON Semiconductor, 1. máje 2230, 756 61 Rožnov pod Radhoštěm, Czech Republic

*lukas.valek@onsemi.com*

Silicon-On-Insulator (SOI) technology has become an important part of microelectronic industry during last years. In the technology of direct bonding, two silicon wafers are bonded together while at least one of the bonded surfaces is covered by silicon dioxide. The top wafer (device wafer) is then thinned by mechanical or/and chemical means until the device layer remains. As electronic devices are manufactured in the device layer, the quality of the near-surface region of the device wafer is critical for the SOI technology.

Czochralski-grown silicon single crystals usually contain various types of defects, which may induce serious issues when located in the active area of the device. In this work we investigate the influence of crystalline quality of the Czochralski grown device wafer on the SOI manufacturing process.

Test devices formed by upper portion of an active structure of the NPN bipolar transistor were manufactured on the polished wafers; several wafers with 10 micron epitaxial layer were used as the reference wafers. Some of the substrate wafers passed denudation annealing to form a defect-free near surface layer. The test was performed on polished wafers and the impact to SOI manufacturing was concluded from the results.

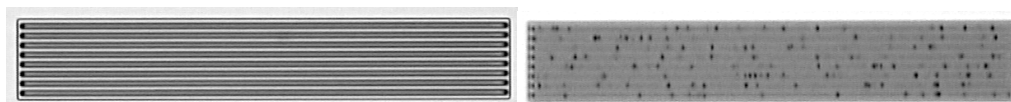


Fig. 1: Test field of deep trenches: (left) properly etched, (right) containing etch defects.

Manufacturing issues were observed during formation of the deep trenches by fluorine-based dry etching. Defectively etched trenches were observed on some of the wafers, while perfect trench etching was achieved on others. The defects appear as dots under the optical microscope (Fig. 1). The SEM analysis reveals the defects as randomly distributed spikes of unetched silicon (Fig. 2 left). Several micro masking effects were proposed as the origin of the etch residues observed during various trench etch processes, e.g. [1,2]. Based on the random height of the spikes and chemistry of the etching process, oxide precipitation has been identified as the origin of micro masking in our case.

Distribution of the spikes across the wafer surface was compared to the distribution of crystal defects. The highest amount of spikes was observed near the vacancy-interstitial boundary [3], fewer spikes were present in the vacancy-rich region and no spikes were formed in the interstitial-rich silicon. Such distribution indeed follows classical features of oxygen precipitation. The density of the spikes was compared to the density of bulk micro defects and a good correlation was found, see Fig. 2 right. Significantly lower spike density

(mostly zero) is observed on the denudation annealed wafers as the consequence of precipitate dissolution and oxygen out-diffusion during the denudation anneal. No spikes were observed also in the epitaxial wafers, naturally free of any oxide precipitates.

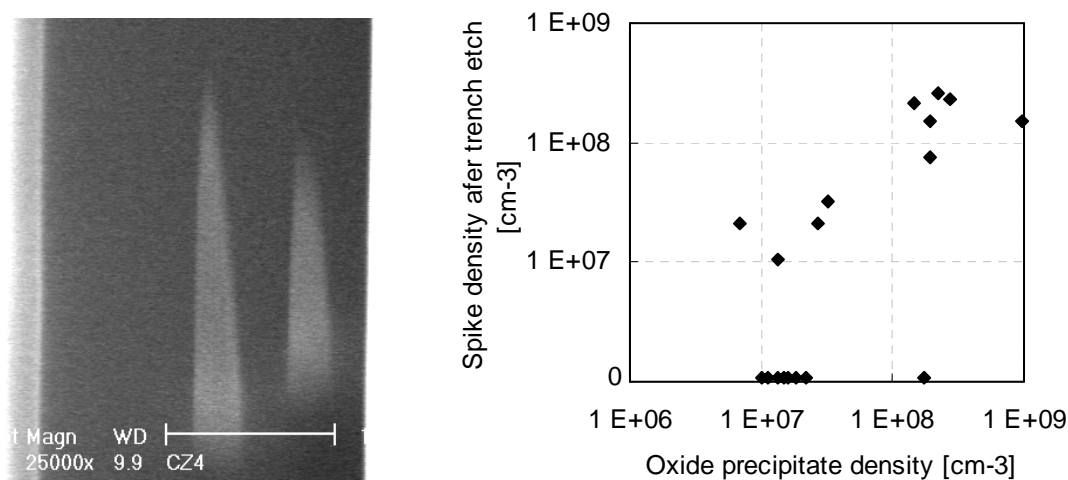


Fig. 2: (left) Spikes in the trenches after dry etching. (right) Correlation of the spike density to the oxide precipitate density in the center of the wafers.

Our results show that occurrence of the defects during plasma etching can be prevented by suppression of oxygen precipitation by means of (a) use of the epitaxial layer on top of the polished silicon surface, or (b) implementation of denudation annealing into the production flow of the wafer prior the plasma etching step. There are also other methods possible such as selecting the substrate being interstitial-rich over the whole wafer surface or CZ silicon growth in magnetic field for extremely low oxygen content. As the epitaxial layer increases the cost and crystal growth in interstitial-rich regime may be difficult as well as magnetic CZ process, denudation annealing seems to be the best option.

Polished silicon wafers of various types were studied from the crystal defect point of view and the impact of quality of the SOI device wafer on the SOI manufacturing process was evaluated. Crystal defects causing manufacturing issues during plasma etching process were identified to be oxygen precipitates and the solution based on defect engineering of silicon wafer was proposed. Measurements of electrical performance of the test devices show that the proposed solution is competitive to epitaxial wafers. Properly treated polished silicon wafer can be used as the SOI device wafer in SOI technology.

- [1] I.W. Rangelow, P. Thoren, K. Masseli, R. Kassing, *Secondary effects of single crystalline silicon deep- trench etching in a chlorine-containing plasma for 3-dimensional capacitor cells*, *Microelctr. Eng.* 5 (1986) 387.
- [2] T.Hayakawa, T.Suzuki, T. Uesugi, Y. Mitsushima, *Mechanism of residue formation in silicon trench etching using a bromine-based plasma*, *Jpn. J. Appl. Phys.* 37 (1998) 5.
- [3] L. Válek, M. Lorenc and J. Šik, *Radial distribution of point defects in CZ silicon*, *Proceedings of the 15th Joint Seminar DMSRE, Czechoslovak Association for Crystal Growth (ISBN 80-89088-42-2), 72-73 (2005).*

## PD NANOLAYERS FOR HYDROGEN SENSORS

R. Yatskiv<sup>(a)</sup>, K. Zdansky<sup>(a)</sup>, J. Grym<sup>(a)</sup>, K. Piksová<sup>(b)</sup>

(a) Institute of Photonics and Electronics v.v.i. AS CR, Chaberska 57, 18251 Prague 8

(b) Faculty of Nuclear Science and Physical Engineering, Czech Technical University in Prague, Brehova 7, 11519 Prague 1, Czech Republic

yatskiv@ufe.cz

The technology of preparation of the metal/InP interfaces plays an important role in the performance of gas sensors [1-3] particle detectors [4] and other applications based on InP. Metal-semiconductor interfaces formed on n-type InP by various conventional metal deposition techniques are known to exhibit low Schottky barrier heights due to the Fermi level pinning effect by extrinsic damages at metal/InP interfaces. Alternatively, the chemical wetness techniques such as electroplating, electroless plating and electrophoretic deposition technique have been proposed to achieve superior interface qualities. In this paper we present hydrogen-sensitive Pd-InP Schottky diodes prepared by electrophoretic deposition (EPD) of Pd nanoparticles with the diameters of 10 nm on the surface of n-type InP substrates. The Pd nanoparticles were prepared by the reverse micelle technique due reduced water solution of PdCl<sub>2</sub> by hydrazine in reverse micelles of sodium-di-2-ethylhexylsufosuccinate (AOT). The Pd-InP Schottky diodes were fabricated on n-type tin doped InP substrates using in-situ pulsed EPD whose set-up is shown in Fig. 1.

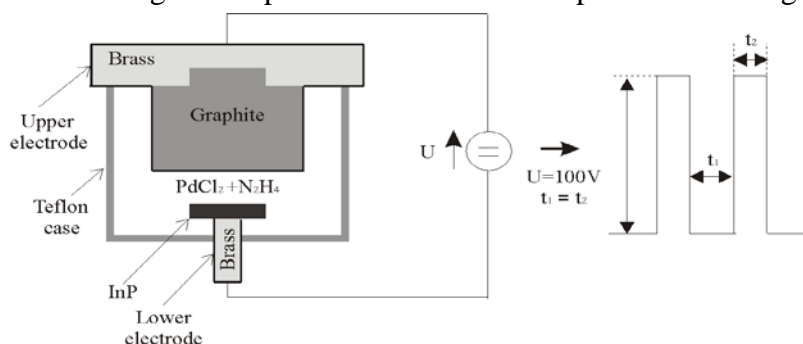


Fig. 1: Electrophoretic cell and pulse waveforms used for in-situ metal deposition

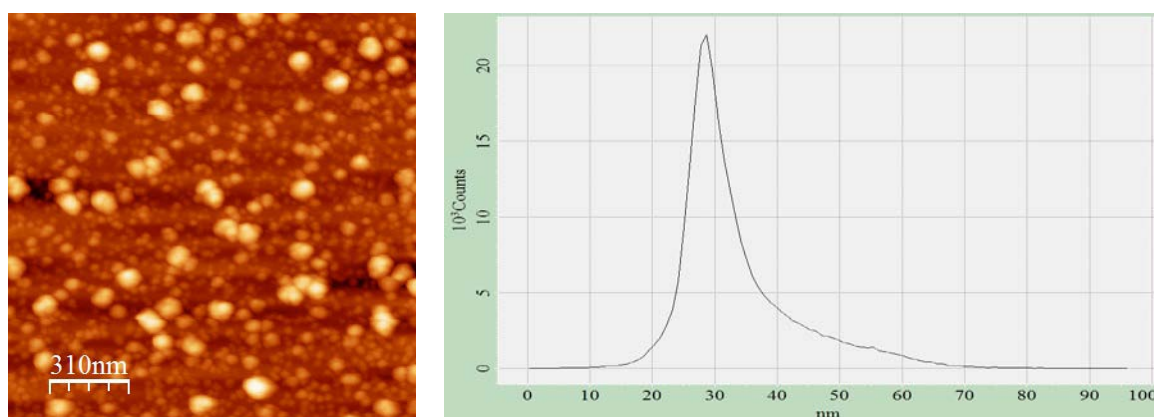


Fig. 2: AFM image of Pd NL and size distribution of Pd nanoparticles EPD on InP surface.

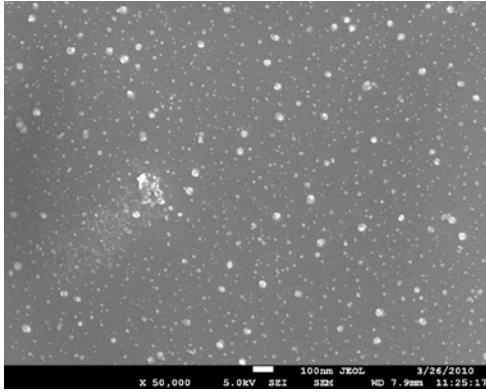


Fig. 3: SEM image of a nanolayer of Pd nanoparticles EPD on InP surface

Crystals of InP:Sn were grown by the Czochralski technique. The n-type concentration was about  $5 \times 10^{17} \text{ cm}^{-3}$ . Wafers of 1 mm thickness were sawed from a crystal, lapped and polished on one side chemo-mechanically with the substance 8% of sodium hydrochloride and 10% of aluminium oxide to the final thickness 450  $\mu\text{m}$ . Ohmic contacts on the back side were formed by rubbing liquid gallium. Schottky barrier electrode was formed by EPD nanolayers (NL) of Pd nanoparticles. Fig. 2 shows AFM image and the size distributions of Pd nanoparticles on InP substrate. Their mean diameter was between 10 nm and 40 nm. The

scanning electron microscope (SEM) image Pd nanoparticles on the InP substrate is shown in Fig. 3. The size of Pd nanoparticles determined by SEM is in a good agreement with their size established by AFM (see Fig. 2 and Fig. 3). The diodes were characterized by the measurement forward and reverse current-voltage characteristics (Fig. 4(i)). Diodes were also tested for their sensitivity to hydrogen Fig.4(ii) in a cell with a through-flow gas system. The detection mechanism in Schottky diodes may be explained by creating dipole layers on the Pd/InP interface due to the diffusion of atomic hydrogen. This layer influences the energy barrier at the interface and decreases the work function between metal and semiconductor.

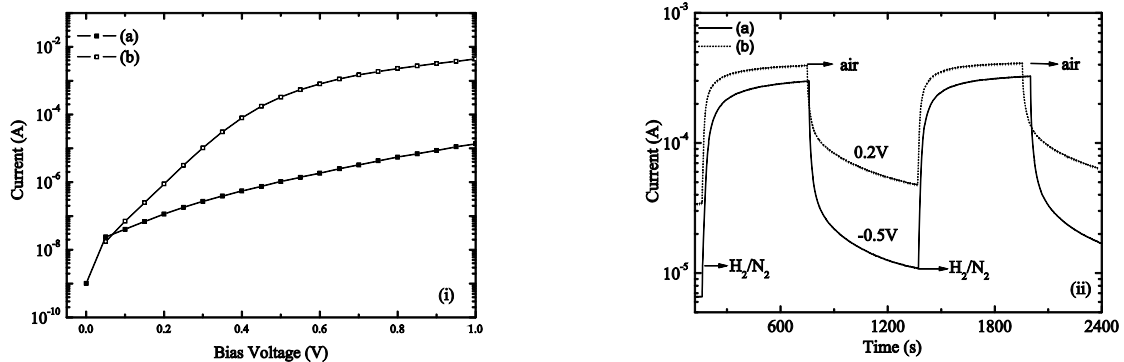


Fig. 4: Current-voltage (i) and current transient (ii) characteristics of Pd-InP diode measured at forward (a) and reverse (b) bias voltage.

*The work has been supported by the projects COST OC10021 of the Ministry of Education CR, KJB200670901 and KAN401220801 of the ASCR. We would like thank to V. Komarnitsky from the Faculty of Electrical Engineering, CTU Prague for AFM measurements.*

References:

- [1] V. Battut, J.B. Blanc, C. Maleysson, Sensors and Actuators B 44 (1977) 503
- [2] M. Yousuf, B.Kuliyev, B. Lalevic and T. Poteat, Solid-State Electron., 25 (1982) 753
- [3] Y.I.Chou, C.M.Chen, W.C.Liu, IEEE Elect. Dev. Let. 36 (2005) 62
- [4] R. Yatskiv, J.Grym, K. Zdansky, L. Pekarek, Nucl. Instr. Meth. A612 (2010) 334

## Author Index

- Babchenko O., 7, 21, 33  
Behúlová M., 9  
Beitlerová A., 47  
Bouda V., 37  
Bryknar Z., 55
- Cihlář A., 57  
Ciprian D., 39
- Davydova M., 33  
Demo P., 31, 63  
Drahokoupil J., 25  
Drápala J., 11, 45
- Galle J., 13  
Ganev N., 13, 15  
Gregora I., 29  
Grym J., 17, 67
- Hanuš M., 19  
Heczko O., 25  
Hlubina P., 39, 41  
Hruška K., 7, 21
- Ignácová-Sedláková S., 25  
Izak T., 7, 21, 33
- Jarošová M., 25  
Jurek K., 25
- Klimsza A., 65  
Kolařík K., 13, 15  
Koleňák R., 49  
Koman M., 23  
Kopeček J., 25  
Kostelník P., 27, 59, 65  
Koudelka L., 29, 61  
Kozak H., 51  
Kožíšek Z., 31, 63  
Král R., 57  
Kromka A., 7, 21, 33, 51  
Kucek V., 35  
Kučera M., 19, 47  
Kursa M., 11, 45
- Křivý I., 53
- Ladman D., 63  
Ledinsky M., 7  
Lipták J., 37  
Luňáček J., 39, 41  
Luňáčková M., 41  
Lysáček D., 43
- Madaj M., 45  
Majtás D., 25  
Mareš J., 19, 47  
Maroszová J., 23  
Martinkovič M., 49  
Michalka M., 21  
Mikloš D., 23  
Moncoľ J., 23  
Montagne L., 61  
Mošner P., 29
- Neykova N., 51  
Nikl M., 19, 47  
Nitsch K., 19, 47, 57  
Nohavica D., 17
- Onderišinová Z., 19
- Pala Z., 13, 15  
Piksová K., 67  
Pilarčíková I., 37, 53  
Pocisková Dimová K., 49  
Potocky S., 33  
Potůček Z., 41, 55  
Průša P., 19, 47
- Rezek B., 7, 33  
Rodová M., 57
- Sedláček J., 37  
Šik J., 59  
Špirková J., 55  
Stará S., 55  
Šubčík J., 29, 61  
Sveshnikov A., 31, 57, 63

Tichá P., 31, 63

Tricot G., 61

Válek L., 65

Yatskiv R., 67

Zdansky K., 67

# LIST OF PARTICIPANTS

Ing. Oleg Babchenko  
Institute of Physics AS CR  
Cukrovarnicka 10  
162 00 Praha 6  
Czech Republic  
*babchenko@fzu.cz*

Ing. Jaromír Galle  
ČVUT FJFI v Praze  
Katedra inženýrství pevných látek  
Břehová 7  
Praha 1, 115 19  
Česká Republika  
*j.galle@seznam.cz*

Doc Mária Behúlová  
Slovak University of Technology in Bratislava  
Faculty of Materials Science and Technology in Trnava  
Paulínska 16  
917 24 Trnava, SR  
Slovakia  
*maria.behulova@stuba.sk*

Prof. Nikolaj Ganev  
Czech Technical University in Prague  
Břehová 7  
115 19 Praha 1  
Czech Republic  
*nikolaj.ganev@fjfi.cvut.cz*

Ing. Alena Beitlerová  
Institute of Physics AS CR  
Cukrovarnická 10  
162 00 Praha 6  
Czech Republic  
*beitler@fzu.cz*

Dr. Jan Grym  
Inst. of Photonics and Electronics AS CR  
Chaberská 57  
18251 Praha 8  
Czech Republic  
*grym@ufe.cz*

Antonín Cihlár  
Institute of Physics AS CR  
Cukrovarnická 10  
162 00 Praha 6  
Czech Republic  
*cihlar@fzu.cz*

Martin Hanuš  
Institute of Physics of Charles University in Prague  
Ke Karlovu 5  
Praha, 121 16  
Czech Republic  
*hamatr@seznam.cz*

Prof. Pavel Demo  
Institute of Physics AS CR  
Cukrovarnicka 10  
162 00 Praha 6  
Czech Republic  
*demo@fzu.cz*

Ing. Tibor Izak  
Institute of Physics AS CR  
Cukrovarnicka 10  
162 00 Praha 6  
Czech Republic  
*izak@fzu.cz*

Prof. Jaromír Drápala  
Vysoká škola báňská - TU Ostrava  
Katedra neželezných kovů, rafinace a recyklace  
Tř. 17. listopadu 15  
708 33 Ostrava - Poruba  
Czech Republic  
*Jaromir.Drapala@vsb.cz*

Prof. Marian Koman  
Fakulta chemickej a potravinárskej technológie STU  
Oddelenie anorganickej chémie ÚACHTM  
Radlinského 9  
812 37 Bratislava  
Slovakia  
*marian.koman@stuba.sk*

Dr. Jaromír Kopeček  
Institute of Physics of the AS CR  
Na Slovance 2  
Praha 182 21  
Česká republika  
*kopecek@fzu.cz*

Doc Miroslav Kučera  
Charles University in Prague  
Ke Karlovu 5  
12116 - Praha 2  
Czech Republic  
*kucera@karlov.mff.cuni.cz*

Dr. Petr Kostelník  
ON Semiconductor Czech Republic  
1. máje 2230  
756 61 Rožnov pod Radhoštěm  
Czech Republic  
*petr.kostelnik@onsemi.com*

Dr. Jan Lipták  
FEL ČVUT Praha  
Czech Technical University in Prague  
Technická 2  
166 27 Praha 6  
Czech Republic  
*liptak@fel.cvut.cz*

Prof. Ladislav Koudelka  
University of Pardubice, FCHT  
Studentska 573  
Pardubice 532 10  
Czech Republic  
*ladislav.koudelka@upce.cz*

Dr. Jiří Luňáček  
Institut fyziky VŠB - TU Ostrava  
17. listopadu 15  
708 33 Ostrava-Poruba  
Czech Republic  
*jiri.lunacek@vsb.cz*

Dr. Zdeněk Kožíšek  
Institute of Physics  
Academy of Sciences of the Czech Republic  
Cukrovarnická 10  
162 00 Praha 6  
Czech Republic  
*kozisek@fzu.cz*

Dr. Milena Luňáčková  
katedra matematiky a deskriptivní geometrie  
VŠB - TU Ostrava  
17. listopadu 15  
708 33 Ostrava-Poruba  
Česká republika  
*milena.lunackova@vsb.cz*

Alexander Kromka  
Institute of Physics AS CR  
Cukrovarnicka 10  
162 00 Praha  
Czech Republic  
*kromka@fzu.cz*

Dr. David Lysáček  
ON Semiconductor Czech Republic  
1. máje 2230  
Rožnov pod Radhoštěm, 756 61  
Czech Republic  
*david.lysacek@onsemi.com*

Ing. Vladimír Kucek  
University of Pardubice  
Studentská 573  
Pardubice 53210  
Česká Republika  
*vladimir.kucek@gmail.com*

Ing. Michal Madaj  
Vysoká škola báňská – Technical University of Ostrava,  
Faculty of Metallurgy and Materials Science  
17. listopadu 15  
Ostrava, 708 33  
Czech Republic  
*michal.madaj@seznam.cz*

Dr. Jiří A. Mareš  
Institute of Physics AS CR  
Cukrovarnická 10  
162 00 Praha 6  
Czech Republic  
*amares@fzu.cz*

Dr. Zdeněk Potůček  
Institute of Physics AS CR  
Na Slovance 2  
182 21 Praha 8  
Czech Republic  
*potucek@fzu.cz*

Doc Maroš Martinkovič  
Faculty of Material Science and Technology SUT  
Pavliška 16  
Trnava 91724  
Slovak Republic  
*maros.martinkovic@stuba.sk*

Zdeněk Remeš  
Institute of Physics AS CR  
Cukrovarnická 10  
162 00 Praha 6  
Czech Republic  
*remes@fzu.cz*

Ing. Neda Neykova  
Institute of Physics AS CR  
Cukrovarnicka 10  
162 00 Praha 6  
Czech Republic  
*neykova@fzu.cz*

Ing. Miroslava Rodová  
Institute of Physics AS CR  
Cukrovarnická 10  
162 00 Praha 6  
Czech Republic  
*rodova@fzu.cz*

Dr. Karel Nitsch  
Institute of Physics AS CR  
Cukrovarnická 10  
162 00 Praha 6  
Czech Republic  
*nitsch@fzu.cz*

Dr. Jan Šik  
ON Semiconductor Czech Republic  
1. máje 2230  
Rožnov pod Radhoštěm, 756 61  
Czech Republic  
*jan.sik@onsemi.com*

Dr. Ivana Pilarčíková  
Faculty of Electrical Engineering - CTU  
Department of Electrotechnology  
Technická 2  
Praha 6 , 16627  
Czech Republic  
*pilarcik@fel.cvut.cz*

Ing. Jiří Šubčík  
University of Pardubice, FChT  
Studentska 573  
53210 Pardubice  
Czech Republic  
*jiri.subcik@student.upce.cz*

Dr. Jan Polák  
Crytur  
Palackeho 175  
Turnov 51101  
ČR  
*polak@crytur.cz*

Dr. Alexej Sveshnikov  
Institute of Physics AS CR  
Cukrovarnická 10  
162 00 Praha 6  
Czech Republic  
*sveshnik@fzu.cz*

Ing. Lukáš Válek  
ON Semiconductor Czech Republic  
1. máje 2230  
Rožnov pod Radhoštěm, 756 61  
Czech Republic  
*lukas.valek@onsemi.com*

Prof. Vlastimil Vodárek  
VSB-Technical University of Ostrava  
17. listopadu 15/2172  
Ostrava - Poruba, 708 33  
Czech Republic  
*vlastimil.vodarek@vsb.cz*

Dr. Roman Yatskiv  
Inst. of Photonics and Electronics AS CR  
Chaberská 57  
18251 Praha 8  
Czech Republic  
*yatskiv@ufe.cz*